Department of Structural Engineering
Faculty of Engineering Science and Technology
NTNU- Norwegian University of Science and Technology

ACCESSIBILITY
OPEN

MASTER THESIS 2010

SUBJECT AREA:	DATE:14.06.10	NO. OF PAGES: 87
Structural engineering		

TITLE:

Numerical modelling of the effects of crystallographic texture and grain structure on the macroscopic behaviour of metals

Numerisk modellering av effektene av krystallografisk tekstur og kornstrukturmorfologi på den makroskopiske oppførselen av metaller

BY:

Mikhail Khadyko

SUMMARY:

Crystal plasticity theory gives mathematical relations that connect the microstructure of crystalline materials, , with their macroscopic properties. These relations can be implemented into the numerical models. Aluminium samples of different microstructure are represented by such models. Plastic properties of these samples are studied. Yield surfaces are found and described for cases of different crystallographic texture and morphology. Analytical functions are found, that fit these yield surfaces.

RESPONSIBLE TEACHER: Odd Store Hopperstad

SUPERVISOR(S) Odd Store Hopperstad, Afaf Saai and Stephane Dumoulin

CARRIED OUT AT: NTNU

MASTER THESIS 2010

Mikhail Khadyko

Numerical modelling of the effects of crystallographic texture and grain structure on the macroscopic behaviour of metals

(Numerisk modellering av effektene av krystallografisk tekstur og kornstrukturmorfologi på den makroskopiske oppførselen av metaller)

The mechanical behaviour of crystalline materials is strongly influenced by microstructural properties such as crystallographic texture and grain structure. Today, micromechanical models are powerful tools to gain an understanding of the underpinning mechanisms of metal behaviour. These models, which are based on the theory of crystal plasticity and the finite element method, provide a direct link between the macroscopic behaviour of the metal and the characteristics of the microstructure.

This project aims at using a micromechanical model to study the effects of crystallographic texture and grain structure on the macroscopic response of the metal, which is here represented by the yield surface. Only fcc materials (like aluminium alloys) will be considered. To this end, finite element (FE) models of representative volume elements (RVEs) of the material will be defined, where the crystallographic texture and grain structure may be varied. The grain structure of the material will be explicitly modelled, and structures with equi-axed and elongated grains will be investigated. The FE modelling will be carried out with the nonlinear finite element code LS-DYNA.

The thesis work consists of the following tasks:

1. Literature study on the mechanisms of plastic deformation and crystallographic texture
2. Literature study on the theory of crystal plasticity
3. Calculation of yield surface for different textures using a one-element approach and the Taylor hypothesis
4. Calculation of yield surface for different textures and grain structures using FE models of RVEs with explicit discretization of the grains
5. Comparison of the results obtained with the two approaches and to results from the literature

The thesis should be organized according to prevailing guidelines.
Supervisors: Afaf Saai, Stephane Dumoulin and Odd Sture Hopperstad

The thesis should be submitted to the Department of Structural Engineering within 14. juni 2010.

NTNU, January 18, 2010

Odd Sture Hopperstad

Main supervisor

Foreword

Finite element modelling of morphology turned out to be more complicated than expected. By the time the report should be submitted only some preliminary results were obtained. So it was agreed with the supervisors that a chapter about fitting of results already obtained for Taylor model to analytical functions will be written instead (which is a useful and interesting subject by itself).

While working on this thesis I found a vast, new and very interesting area of crystal plasticity and its numerical models. I find things like this beautiful – a complex structure is built on several rather simple principles. For all help I have got while working on this, I want to thank my supervisors. Afaf Saai showed me the way, Stephane Dumoulin introduced me to the domain of CP numerical models and Odd Hopperstad coordinated it all. I just wish we had a little more time and made this thesis a little more perfect.

Abstract.

The crystal plasticity theory derives the response of a crystalline material from its structure and the structural defects. This work tries to find this connection. The first part revises the main concepts of the plasticity theory, structure of the crystalline material and its crystallographic texture, and shows how plastic deformations are explained by slip on the slip systems, which in turn is realized through the movement of the dislocations. Then the mathematical relations of the crystal plasticity are introduced, the main of which are Schmid's law, maximum plastic work principle, Voce law, viscoplastic constitutive relation and Taylor model. Taylor model particularly represents the polycrystal as homogeneous in terms of strains in it. This simplified approach and other relations are used to establish a numerical model of an aluminium sample where texture is represented by a set of Euler angles. This model is then used to derive the yield surfaces of samples with different sharp textures for plane stress situation by two different methods. One of them is the direct Taylor approach, where the load is applied as a deviatoric strain rate tensor. The other is a finite element model with one element. These yield surfaces show a strong unambiguous influence of texture on the plastic properties of the sample. These yield surfaces are analyzed and then represented as analytical yield functions. Finally, the morphology of the sample is introduced into the simulations and some preliminary results, showing its influence, are obtained.

Notation

A_0	cross sectional area
A_S	slip plane area
$\mathbf{b}$	Burger's vector
$\mathbf{C}$	stiffness tensor
c'_{ij}, c''_{ij}	transformation matrix
$\tilde{d}_{ij}$	transformed deviatoric stress
d_{ij}	deviatoric stress
D_{ij}	principal values of deviatoric stress
E	Young's modulus
$E(c'_{ij}, c''_{ij})$	error function
$f(\sigma)$	yield function
f_g	volume fraction of the grain
f_y	yield stress
F	force
m	strain rate sensitivity
m_{ij}	Schmid's orientation matrix
M_{ij}	rotational matrix
n^α, m^α	slip system orientation vectors
n_s	number of slip systems
ODF	orientation distribution function
$q_{\alpha\beta}$	latent hardening matrix
S_{ij}	normalized stress
t	time
t_i	traction
$\mathbf{T, L, L', L''}$	additional transformation matrices
$\mathbf{v}$	velocity field tensor
w^p	plastic work
w_p	weight coefficient
α	index of current slip system
$\gamma^{(\alpha)}$	resolved shear strain
$\gamma_*^{(\alpha)}$	kinematically equivalent shear strain
γ	relation between stress in x direction and shear stress
Γ	accumulated shear strain
Γ_{ch}^k	characteristic shear strain of k-th term
ε_p	plastic strain
ε	strain

$\left\langle \dot{\varepsilon}_{ij} \right\rangle$ volume averaged strain rate

θ shear strain rate

θ_k strain rate of k-th term

ρ relation between stress in x and y direction

σ_{02} equivalent stress

σ_{ij} stress tensor

σ_i principal stress

σ^0 isotropic stress

σ' deviatoric stress

σ_* statically equivalent stress

σ_p^{pr} approximated stress

σ_p^{sim} simulated stress

$\left\langle \sigma_{ij} \right\rangle$ volume averaged stress

τ_S resolved shear stress

τ_{CS} critical resolved shear stress

τ_0 initial critical resolved shear stress

τ_{sk} saturation shear stress for k-th term

$\varphi(S)$ isotropic yield function

φ, θ, ω Euler angles

ω_{ij} rotation tensor

ω_0 scatter width of texture component

ω angle between a given orientation and the ideal orientation

Contents

1. Introduction.

Aluminium is one of the most important structural materials. The plastic behaviour of aluminium is of a special interest because it undergoes plastic deformations in many cases: during production of details by sheet rolling, extrusion or pressing, during exploitation or collapse of construction.

In phenomenological models used in engineering, aluminium is usually treated as isotropic, homogeneous and continuous. This is also true for the models that try to predict the plastic properties of aluminium, but it is not a correct assumption for most cases. Metals have complex anisotropic microstructure that can considerably influence their properties. Multiscale modelling tries to determine properties of a material on some level as a consequence of its properties on a smaller scale. In our case the macroscopic properties of an aluminium sample, like the stress-strain curve or the yield surface, are derived from its microstructure – the orientation and plastic properties of the constituent grains. For this, the crystal plasticity models are used, which couple the microscopic properties and orientations of grains and the macroscopic response of a sample to the exterior load. When these models are used in numerical modelling of metal behaviour they allow getting more accurate results than the phenomenological relations that do not consider the inner structure of the metal. More specifically, the plastic behaviour under different straining of a sample –represented by its yield surface – depends on the distribution of orientations of the grains in that sample. While crystal plasticity models allow us to find those different yield surfaces by use of numerical models (using Finite Element Method (FEM) or other), the usual methods do not, despite the fact that the influence of microstructure on these surfaces may be considerable.

The objective of this work is to examine the influence of microstructural anisotropy (namely the typical textures) on the plastic properties of a rolled or annealed sheet aluminium sample (described by its yield surface) by means of a crystal plasticity model implemented in numerical simulation programs.

Only aluminium is considered and only a number of sharp idealized textures of aluminium (as explained in 3.3). Only one rate dependent constitutive model of single crystal plasticity with latent hardening is used (explained in 2.3). The situation of plane stress (which is the most common approximation, when we describe the rolled sheet metal) is assumed. Only several combinations of texture-morphology are simulated.

In this work it is shown what microstructure aluminium has and how we can use the mathematical relations based on its microstructure to predict macroscopic response. Firstly, a custom program developed by S. Dumoulin is used for numerical simulation that uses the Taylor approach directly. Then, a FEM program LS-DYNA is used, with microstructural properties implemented in a user-defined material model. Finally this material model is used for grain morphology study. Yield surfaces are obtained and analysed. A form of an approximate analytical yield function is found for them.

2. Theoretical foundation.

In the first part of the work, we will represent the theoretical basis for the numerical simulations. Firstly an overview of the concept of yield surface will be given, as a primary tool for understanding the plastic behaviour of the material. Then we will describe the microstructure of a metal – a polycrystalline microstructure – and show how it may be described in mathematical terms so as to be used in the crystal plasticity models. We will define crystalline material and its most important properties as well as such important concepts as grain orientation and texture. Then the mechanism of crystal plasticity will be explained as slip in the crystal lattice by means of dislocation displacement. We will introduce the relations for plasticity in a single crystal. Then we will use these relations in the model of polycrystal plasticity – the Taylor model. Finally we will show how the texture - as a property of microstructure - is connected with the macroscopic properties of a sample [7, 29].

In this work we make some general assumptions. We assume that all processes are quasistatic, which means that although we have some development of them in time, all accelerations are negligibly small and so are the inertia forces connected to them. We assume that all deformations are infinitesimal (so we can use the starting undeformed configuration of the body as a reference configuration). We also assume that the temperature is constant or it does not change enough to affect the deformations (isothermal conditions). Well known relations of continuum mechanics will be used throughout this work [3].

2.1 Yield surface.

2.1.1 Yield stress.

The first question that must be answered when we study the plastic behavior of a material is – at what value of load (stress) or deformation (strain) does this material start to yield (or we get plastic deformations). Figure 1 shows a relation between stress and strain for a simple case of uniaxial tension/compression. For some materials, especially mild steel, the stress-strain curve shows a distinct region of elastic proportionality and flat plastic region (Figure 2). The value of stress at which the material starts to yield can then be easily identified. It is called **yield stress** f_y [2, 3]. In these materials the elastic region is almost exactly linear and plastic strains accumulate without increase in stress (stress remains equal to the yield stress in a broad range of strains; this behavior is called perfect plastic). But for a general stress-strain curve it is not that simple. The elastic part is not exactly linear and it turns gradually into the plastic region, which is also not perfectly plastic, but shows some complex relation between stress and strain (such behavior, when yield stress is not constant, but some function of strain in plastic region is called hardening). So the transition part between pure elastic and plastic-dominated parts is rather broad (Figure 1). In this case, the yield stress is not as definite as in the previous. There are several methods of how to define it. The most common one is to define yield stress f_y equal to the stress $\sigma_{0.2}$ resulting in a plastic strain $\varepsilon^{\mathrm{p}} = 0.002 = 0.2\%$. But other values of strain or other methods and definitions are also used, as illustrated on

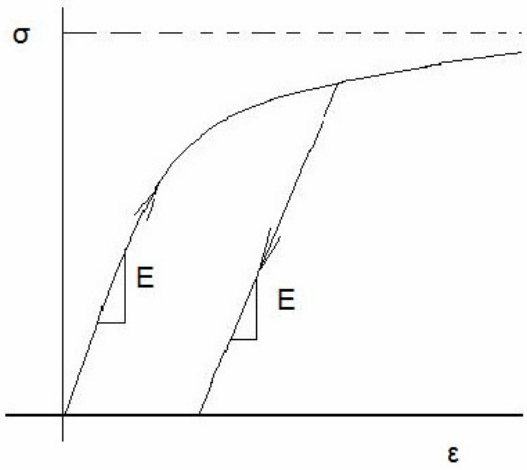

Figure 1 Typical stress-strain relation curve for a metal.

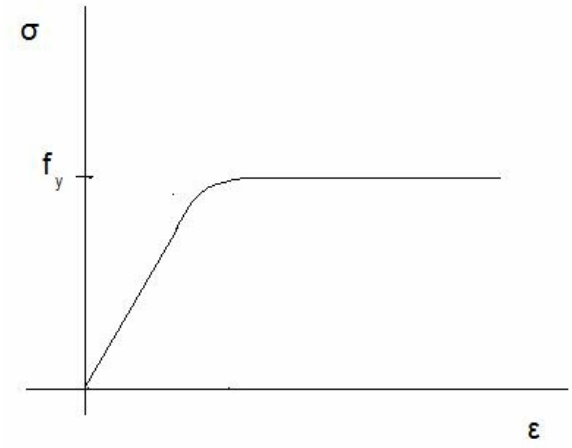

Figure 2. Perfect plasticity curve.

Figure 3. We can base these methods on stresses but also on strains and strain energy. The choice of a method to define a yield stress is mostly arbitrary.

Anyway, we can define a certain value of stress f_y for a material, which corresponds to yield in a uniaxial test and is a characteristic property of a material like e.g. Young's modulus and the bulk modulus.

2.1.2 Yield criteria. Yield surfaces.

In the uniaxial test case yielding starts when the stress value reaches the yield stress. In the general case we have the stress state of a solid defined not by a single value σ, but by a stress tensor $\boldsymbol{\sigma}$. Yielding starts when a combination of components of the stress tensor reaches some value. We need a way to describe this combination and link it to the material properties. The material properties are usually scalar, so let $f(\boldsymbol{\sigma})$ be a scalar valued function of the stress tensor $\boldsymbol{\sigma}$. Then we

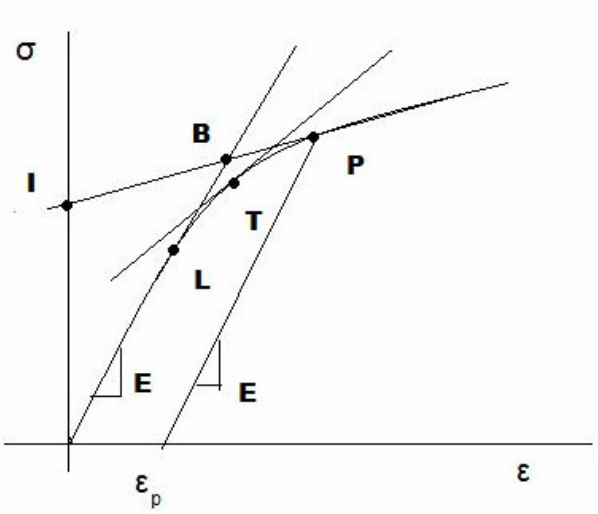

Figure 3. Definitions of yield stress. I – Intercept stress, L-Limit of proportionality, P-Proof stress, T-Tangent stress [2].

can formulate the yield criterion: yielding starts when $f(\boldsymbol{\sigma}) = 0$, if $f(\boldsymbol{\sigma}) < 0$ we have elastic behavior, $f(\boldsymbol{\sigma}) > 0$ is not acceptable.

The function $f(\boldsymbol{\sigma})$ is called the **yield function** for the material. It contains the stress tensor components in some form as arguments and material properties like e.g. uniaxial yield stress or hardening parameters. So the **yield criterion** is expressed mathematically by the yield function. The two most common yield criteria are the von Mises and Tresca criteria [2, 3]. The first one combines the equivalent stress, which is the norm of the stress tensor, and the yield stress in a uniaxial test. It may also be derived from strain energy considerations (yielding starts when the strain energy reaches a certain value). The other one uses the maximum shear stress as a main parameter. But generally we can use other criteria, based on stress or strain or strain energy. For a general material the yield stress is difficult to define as we already said, it is arbitrary, and so is the yield criterion.

In order to obtain useful yield functions some fundamental hypotheses are usually formulated. These hypotheses are based on experiments and experience. For us the most important are the following two:

1. The yield function is symmetric with respect to reversing of the stresses. $\mathrm{f}(-\boldsymbol{\sigma}) = \mathrm{f}(\boldsymbol{\sigma})$ It is analogous to similarity of tension and compression curves for the uniaxial test.

2. Isotropic states of stress or superposition of isotropic stress on states of stress corresponding to elastic response do not lead to yielding. The consequence of this is that we may assume that only the deviatoric part of the stress tensor appears in the yield function.

The deviatoric and isotropic parts of stress tensor are basic concepts in continuum mechanics. Here we'll just say that any stress tensor $\boldsymbol{\sigma}$ can be represented as a superposition of two parts

$$\boldsymbol{\sigma} = \boldsymbol{\sigma}^0 + \boldsymbol{\sigma}' \tag{1}$$

where $\boldsymbol{\sigma}^0$ is the isotropic part:

$$\boldsymbol{\sigma}^0 = \frac{1}{3} tr(\boldsymbol{\sigma})\mathbf{I} \tag{2}$$

and $\boldsymbol{\sigma}'$ is the deviatoric part:

$$\boldsymbol{\sigma}' = \boldsymbol{\sigma} - \boldsymbol{\sigma}^0 \tag{3}$$

where $\mathbf{I}$ is a unit matrix. So we can say that $f(\boldsymbol{\sigma}) = f(\boldsymbol{\sigma}')$.We should mention that for $\boldsymbol{\sigma}^0$, $\sigma_{11} = \sigma_{22} = \sigma_{33}$, and for $\boldsymbol{\sigma}'$ we have $\sigma_{11} + \sigma_{22} + \sigma_{33} = 0$. The second hypothesis has an important consequence. All the volume changes in the material when it is deformed are due to the isotropic components of the strain and consequently the stress. So the deviatoric component can not change the volume of a body. It means that plastic deformations are **isochoric** in nature – they occur without change of volume [2, 3].

As the yield function is most often some continuous function of stress, it may be represented graphically as a surface in a stress space. This surface is called a **yield surface**. When the stress state, represented as a vector in stress space, lies inside the surface, we have elastic behaviour, when it reaches the surface, it becomes plastic. Hardening means that the surface moves from its original position. The yield surface can be obtained for any space with independent stress components ($(\sigma_x, \sigma_y, \tau_{xy})$, $(\sigma_1, \sigma_2, \sigma_3)$ etc.) as base vectors. A general stress tensor has 6 independent components, but if we use the deviatoric nature of plasticity we can see that the three components of stress tensor lying on the main diagonal of the stress tensor are connected and the total number of independent components is 5. So in general the yield surface is a hypersurface in a 5-dimensional space. The form of this surface may vary, depending on the material properties and the stress space which we use (or which projection of 5D hypersurface on a 3D or 2D space is used), but it always reflects the basic properties of the material and plasticity. The simplest yield surface for an isotropic solid, the von Mises yield function, is shown in Figure 4. The second hypothesis means that the isotropic stress (which is corresponding to the line in the principal stress space, defined by the vector $\mathbf{e} = [1,1,1]$) does not influence the yield surface, so this surface must be cylindrical in form with the $\mathbf{e}$ vector as its axis. The plane $\sigma_1 + \sigma_2 + \sigma_3 = 0$ is called the deviatoric plane or π-plane, because all points lying on it correspond to pure deviatoric states of stress. The curve formed by the intersection between the yield surface and the deviatoric plane is a circle for the von Mises criterion (which reflects the isotropy of the material) and a central-symmetric polygon for the Tresca criterion, which also represents the difference in these yield functions [3].

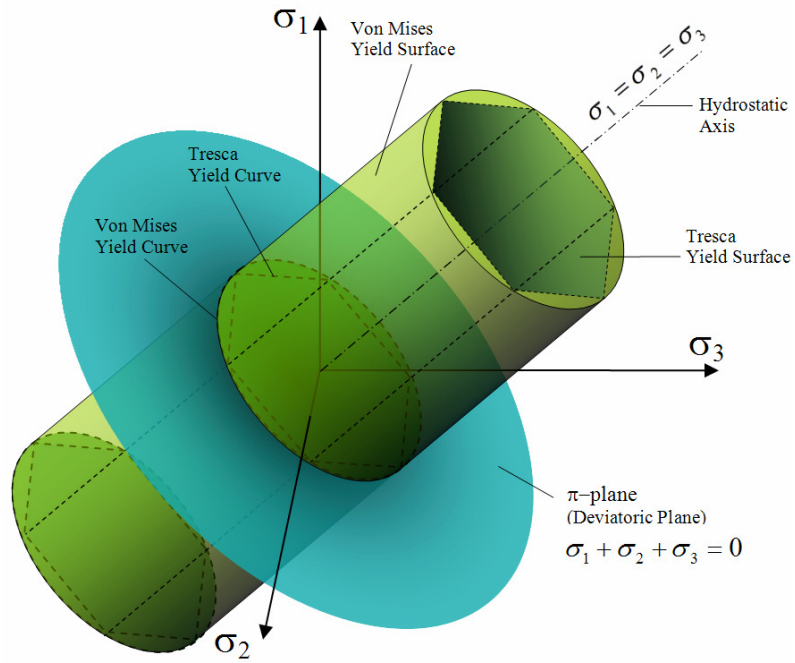

Figure 4. Von Mises and Tresca yield surface [11].

If the solid has some anisotropy in its properties, then the symmetry will be violated in the yield surface too, and the curve will distort in the appropriate direction. So the yield surface is a handy tool for representing material properties and limits of elasticity for a given material (it should be noted that it is generally impossible to represent an anisotropic yield surface in the principal stress space like the one in Figure 4 so other stress space could be used).

2.2 Crystals and Polycrystals.

2.2.1 Single crystals. Basic definitions. Anisotropy and symmetry.

A crystal or crystalline solid is a solid material, whose constituent atoms, molecules, or ions are arranged in an orderly repeating pattern extending in all three spatial dimensions. Most commonly used manmade materials and naturally occurring substances (as well as aluminium which is a subject of this work) are aggregates of crystals or polycrystals. Many important properties which differentiate crystals from non-crystallic materials are due to their ordered structure and can be predicted or derived from it. Two important properties that are particular for the crystals are anisotropy and symmetry.

A material property is **isotropic** when it is the same if measured along any direction in a sample, it does not depend on how sample is 'turned'; it is **anisotropic** when it varies with different orientations of the sample in some reference coordinate system. Anisotropy of a property in a sample (macrolevel) appears as a result of anisotropy in the microstructure of the sample (microlevel). Property in this context means a relation between a macroscopic influence on the sample and its macroscopic response (for example the elastic modulus).

The structure of crystals can be idealized into having translation symmetry at the atomic level. The constituent atoms of the crystal may be grouped in different ways, but on one or another scale these groups will be repeated again and again in a global orderly 3 dimensional structure called **lattice** [4]. Real materials differ from idealized ones by having 'lattice defects' which are errors in this repeating order (such as vacancies, dislocations, stacking faults [5] etc, some of them also define macroscopic properties and will be discussed further) and by being finite in extent (having surfaces and interfaces). Nevertheless the symmetry properties of crystals are predominantly determined by the symmetry of the lattice and the symmetry of the groups of atoms that are repeated in the lattice.

A lattice may be described by a **unit cell** which is the smallest part of the lattice which still has the same properties (symmetries) as the whole lattice. The arrangements of atoms in the unit cell which are most common are shown in Figure 5. Aluminium has face-centred cubic cell structure (FCC). The symmetries of aluminium single crystal properties are the same as symmetries of its FCC unit cell.

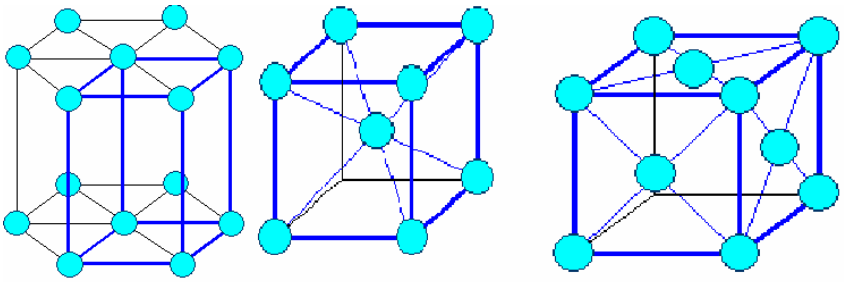

Figure 5. Hexagonal, body centred cubic and face centred cubic cell.

To describe the properties and processes in single crystals we need a way to define planes and directions in some reference frame connected to the crystal. The symmetry axes of the unit cell are a natural choice for the axes of this reference frame. They are connected to the structure of the crystal and are parallel for the whole lattice of the crystal. To define a direction in this reference frame so called **Miller indices** are used. Within a crystal frame, it is possible to describe lattice directions and lattice planes by integer indices. The definitions of these indices may be found in [4]. To denote that it is the direction which we describe the indices are taken into brackets [uvw]. To denote that we describe a plane they are taken in parentheses (hkl). The notation {hkl} denotes the set of all planes that are equivalent to (hkl) by the symmetry of the lattice.The notation <uvw> denotes the set of all directions that are equivalent to [uvw] by symmetry (Figure 6).

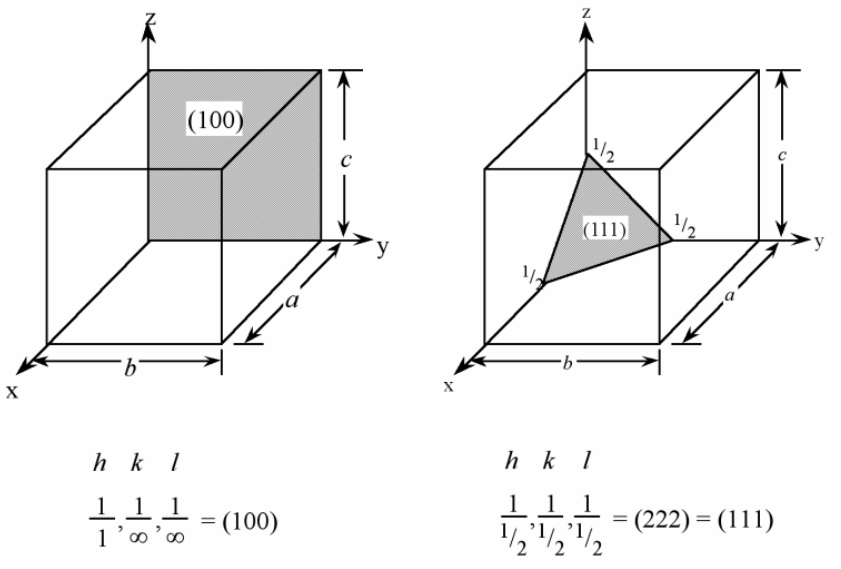

Figure 6. Miller indices [4].

2.2.2 Polycrystals. Texture.

Polycrystal is a solid that consists of many crystals (crystallites or grains). The properties of a polycrystal are defined by both properties of grains and their interaction. Each grain of polycrystal has its own orientation of lattice, so called crystallographic orientation (the spatial rotation of the crystallographic reference compared to the macroscopic reference of the specimen); an important concept here is the grain boundary, which is the border between two or more grains. The strain compatibility and stress equilibrium on the boundaries and their role in plasticity will be discussed later.

The properties of single crystals are direction-dependent (anisotropic), so the properties of a polycrystal must be largely dependent on the orientations of its grains relative to its global reference frame. This orientation can be random but in many cases the research shows that a bigger part of grains have orientations around some distinct values. The non-random distribution of crystallographic orientations is called **texture**.

We speak about texture when this distribution shows some preferred orientations, if this distribution is even and random it is said that the polycrystal has no texture. It can be easily seen that a material with texture will show some degree of anisotropy, because it will have some directions that are distinct from all others, and vice versa the polycrystal without texture will be isotropic. Texture also reflects the symmetry of the solid (sample). The number of

grains in real crystal is always finite, so the symmetry in a sample is always statistical in nature, unlike the single crystals where lattice is truly symmetric.

Some textures can be described very well by '**components**', which are a superposition of a small number of orientations with some spread around them (which may be quantified by a Gaussian distribution). Others can be well represented as fibers in orientation space (see next chapter) in which a single angle can be used to specify an orientation within the fiber [4].

The textures usually form as a result of some physical process or the treatment of metals. The textures in metallic materials are traditionally divided into deformation textures and annealing or recrystallizaion textures [4]. For example when sheet metal is produced by rolling, the grains in the treated piece of metal tend to rotate near particular orientations which differ according to microstructural features other than crystallography. The textures that develop in process of rolling are not the same in two metals even if they have the same FCC crystal lattice. The result is more depending on materials parameters (stacking fault energy, solute content [5]). In aluminium alloys, the texture tends to develop around the particular components, so called copper, brass and S texture components. Then the texture of the rolled material can be represented by some of these components in varying amount together with some amount of randomly distributed grains. In real material there is also always a certain distribution of orientation of the grains around these ideal components.

After annealing the material does not lose all texture as could be expected (because new grains are formed), but some textures particular for this process appear in the material. These new recrystallization textures depend on the starting texture and also on the kinetics of the recrystallization process, like annealing time, heating and cooling rate and temperature. In aluminium alloys the most frequent recrystallization texture is the cubic texture, the second most frequent is the Goss texture (Table 1).

Texture	Indices	Type
Cu	{112}<11-1>	Rolling
Brass	{110}<1-12>	textures
S	{123}<63-4>	
Cube	{100}<001>	Recrystallization
Goss	{440}<001>	textures

Table 1. Components of textures frequently found in aluminium alloys [6].

It should be mentioned that sometimes a texture is referred to as the texture of a material, not a sample. Some materials might have a characteristic texture which is always present in a sample of representative size.

2.2.3 Representation of directions. Euler angles.

If we need to represent a direction in general (not just within a crystal lattice like in case of Miller indices), the problem is basically the same as describing a unit vector. A unit vector may be described by its coordinates, but in our case it is more convenient to describe a unit vector by the coordinates of the point on the unit sphere where this vector touches the sphere. We can use the reference frame connected to the crystal or to the sample, in this case the reference frame of the sample is often defined by so called normal, transverse and rolling directions (because it was first introduced for analysis of the rolled sheet samples).

If we need to describe the position of a plane (for example the crystallographic plane) then the easy way is to imagine the plane of interest in the center of a unit sphere, then the plane's normal taken in the center of the sphere intersects it at two diametrically opposed points. We may define one of them as positive and negative as it is most convenient. Or if the sign is of no interest we can leave this set of normals unsigned, in this case the unsigned normals are called a **pole**.

So the two numbers that specify the direction are most conveniently chosen as the coordinates on the surface of a sphere; if the normals are unsigned (poles), it is enough to describe their intersection with a hemisphere. Then we may map the points of intersection of these normals with the sphere or hemisphere on two circles or a circle (for hemisphere). Such representation of a distribution of some directional properties (for example the direction of some crystallographic axes) is called a **pole figure**. There are several methods to map the surface of a hemisphere onto a circle for representation purposes [4]. The directions on the pole figure may be represented as discrete points, but then in some cases in high density areas the individual symbols overlap too much and then seem under-represented. More often a continuous distribution of poles is plotted, where the discrete points are assigned with their respective intrinsic weights to small area pieces.

Pole figures represent the directions in the sample reference frame. We can also plot one direction (e.g. tensile axis) in the reference frames connected to each individual grain's lattice. We also get a set of points; each of these points represents the orientation of the tensile axis in a reference frame connected to one grain. This figure is called the **inverse pole figure**. In some cases the inverse pole figure represents important features of a texture that can not be seen on a 'usual' pole figure (for example in samples with fiber symmetry).

There is another way to define the coordinates of a point on a spherical surface (i. e. the direction). We use XYZ for sample axes. We define the North pole as the point of intersection between the Z axis and the sphere. We define the standard meridian as the line of intersection between positive half of XZ plane and the sphere. We then use the pole distance θ and an angle ω from a standard meridian to describe any point on the sphere. We count ω as increasing when we go from positive X to positive Y. Alternatively these angles can be introduced as two rotations: first we rotate by ω clockwise around positive Z, then by θ clockwise around new positive Y. These two angles are the **Euler angles** for locations on the sphere.

In the other case as with the inverse pole figures we may use the crystallographic axes of a crystal for reference and describe for example the tensile axis for the whole sample. Now we define North pole as the intersection between the unit sphere and the positive z axis of the crystal. If we look at the connection between the system (North pole and standard meridian) in the first case and the second we can see that while the angle θ between the z and Z axis is the same and goes from one type of description to another without change, the second angle depends on how the crystal x axis is put, so we use a third angle φ instead of ω (Figure 7). Euler angles are given here as defined in [4]. Other definitions and notations are also used in other sources.

To sum up, for some purposes we just need to specify one direction which is of most importance, either a direction in sample coordinate frame or in the single crystal coordinate frame (inverse system). To specify a direction just two numbers are enough. They are usually the coordinates on the surface of a sphere or the angles. The direction may also have a sign (be a unit vector) or be unsigned (when it is not important if it goes through positive or negative hemisphere). For unsigned direction we use the term 'pole'. The points where poles (or unit vectors) intersect with the hemisphere may be mapped on a circle (or two circles for unit vectors).

2.2.4 Representation of orientations.

What we described in the second example is the direction of the axis (the tensile axis) with respect to a crystallographic coordinate system. Often this is referred to as the 'orientation' of the tensile axis. We shall use the word orientation here only when it is implied that the entire relation between two coordinate frames is to be described (which requires three rather than two numbers). Complete textures are described exactly by a set of complete orientations. Sometimes though, only one direction is enough to give necessary information about texture.

In some simple cases we can describe orientation as a plane and a direction on it using Miller indices. We give a normal to the plane and a line in it. For example if we have a rolling texture, we use the rolling plane and the rolling direction as a reference and describe the texture as {211}<111>, which means that the {211} of the grain crystal plane is parallel to the rolling plane, and the <111> direction is parallel to the rolling direction. For example, the orientations of the mentioned texture components that we observe in aluminium are given in Table 1 taken from [6].

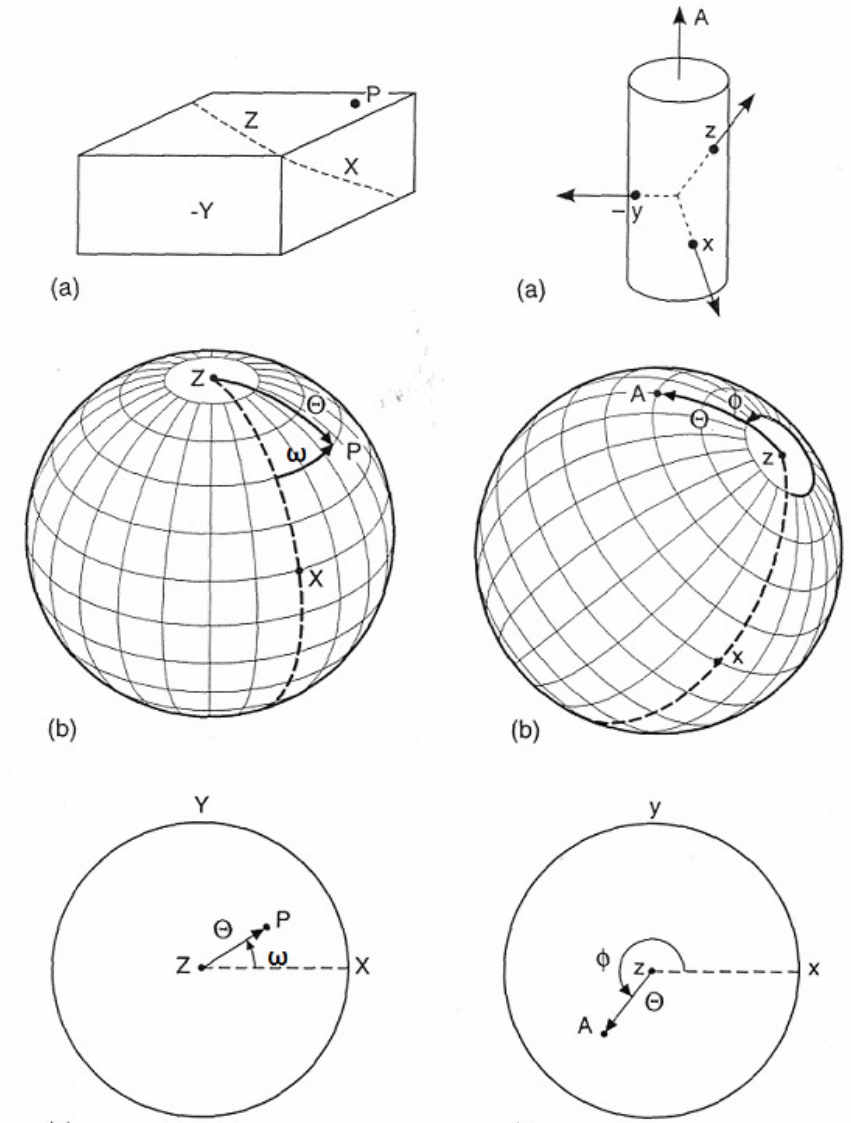

Figure 7. Definition of Euler angles representing directions. Left: direction of a crystal axis in sample system; right: direction of tensile axis in crystal system [4].

In general the relation between two coordinate frames can be represented in various ways. We can express either the axes of the crystal with respect to those of the sample ('crystal orientation') or vice versa ('sample orientation'). These expressions are entirely equivalent. Symmetries also play a major role in descriptions of orientations – sometimes they make the relation between two coordinate frames simpler.

An orientation of some general crystallographic frame can be described by for example three poles or a vector on a surface of a unit sphere, but these will not be discussed here. In case of the FCC crystal lattice of aluminium we have orthogonal coordinate systems of both the crystals and the sample. We can describe the relation (not including translations) between two orthogonal coordinate systems by transforming one into the other by a series of rotations. These rotations can be described by the same Euler angles which we already defined in the previous part. For the case that we also have cubic crystal symmetry and orthotropic sample symmetry, we can also keep all the angles in the range 0^o to 90^o (Figure 8).

A convenient way to represent orientation in a numerical model is to construct the rotation matrix from the Euler angles. This matrix will transform any vector or a coordinate frame from one reference system to another. It may be used for example to find the change of grain orientation after some plastic strain was applied in FEM analysis.

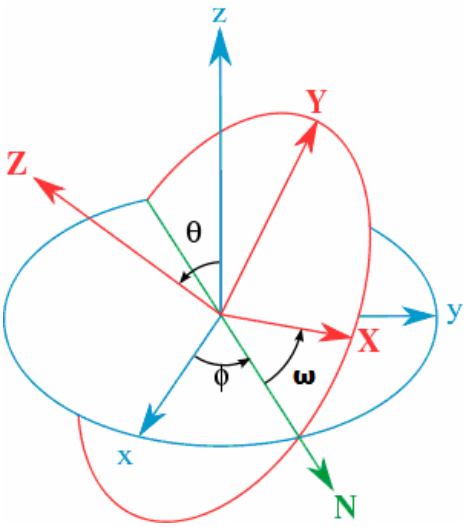

Figure 8. Definition of Euler angles representing orientation [14].

We denote the basis vectors of the global reference system $\mathbf{e}_i$ and the vectors of the reference system of some single crystal as $\mathbf{e}_i^c$. We will use subscript c from here on to denote the variables that relate to single crystals (grains). The relation between these two reference systems may found by using the cosine of angles between each pair of vectors. The relation has the form

$$\mathbf{e}_i = M_{ij}\mathbf{e}_j^c \tag{4}$$

M_{ij} is this rotation matrix for a general transformation. To find the components of $\mathbf{M}$ we can use a series of simple rotations, each by one of Euler angles: $0 \le \phi \le 2\pi$, $0 \le \theta \le \pi$ and $0 \le \omega \le 2\pi$. [1, 4].

2.2.5 Representation of textures.

Now we can describe a texture in our model qualitatively and quantitatively by a distribution of directions (in some simple cases) or orientations (in more general cases). We assume that a large number of individual orientations of the grains are known. We can construct a three dimensional orientation space (three numbers are necessary to define the orientation) then these individual orientations will correspond to a set of points in this space. Another possibility is that one has a continuous distribution of points in the orientation space. This space may be divided in a number of finite cells and to each cell some occupation density will be assigned. A continuous distribution may also be expressed as a number of coefficients of a series expansion. Any of these representations will be referred to as an **orientation distribution function** (ODF) [4, 28].

The orientation of the crystal with respect to the global frame may be defined by the set of Euler angles (ϕ, θ, ω). Then the ODF is defined as the volume fraction of grains oriented along a certain direction $\mathbf{g}$, where $\mathbf{g}$ is taken to denote the set of Euler angles (ϕ, θ, ω), and thus

$$\mathrm{ODF}(\mathbf{g}) = \frac{1}{V}\frac{dV(\mathbf{g})}{d\mathbf{g}} \tag{5}$$

Orientation of single crystals can be determined by various methods such as x-ray diffraction or the electron backscatter diffraction (EBSD) method in the scanning electron microscope (SEM). But the ODF and texture cannot be measured directly by any technique. Traditionally both x-ray diffraction and EBSD may collect pole figures for orientations of a number of grains. Then ODF is derived from these results by a number of methods. They can be classified based on how they represent the ODF. Some represent the ODF as a function, a sum of functions or expand it in a series of harmonic functions. Others, known as discrete methods, divide the orientation space in cells and focus on determining the value of the ODF in each cell [4].

2.3 Single crystal plasticity.

In the previous parts it was discussed how the solids behave plastically, but it was not said why they do it so. Any deformations in solids (and accordingly strains and stresses) mean displacement of atoms or molecules that they consist of, stresses appear because of the forces of interatomic interaction (interatomic bonds). If the distance between the constituent particles varies with the deformation but the atomic bonds remain in the same general state, then the deformations are elastic. If the displacement of the particles leads to some redistribution of the interatomic bonds, then the deformations are plastic. In metallic and other crystalline solids the atoms are positioned in some order in the crystal lattice. Here the plastic deformations mean that atoms that constitute this lattice undergo some redistributions. For example we can consider a plane of atoms in a crystal. If we apply a large enough shear force upon this plane, its bonds with the neighbouring plane will be broken, it will irreversibly 'slip' relative to it, and new bonds will form between the atoms of the planes but now shifted one position relative to the primary configuration. This may explain the plastic incompressibility – the volume changes only when the interatomic distances change, i.e. it is only characteristic for the elastic deformations.

We can use the knowledge about atomic structure of a material for deriving numerical models that will describe its behaviour. This way our models will include the microstructural properties of material, unlike the phenomenological models. We may find the properties of a single crystal of a metal, then find the texture of the sample and couple these two properties together to predict the response of this sample. The obvious simple model that is natural to assume is, as said before, a slip along some plane by breaking the interatomic bonds between two layers of atoms. But this simple model has some serious problems. The interatomic bonds are relatively strong and breaking them all at once so that such slip could occur demands a very big magnitude of shear force. The shear stress computed from this model is tens of thousands times more than the shear stress measured in experiment [5]. This difference exists because of imperfections in the crystal lattice that allow other ways for it to deform rather than simultaneous breaking of a large number of atomic bonds along the slip plane. These imperfections or defects are called dislocations.

2.3.1 Dislocations. Dislocation types.

One important type of defect that can be observed in the crystals is the **edge dislocation**. The defect can be considered to be an additional partial plane of atoms inserted into the upper portion of the crystal and terminating on a {100} plane. Figure 9 shows how the edge dislocation can move by selectively displacing atoms. The shear stress is applied on the top and bottom faces of the crystal in a direction to produce shearing forces in a <100> direction. If one considers the disturbed atomic arrangement at the zone of partial plane termination (called **dislocation core**), it can be seen that there is an atom that is situated at equal distance from two neighbouring atoms, so it is equally attracted to both of them if no external stress is applied. When we apply the external shear stress in the right direction the equilibrium is disturbed and this atom is attracted preferentially to the right neighbour rather than the left one. As a result new interatomic bonds are created, small shift of atoms in the vicinity occurs so that the plane to the right now becomes the partial terminated plane, as shown in part 2 of Figure 9. It may be also seen as shift of the partial plane (and the edge dislocation) to the right, while physically there was almost nothing moving, just some minor rearrangement of atoms. So it is said that the dislocation moves. The dislocation continues to move in the same direction as long as the external shear stress is applied. Naturally, it stops when it reaches the surface (or interface) of the crystal. Then there are no new atoms to rearrange, so the upper half of the crystal becomes shifted relatively to the bottom part as shown in the final part of Figure 9. The crystal becomes deformed. This deformation is irreversible in nature (when dislocation reaches the surface it dissipates and can not shift the crystal back to its former state) which means it is a plastic deformation. Its reason is the dislocation motion.

The plane containing the dislocation is called the **slip plane** and the **slip direction** is the direction of the motion of the dislocation line (and naturally it is the plane along which the crystal irreversibly deforms and the direction in which the crystal is deformed). It is obvious that the stress required to shift equilibrium of forces between the atoms at the dislocation core is much less than the stress required to break all bonds in the plane at once. This small stress that needs to be applied to the dislocation to move it is called frictional stress (Peierls stress) [5].

The stress found from dislocation model is much closer to the real values than the stress we found from “breaking all bonds” model. The dislocations and their evolutions were observed

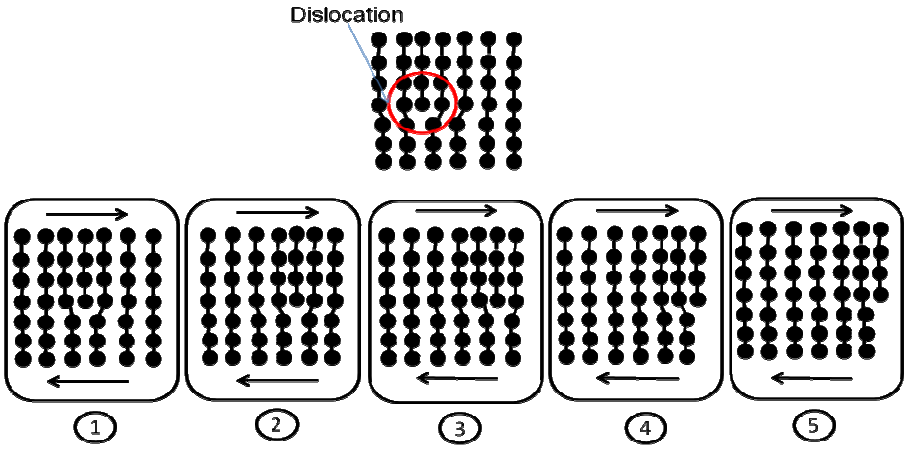

Figure 9. Deformation of a crystal by a consecutive displacement of a dislocation [1].

in real samples, so dislocation model is a commonly accepted one [5, 2]. The dislocation is a line defect, the length of partial plane is much more than distances at the dislocation core.

To describe the dislocation a so called **Burger vector b** is used. It is derived from Burger circuit (Figure 10). Its magnitude is equal to the permanent offset that half of the crystal gets as a result of this dislocations motion. Its direction is the slip direction. Thus for the edge dislocation the slip plane contains both **b** and the dislocation line.

Another basic type of dislocation is the **screw dislocation**. While the edge dislocation is moving by 'linear' way, the screw dislocation is an 'angular' type. The arrangement of atoms at the screw dislocation core is shown in Figure 11.

As we can see it is also a line defect with length much larger than width. Slip occurs if the top and bottom of the crystal are subjected to the shear stress. The basic mechanism of screw dislocation is the same as for edge type – minor atomic rearrangements lead to movement of dislocation until it reaches the surface of the crystal. The word 'screw' is derived from the helical nature of the atomic structure in the volume around the dislocation core. The Burgers vector for a screw dislocation can be obtained by taking a Burgers circuit in a way similar to the edge dislocation circuit (Figure 10). It is also parallel to the slip direction and has length equal to the fundamental slip distance. For the screw dislocation the direction of the dislocation line motion is normal to the direction of the applied stress. The Burgers vector for the screw dislocation is, unlike the edge dislocation, parallel to the line and thus this vector and dislocation line do not define a unique slip plane and the dislocation can change slip plane ('cross-slip') [5].

These two basic types of dislocations are mostly an abstraction. In real crystals the dislocations are usually a combination of both types. The Burgers vector of such dislocation makes an angle between 0 and 90^{o} to the dislocation line and defines the slip direction.

The energy of dislocation is proportional to the square of its Burgers vector [5] and we have the general principle of minimum potential energy, so it is natural, that dislocations with the smallest energy, i.e. the smallest Burgers vectors and consequently the smallest interatomic distance, are most frequently observed. Dislocations with larger slip distances are energetically unfavourable in comparison to those with the minimum possible value of **b**. Thus slip directions are usually the directions where atoms are 'packed' most closely. Additionally, the frictional stress necessary for dislocation motion is minimized when the interatomic spacing between glide planes is greatest – it is easier to break and restore the bond between atoms at larger distance than between the closer ones. So slip on a close-packed atomic plane is favoured. The number of close-packed atomic planes in the crystal lattice or a

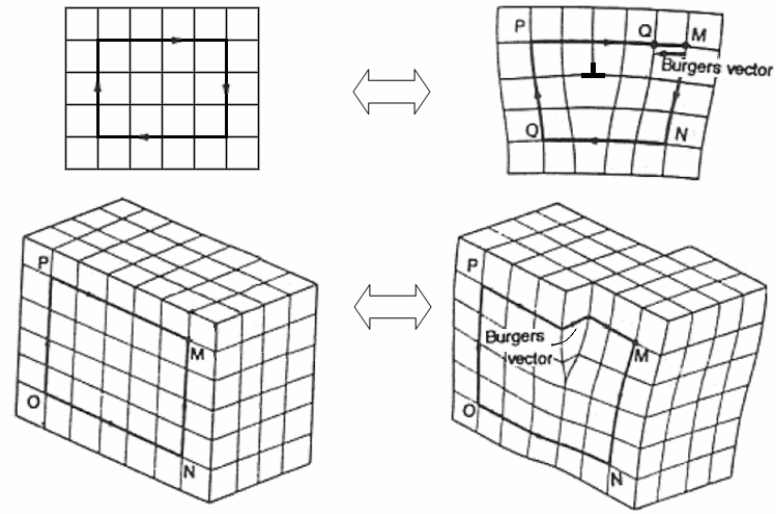

Figure 10. Burgers vector. Edge dislocation (upper) and screw dislocation (lower) [12].

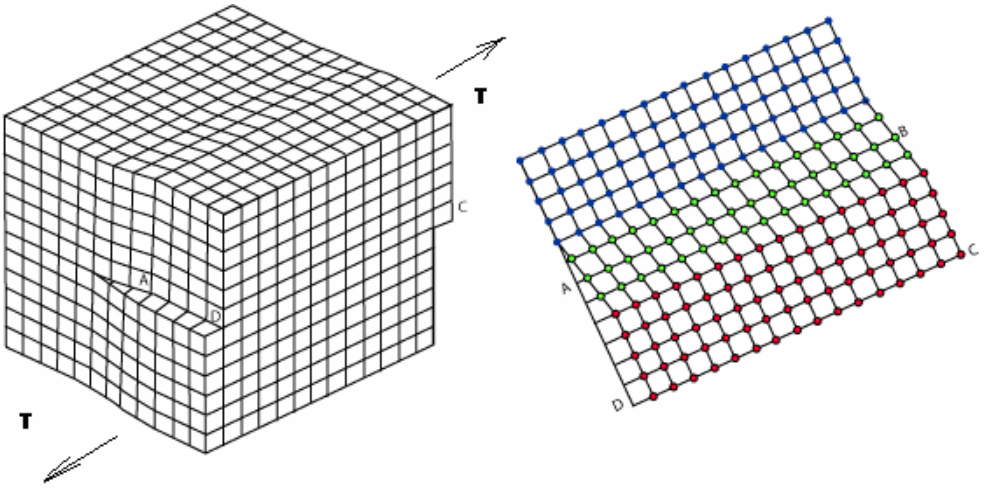

Figure 11. Screw dislocation [13].

unit cell is determined by the arrangement of atoms, so for a given type of lattice and consequently for a given material or a group of materials we have the same slip planes and directions. We call the combination of a slip plane and a slip direction a **slip system**. For example in our case (aluminium FCC lattice) the {111} family of planes are the primary slip planes. The slip directions are the directions which are members of the <110> family.

2.3.2 Resolved shear stress. Schmid's law.

The previous part showed that the physical microstructure of crystalline materials is the reason for existence of specific slip planes and slip directions that coincide with the planes and directions of highest density of atomic packing. Each type of lattice has a specific number of geometrically distinct slip systems (Table 2). There are, for instance, 12 slip systems in FCC materials and as many as 48 in BCC materials. Plastic deformations are realized through the movement of dislocations and, as a consequence, displacement in the sample along the

slip planes in the slip directions. Usually the crystals are subjected not to the shear stress in a slip system but to a more general case of tensile or compressive stress. Plastic flow in these crystals is accomplished also by slip in the slip systems. In some systems slip does not occur, we say that these systems are not **activated**. Whether the system will be activated may be determined in a way similar to the example in Figure 12. For simplicity in this figure we consider only one of the potential slip systems in a sample subjected to an applied tensile force F. The transverse cross sectional area of the crystal is A_0 and the tensile stress is then found as $\sigma = F / A_0$. It follows from the geometry of the system, that shear stress is always smaller than the tensile stress. The angle between normal to the slip plane and tensile direction is φ and angle between the slip direction and tensile axis is λ. It should be noted that in general $\varphi+\lambda \neq 90^o$, i. e. the three directions (tensile axis, slip plane normal and slip direction) are not coplanar. The projection of force on the slip direction is equal to $F\cos\lambda$. As can be seen the slip plane area, A_S is greater than A_0 and the areas are related by $A_S = A_0 / \cos\varphi$. Then shear stress acting on the slip plane in slip direction can be found as

$$\tau_S = \frac{F}{A_0}\cos\phi\cos\lambda = \frac{\sigma}{m} \tag{6}$$

This stress is called the **resolved shear stress**. m is the orientation factor.

Alternatively, let $\mathbf{n}^\alpha$ and $\mathbf{m}^\alpha$ represent the orthonormal vectors defining the normal to the

Slip planes	Slip directions					
	[011]	[0$\bar{1}$1]	[101]	[$\bar{1}$01]	[$\bar{1}$10]	[110]
($\bar{1}$11)		A_2	A_3			A_6
(111)		B_2		B_4	B_5	
($\bar{1}\bar{1}$1)	C_1		C_3		C_5	
(1$\bar{1}$1)	D_1			D_4		D_6

Table 2 Slip systems in FCC materials [18]

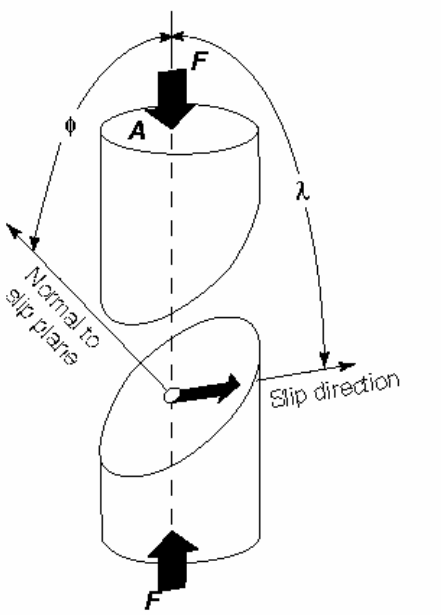

Figure 12. Resolved shear stress [5].

slip plane and the slip direction, respectively, for slip system α, where $\alpha = 1, 2, \ldots n_S$ and n_S is the total number of slip systems that may be activated in the material. The resolved shear stress is then equivalent to the traction force acting in the slip plane along the slip direction. Then we can find it as the projection of the traction force on the slip direction; the traction force in turn is found from the stress tensor and the normal to the slip plane (by definition of the Cauchy stress)

$$\tau_S^{\alpha} = t_i m_i^{(\alpha)} = n_i^{(\alpha)} \sigma_{ij} m_j^{(\alpha)} \tag{7}$$

If we have a randomly oriented crystal, each of the slip systems will have its own orientation and consequently its own resolved shear stress. Some of them will be larger than the others - in this case we speak about favoured orientations. It is natural to expect that slip (and plastic deformation) will initiate in these favoured systems. It should be noted that the value of stress normal to the slip plane has no influence on slip.

Since slip in different slip systems is occurring by the same physical mechanism it is reasonable to assume that to initiate slip the resolved shear stress must reach some certain value which is characteristic for material. We can denote this property τ_{CS} (**critical resolved shear stress**). Its relation to the yield stress may be found from the same geometrical considerations:

$$f_y = m\tau_{CS} \tag{8}$$

The equation (8) is also known as **Schmid's law** [16]. It can alternatively be expressed as: slip occurs at slip system α as soon as $\left|\tau_S^{(\alpha)}\right|$ reaches the critical value $\tau_{CS}^{(\alpha)}$, i.e.

$$\left|\tau_S^{(\alpha)}\right| = \tau_{CS}^{(\alpha)} \tag{9}$$

The Schmid's law has been verified experimentally. A series of tensile tests of single crystal sample was performed. Samples had different orientations of crystallographic axes. Different values of yield stress were measured for each sample. However when they were divided by appropriate values of orientation cosines, it was found that the value of τ_{CS} is invariant for a given material. It was also found that this value depends on the physical conditions of the

experiment that affect the dislocation motion in the crystal lattice such as strain rate and temperature, as well as dislocation density and material purity [5].

The **resolved shear strain** (or glide strain or slip strain) γ corresponding to resolved shear stress is a convenient measure of deformation in crystal plasticity. The plastic spin and plastic strain rate tensors for a slip on several slip systems are found similarly to the stress by summation of slip strain on the appropriate systems multiplied by a combination of orientation factors [7]

$$\dot{\varepsilon}_{ij}^{p} = \sum_{\alpha=1}^{n_s} \frac{\dot{\gamma}^{(\alpha)}}{2}\left(m_i^{(\alpha)} n_j^{(\alpha)} + m_j^{(\alpha)} n_i^{(\alpha)}\right), \quad \dot{\omega}_{ij}^{p} = \sum_{\alpha=1}^{n_s} \frac{\dot{\gamma}^{(\alpha)}}{2}\left(m_i^{(\alpha)} n_j^{(\alpha)} - m_j^{(\alpha)} n_i^{(\alpha)}\right) \tag{10}$$

So if we know all orientations of slip systems then we may find all strain rates and rotation rates in the point from the shear strains on these systems.

2.3.3 Yield surface of a single crystal.

Schmid's law postulated that plastic slip (i.e. plastic deformation in a solid) starts when the resolved shear stress in the slip system reaches its critical value.

First, we will assume that plastic behaviour of a crystal is independent of the strain rate (rate-independent). We may also assume that the crystal has some straining history and that the critical resolved shear stress shows some hardening behaviour (it was never postulated that we have perfect plastic behaviour in slip, on the contrary, the interaction between the dislocations leads to hardening). It means that in general each slip system will have its own strain history and its own critical resolved shear stress. Then we can formulate the following yield function for a single crystal

$$f^{(\alpha)} = \left| n_i^{(\alpha)} \sigma_{ij} m_j^{(\alpha)} \right| - \tau_{cs}^{(\alpha)} = 0, \quad \alpha = 1, 2, ..., n_s \tag{11}$$

This is a set of n_s equations. If $f^{(\alpha)} < 0$ for a given slip system α then the system is not activated, $f^{(\alpha)} > 0$ is inadmissible [1].

Instead of n_i and m_j we can also define a transformation matrix m_{ij} which is called Schmid's factor (or Schmid's matrix).

The yield function may also be represented as a yield surface. As already mentioned it is in general a 5 dimensional surface (in space having 5 independent stress components as base vectors). The form of the yield surface is defined by the yield function, so in this case it is a polyhedron with flat surfaces (hyperplanes). Each hyperplane corresponds to slip in a slip system (when stress vector touches this surface). Two surfaces intersect at edges and several surfaces intersect at the vertices. If the stress vector lies on the edge it corresponds to the slip in two systems. In case of simultaneous slip in several systems at once (just several discrete directions of stress vector correspond to them) the vector is lying in the vertex. We can project this hyper-polyhedron onto a space with fewer dimensions, like for example in this work we use the three independent components of the plane stress tensor; anyway it remains a polyhedron (or a polygon if projected on the plane) [4].

The yield function is basically a scalar field in the stress space and the yield surface is one of its isosurfaces (corresponding to value of yield function equal to zero). The gradients of a function will be normal to the isosurfaces by definition and consequently the gradient of yield function will be normal to the yield surface. The strain rate (which lies in the straining direction) is proportional to the gradient of yield function, or in other words it is normal to the yield surface. Figure 13 illustrates the cases of single and double slip. Here $f^{(\alpha_1)}$ and $f^{(\alpha_2)}$ are the yield functions for the slip systems α_1 and α_2. The strain rate increment $d\varepsilon_{ij}^{p} = d\dot{\varepsilon}_{ij}^{p} dt$

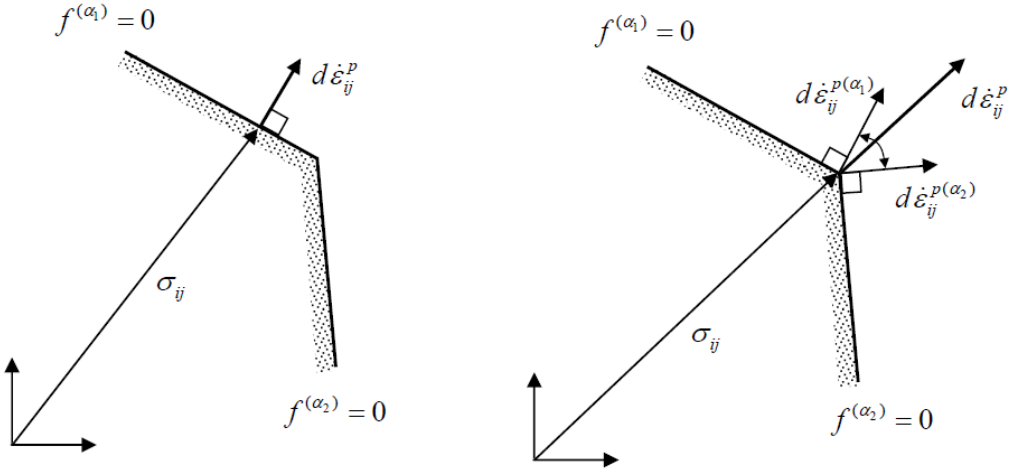

Figure 13. Yield surface with vertex and single slip (left) and double slip [4].

has the same direction as the strain rate and is normal to the hyperplane. When the stress touches the intersection the strain increment becomes undefined. The cone of normals bounded by strain increments of intersecting planes is shown.[1].

These properties of the single crystal yield surface lead to a problem. The faces of polyhedron correspond only to several discrete straining directions, so any straining may be found in the continuous spectrums of strainings connected to the vertices. But the same straining direction may be found in two or more different vertices and consequently correspond to two or more different stresses. Bishop and Hill (1951) [17, 22] suggested a method that made finding the right values of stress for the given straining directions algorithmically easy. It is called the **principle of maximum plastic work**. We assume that we know several stresses $\sigma*$, each of them lies in the vertex and may correspond to the given straining direction. Then the correct stress is the one that maximizes the plastic work done over the given strain increment

$$(\sigma_{ij}-\sigma_{ij}^{*})\dot{\varepsilon}_{ij}^{p}\geq 0 \tag{12}$$

In other words, one straining direction may be realized through slip on different combinations of slip systems. So we may formulate the principle in another way, so that it will allow us to choose the correct combination of slip systems that corresponds to a given straining rate. Let the plastic strain rate $\dot{\varepsilon}_{ij}^{p}$ be prescribed; we assume that an unknown stress σ_{ij} produces this strain rate by a set of shear strain rates (slip rates) on individual slip systems $\dot{\gamma}^{(\alpha)}$. In any crystal there always exist several sets of slip rates that give the same strain rate. We denote another, kinematically equivalent set of slip rates $\dot{\gamma}_{*}^{(\alpha)}$(it is not necessarily so that this set of slip rates may be achieved with the stress, fulfilling yield condition, it is just that they are possible kinematically). Then the **complementary minimum principle** helps to choose the physically correct system [1, 7]. It says that the plastic power expended by the physically possible slip rates producing a given plastic strain rate is less than that for a set of slip rates which is only kinematically possible:

$$\sum_{\alpha=1}^{n_s} |\dot{\gamma}^{(\alpha)}| \le \sum_{\alpha=1}^{n_s} |\dot{\gamma}_*^{(\alpha)}| \tag{13}$$

2.3.4 Work-hardening. Latent hardening. Voce law.

Taylor and Elam (1923) (after them Khan and Huang, 1995) [7, 15] draw the following two conclusions from experiment observations.
1. Slip systems are hardened by slip on other systems (whether they themselves are active or not). This hardening is called **latent hardening** to distinguish from the **self-hardening**.
2. The latent hardening rate is at least comparable in magnitude to the self-hardening rate, i.e. the hardening of the active system by slip on itself.

We can use a form of 'Voce law' (which assumes exponential behaviour of stress-strain curve at plasticity) together with latent hardening matrix in one model [19, 20, 21]. Other models were also developed, but this one is implemented in the numerical simulation [7]. Let the accumulated plastic shear strain be denoted Γ and its rate of change defined by

$$\dot{\Gamma} = \sum_{\alpha=1}^{n_s} |\dot{\gamma}^{(\alpha)}| \tag{14}$$

We define strain-hardening rate for slip system α as

$$\theta(\Gamma) = \frac{d\tau_{cs}(\Gamma)}{d\Gamma} \tag{15}$$

The work-hardening relation now takes the form

$$\dot{\tau}_{cs}^{(\alpha)} = \theta(\Gamma) \sum_{\beta=1}^{n_s} q_{\alpha\beta} \left|\dot{\gamma}^{(\beta)}\right| \tag{16}$$

where θ defines the hardening rate for a given accumulated plastic strain and $q_{\alpha\beta}$ is the latent hardening matrix:

$$\left[q_{\alpha\beta}\right] = \begin{bmatrix} A & qA & qA & qA \\ qA & A & qA & qA \\ qA & qA & A & qA \\ qA & qA & qA & A \end{bmatrix} \qquad [A] = \begin{bmatrix} 1 & 1 & 1 \\ 1 & 1 & 1 \\ 1 & 1 & 1 \end{bmatrix} \tag{17}$$

The diagonal terms of $q_{\alpha\beta}$ representing self-hardening are all equal to unity, while the off-diagonal terms that represent latent hardening might be unity or somewhat higher, depending on the latent hardening parameter q. The work-hardening rate θ is defined as the derivative with respect to Γ of a hardening curve (critical resolved shear stress as a function of accumulated plastic shear strain) in the form

$$\tau_{cs}(\Gamma) = \tau_0 + \sum_{k=1}^{N} \tau_{sk} \left(1 - \exp\left(-\frac{\theta_k \Gamma}{\tau_{sk}}\right)\right) \tag{18}$$

where τ_0 is the initial critical resolved shear stress, assumed to be the same for all slip systems, θ_k determines the initial hardening rate, and τ_{sk} represents the saturation for the term number k of total N terms. It is seen that (18) is basically an exponential curve and thus represents a form of Voce hardening law with N hardening rates θ_k. θ is then calculated as

$$\theta(\Gamma) = \frac{d\tau_{cs}(\Gamma)}{d\Gamma} = \sum_{k=1}^{N} \theta_k \exp(-\frac{\Gamma}{\Gamma_k^{ch}}) \tag{19}$$

The characteristic shear strain $\Gamma_k^{ch} = \frac{\tau_{sk}}{\theta_k}$ represents the strain scale for the saturation with strain in term number k. We use $N = 2$ in our model.

2.3.4 Rate dependent behaviour.

All of the previous arguments are based on the assumption that parameters of material like flow stress and work hardening do not depend on the plastic strain rate. This assumption makes derivations simpler, but physically that is not the case for most metallic materials. Strain rate affects the behaviour of materials. Physically it is connected to the dislocations movement and interaction [4, 5]. **Rate dependence** varies for different materials and for different temperatures in one material. Usually higher strain rates increase flow stress for the same strains. Rate dependent plasticity of materials is denoted **viscoplasticity**.

To establish a model for viscoplastic behaviour which may be implemented in a numerical model we first make some assumptions. For simplicity we assume that slip rate in a material is defined by the state of the material, i.e. the stress state and the structural parameters. A power law is often used [20, 21, 25]:

$$\dot{\gamma}^{(\alpha)} = \dot{\gamma}_0 \left(\frac{\left| \tau^{(\alpha)} \right|}{\tau_{cs}^{(\alpha)}} \right)^{\frac{1}{m}} \operatorname{sgn}\left(\tau^{(\alpha)} \right) \tag{20}$$

where $\dot{\gamma}_0$ is a reference shearing, m is the instantaneous strain rate sensitivity of the material which reflects its viscoplastic properties (we assume that it is the same for all slip systems), $\tau_{cs}^{(\alpha)}$ is the critical resolved shear stress of slip system α (it represents the properties of the material in form of the hardening law), and the stress state is described by the resolved shear stress $\tau^{(\alpha)}$. In (20) function $\operatorname{sgn}(x)$ denotes the sign of the variable x. It should be mentioned that according to this model slip will occur for all resolved shear stresses different from zero, and, as such, no yield criterion exists. This may seem problematic, but for metals m often takes a relatively high value, so shearing rate becomes negligible when $\left|\tau^{(\alpha)}\right| < \tau_{cs}^{(\alpha)}$ and model gives accurate enough predictions.

2.4 Polycrystal plasticity.

When the properties and relations for single crystals are established, the main question is how to find the properties of the aggregate consisting of these crystals from these known properties of individual crystal. As we already mentioned the properties of a polycrystal are defined not only by the properties of constitutive crystals but also by their interaction on the grain boundaries (interfaces): these interactions require both equilibrium of forces and kinematic compatibility conditions. For our first numerical model we do not model the interactions of large numbers of grains between each other individually (it requires too much computational time) but use some sort of averaging. Also to describe the solid consisting of large number of grains we can use a part of this solid which still has the same properties (texture) as a whole and use this smaller part for calculations. This process of describing a solid as homogeneous on average, consisting of a number of smaller parts each with the same properties as a whole is called **homogenisation**. Homogenization may be numerical (or computational, in FEM) or analytical.

2.4.1 Taylor model.

An example of analytical homogenization is the Taylor model, developed in 1930s [18]. Every material point of a solid is assumed to be composed of a finite number n_g of grains. The set of grains may have a given texture.

Taylor made the following assumptions:

1. The elastic deformations are small compared to the plastic ones.
2. Each grain is subjected to the same homogeneous deformation as the polycrystalline aggregate.
3. The material behaviour is rate independent.
4. All slip systems have the same hardening rate.

The first assumption implies that $\dot{\varepsilon}_{ij} \approx \dot{\varepsilon}_{ij}^{p}$ and $\dot{\omega}_{ij} \approx \dot{\omega}_{ij}^{p}$. It also implies bulk plasticity *slip on many slip systems at once), because single slip plasticity can not guarantee the kinematic compatibility [4]. The second assumption is the main point of Taylor's approach; it is sometimes even called the constant strain approach because of it. It may be written as

$$\left\langle \dot{\varepsilon}_{ij} \right\rangle = \sum_{g=1}^{n_g} f_g \dot{\varepsilon}_{ij}^{g} = \dot{\varepsilon}_{ij}^{g} = \dot{\varepsilon}_{ij} \tag{21}$$

where $\left\langle \dot{\varepsilon}_{ij} \right\rangle$ is the volume averaged strain rate tensor, f_g is the volume fraction of grain g. Naturally $\sum_{g=1}^{n_g} f_g = 1$. $\dot{\varepsilon}_{ij}^{g}$ is the strain rate tensor in individual grains.

The fourth assumption says that $h_{\alpha\beta} = h$. It means that all slip systems harden together and the critical stress at any slip system is the same: $\tau_{cs}^{(\alpha)} = \tau_{cs}$ and thus the active slip systems fulfil the yield condition in the form $f^{(\alpha)} = \left|\tau^{(\alpha)}\right| - \tau_{cs} = 0$. Taylor assumed further that the active slip systems are those that minimize the plastic power. The stresses are found by direct volume averaging. We denote σ_{ij}^{g} the Cauchy stress in grain g (we assume stress constant within the grain). The Cauchy stress at the material point is equal to

$$\left\langle \sigma_{ij} \right\rangle = \sum_{g=1}^{n_g} f_g \sigma_{ij}^{g} \tag{22}$$

It is obvious that stress equilibrium at the grain boundaries may not be ensured if we assume homogeneous strain (although we may account for non-equilibrium by superimposing an elastic stress field on the solid). The other assumption that may be a source of inaccuracy is that stress and strain are assumed constant within the grains and some gradients of it may exist. The Taylor model is also expected to fail when plastic heterogeneity is too great (for example at the presence of strong strain hardening or rate sensitivity [4]). But for a range of materials and strain situations we may use it to derive the properties of an aggregate (like yield surface, strain-stress curve and strain-hardening parameters) from the known or assumed properties of grains and texture. We apply the straining on the sample (which is also the same for all individual grains), use the maximum plastic work rule to find the combination of shear strains that correspond to this straining and then use Schmid's law to find the stresses in individual grains, which are then averaged. The microparameters, such as the position of the slip systems described by the directional cosines, hardening of a single crystal grain and the texture (orientations of individual grains) described by Euler angles are defining the link between the macroscopic strain and stress.

The classical Taylor approach used rate-independent behaviour of individual grains. It is although possible to modify the model and use rate dependent model for single crystals. Then we use the first two hypotheses of the classical model and omit the third and the fourth. Most of the relations are the same as for the rate independent theory. The difference is in the constitutive relation. Also the strain hardening rate is now supposed to be different on different systems. It means that critical stress is now not the same in different systems and τ_{cs} can not be used as it was used in the rate independent Taylor model [1, 7].

2.5 Concluding remarks

As we showed, the microstructure of a crystal – its atomic arrangement (lattice) and defects (dislocations) may be used as a basis for derivation of models that describe the behaviour of this crystal. The Schmid's law defines the connection between stress applied to the single crystal and the resolved shear stresses on slip systems of this crystal. Schmid's factor is also a link between the resolved shear strains and global strains. Texture, which in this work is given as a set of Euler angles, gives the orientations of constituent grains of a polycrystal. We use this geometric description – Schmid's factor and Euler angles – to connect the stresses and strains in polycrystal as a whole with resolved shear stresses and strains in single crystals. This connection helps us to derive the response of the polycrystal when the response of the single crystals is known. Taylor's model makes some assumptions that make this derivation mathematically simple. Then we may try finding properties (yield surfaces) of polycrystals with different textures using this method. To do this we just use different sets of Euler angles corresponding to different textures. This is what we do in the next part of the report.

3. Generating yield surfaces using Taylor model of crystal plasticity.

3.1 Method of yield surface generation.

On the first stage the yield surfaces were generated with the custom software that utilizes Taylor approach directly. The rate dependent model for the single crystal plasticity is implemented, which means that no yield criterion in explicit form is used.

The calculations are performed stepwise in time steps defined in the beginning. The general procedure is the following.

The number of time step is denoted i. The resolved shear stress rate $\dot{\gamma}^i$ is found from equation (20). The plastic component of the global strain rate tensor $\dot{\varepsilon}^i{}_p$ is found from $\dot{\gamma}^i$ and the geometric factors (slip plane orientation, slip direction and Euler angles) by equation (10) and (4). The complementary minimum principle (13) is used to choose the actual slip systems. The total strain rate tensor is given in the beginning of the calculations and according to the Taylor model it is the same for each grain. Then the elastic component of the strain rate tensor for each grain is found as

$$\dot{\boldsymbol{\varepsilon}}_e^i = \dot{\boldsymbol{\varepsilon}}^i - \dot{\boldsymbol{\varepsilon}}_p^i \tag{23}$$

Strain is then found by linear extrapolation:

$$\boldsymbol{\varepsilon}_e^{i+1} = \boldsymbol{\varepsilon}_e^i + \dot{\boldsymbol{\varepsilon}}_e^i \Delta t \tag{24}$$

Stresses in a grain are then found by Hooke's law

$$\boldsymbol{\sigma}^{i+1} = \mathbf{C}\boldsymbol{\varepsilon}_e^{i+1} \tag{25}$$

where $\mathbf{C}$ is the stiffness tensor. Now the stress tensor is used to find and update $\tau^{(\alpha)}$ in (20). $\tau^{(\alpha)}$ is found by the same geometric considerations as in (7). To update $\tau_{cs}^{(\alpha)}$ the hardening law (16) is used. Then

$$\tau_{cs}^{i+1} = \tau_{cs}^i + \dot{\tau}_{cs}^i \Delta t \tag{26}$$

With equation (20) updated $\dot{\gamma}^{i+1}$ is found in the same way and all calculations are performed again. The value of plastic work is controlled at each time step and the calculations stop once it reaches a certain value defined prior to the calculations. Then a certain stress state that corresponds to this value of plastic work is obtained. The total stress is found from (22).

The sample is assumed isotropic with respect to the elastic properties, so the stiffness tensor has three independent components: C_{11} C_{12} and C_{44} [3]. Basic values of these are $C_{11} = 106{,}43$, $C_{12} = 60{,}35$, $C_{44} = 28{,}21$. But the exact values of these are of no big importance in this work. The stress is defined by (16) and (20). (25) just defines the path to this stress. If we choose higher stiffness constants, the yield stress will be reached sooner and the plastic component in the total strain will dominate sooner, but the value of stress will be the same. Because of this the value of the stiffness constants was changed in some simulations to a more convenient one.

The parameters of the viscoplastic model are the reference shear strain rate $\dot{\gamma}_0$ and the instantaneous strain rate sensitivity m. The values used in most of the calculations are $\dot{\gamma}_0 = 0{,}036$ and $m = 0{,}005$. The influence of the strain rate sensitivity on the yield surface was studied separately and showed that it is a good estimate.

The hardening model parameters are the latent hardening parameter q, the initial critical resolved shear stress τ_0, assumed the same for all slip systems. Two terms are used in (18), which gives us four parameters: $\theta_1, \tau_{s1}, \theta_2$ and τ_{s2}. The values used in the calculations are: $q = 1{,}4 \quad \tau_0 = 75{,}4 \quad \theta_1 = 897 \quad \tau_{s1} = 13{,}7 \quad \theta_2 = 205{,}1 \quad \tau_{s2} = 15{,}7$ All values for the model parameters were obtained by fitting the stress-strain curve of a 6063-T6 aluminium sample in uniaxial tension with a corresponding curve generated by this program [26].

The stress tensor that we obtain in the end of the calculations above gives us one point of the yield surface in the stress space that corresponds to a certain point in the strain rate space. This point in the strain rate space is defined by the strain rate tensor that must be input at the start of the calculations. To obtain a number of points with the same value of plastic work that constitutes a cloud of points (that is further called 'the discrete yield surface'), the calculations must be performed many times with an appropriate varying strain rate tensor. This data is available on the CD. Then the discrete yield surface may be interpolated into a continuous surface (we may assume that between the known points of the surface it is continuous and smooth, so that this interpolation is possible). For this interpolation a program written in Matlab is used. It depicts convex smooth surfaces and most polyhedrons, but very sharp edges and regions on the edge of the discrete surface are problematic for it. E. g. Figure 24 has isoline $S_{12} = 0.4$ on the edge of discrete surface so it could not be depicted properly and was not included in the illustration. On Figure 29 and 30 sharp edge is either depicted with irregular line or deleted from the illustration. But in general these problems are rare and do not prevent from understanding the form of the surface. We also do not use the same exact values of ρ as in [6], just some arbitrary values, because they are of no importance for understanding the properties of yield surfaces.

We assumed the plane stress situation, which implies three stress components - σ_{xx}, σ_{yy} and σ_{xy}. The yield surfaces are also projected on the σ_{xx}-σ_{yy}-σ_{xy} space. To provide these the strain rate tensor must take form

$$\begin{bmatrix} \dot{\varepsilon}_{xx} & \dot{\varepsilon}_{xy} & 0 \\ \dot{\varepsilon}_{xy} & \dot{\varepsilon}_{yy} & 0 \\ 0 & 0 & -(\dot{\varepsilon}_{xx} + \dot{\varepsilon}_{yy}) \end{bmatrix}$$

The third diagonal component reflects the plastic incompressibility. But it also means that we get a stress component σ_{zz}. To get rid of it and provide the plane stress state we impose a hydrostatic stress state on our result with component equal to $-\sigma_{zz}$. As we said, only deviatoric stress tensor defines plasticity, so we may well impose a hydrostatic stress on our result and it will not influence the yield surface. This way the plane stress state is more a consequence of how we find the stress tensor.

Different strain rate tensor imposed on the sample in the program are distinguished by the values of ρ and γ. We define them as

$$\rho = \frac{\dot{\varepsilon}_{yy}}{\dot{\varepsilon}_{xx}} \tag{27}$$

$$\gamma = \frac{\dot{\varepsilon}_{xy}}{\dot{\varepsilon}_{xx}} \tag{28}$$

The program varies these parameters in a given range to obtain different straining states. As we can see $\dot{\varepsilon}_{xx}$ remains the same for each state. As the result of running the software we get a number of different combinations of ρ and γ values with the corresponding stress states.

The stresses are normalized with the value of σ_{xx} corresponding to the uniaxial tension situation, the normalized stresses are denoted as S_{11}, S_{22} and S_{12} so the surface always intersects the S_{11} axis at 1. These stress states are then used for interpolating of a continuous surface that is represented by projecting the lines with equal S_{12} on the S_{12}=0 plane. The lines containing the points with equal ρ which are of a certain interest are represented too.

It may be seen that points corresponding to pure shear ($\dot{\varepsilon}_{xx}=0, \dot{\varepsilon}_{yy}=0$) correspond to undefined values of ρ and γ. The values of γ at this part of the surface are quickly going to infinity and values of ρ to the indeterminacy $\frac{0}{0}$, so this point must be calculated separately and the points in its neighbourhood are usually not calculated at all, because of numerical instabilities.

It should be mentioned that this method is different from FEM. The Taylor model allows a great deal of simplifications. The geometry of the sample, its morphology, boundary conditions, all of these is neglected. Homogeneous behaviour throughout the sample is assumed.

3.2 Generating yield surfaces of single crystals.

Generating the yield surfaces of the single crystals with this software has several goals. Firstly these surfaces for the single crystals have certain properties determined by the crystal plasticity theory. These properties were for the most part described in the theoretical foundation chapter. Varying certain parameters of the simulation must lead to the predictable consequences which may be observed on the generated surfaces. All this will partly verify that any results obtained with this software are in accordance with the crystal plasticity model. These surfaces may also have another use. We will be simulating the straining of the strongly textured polycrystals. The textures of these polycrystals are well described by a component with small scatter and a randomly distributed rest of the grain orientations. This one component corresponds to a single orientation of a grain. Building the yield surface of this single grain and comparing it with the polycrystal yield surface may provide some verification/explanation of the latter.

The crystal plasticity, and more specifically Schmid's law (or the viscoelastic constitutive relation), predicts that the yield surface of a single crystal is a polyhedron. In general it is 5-dimensional, but we project it on the plane stress space with three independent components of the stress tensor and get a 3D polyhedron. Figure 15 shows a yield surface generated for a grain with Euler angles (0,0,0). Rotating the grain, i. e. assuming other values of Euler angles, must rotate the 5D polyhedron, changing its projection. Figures 16 and 17 show the surfaces corresponding to Euler angles (0,0,30) and (0,0,45). The symmetric properties of the FCC crystal lattice lead to some rotational symmetries of the yield surface. The surfaces corresponding to the (0,0,60) and (0,0,90) orientations are coinciding with the ones defined by (0,0,30) and (0,0,0). The other property of a single crystal yield surface that may be considered is connected to normality. As we said in the previous chapter, a broad spectrum of stresses correspond to several discrete straining directions (normal to the planes of the polyhedron), while several discrete stresses pointing at the vertices of the polyhedron will be responsible for a broad spectrum of straining directions. But we must also consider the elasticity influence. Any yield surface produced will be the result of some work done by both elastic and plastic stresses. These two have distinctly different connection with the strains. While the plastic stress-strain relation is as described earlier, the elasticity means

proportionality. If we draw each point of the discrete yield surface generated by the simulation in the strain space we will get a pattern where the points cover the area around the origin relatively even, and the points corresponding to the value of ρ =some constant will lie

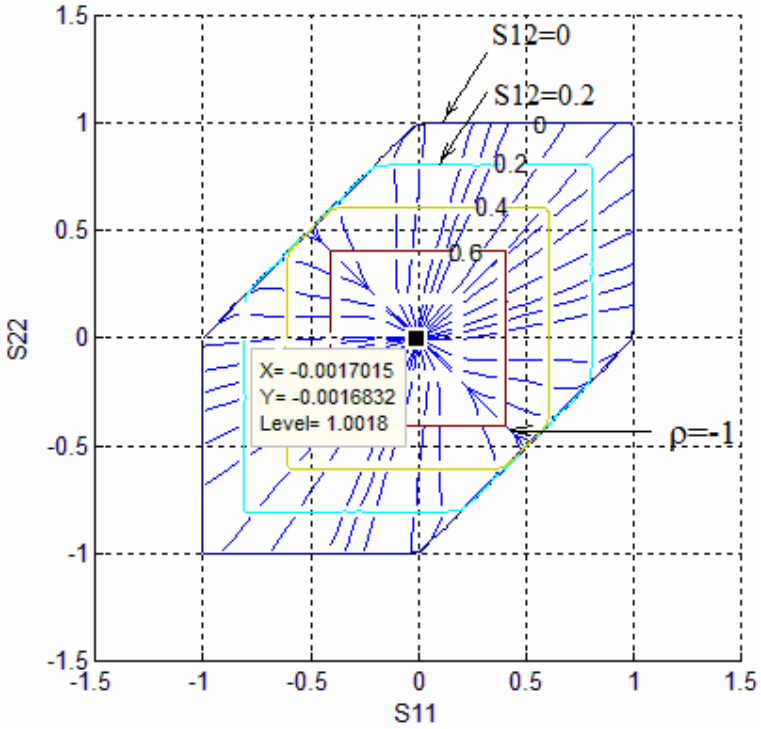

Figure 15. Yield surface of a single crystal with orientation (0,0,0) with lines $\rho = const$.

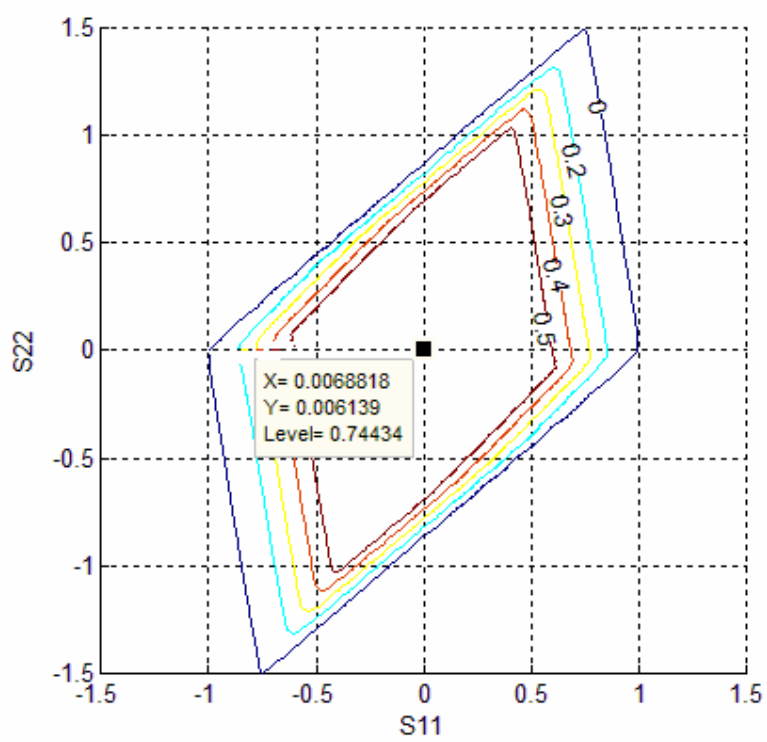

Figure 16. Yield surface of a single crystal with orientation (0,0,30).

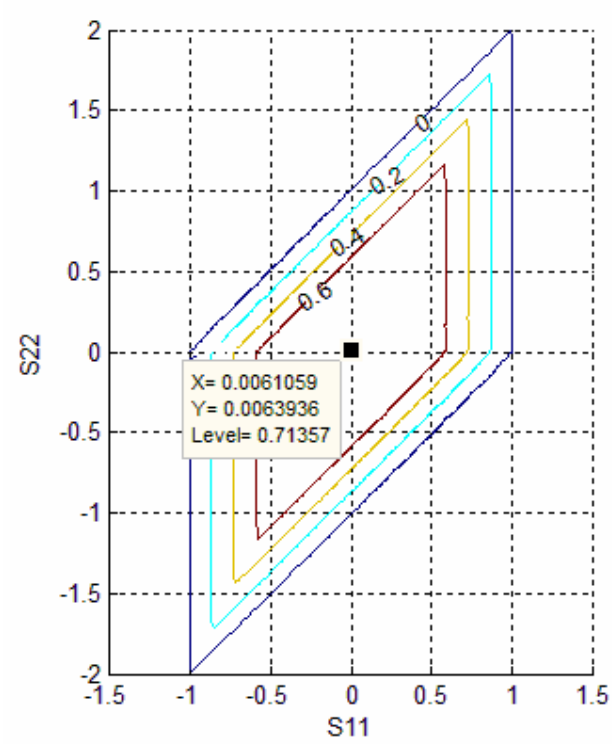

Figure 17. Yield surface of a single crystal with orientation (0,0,45).

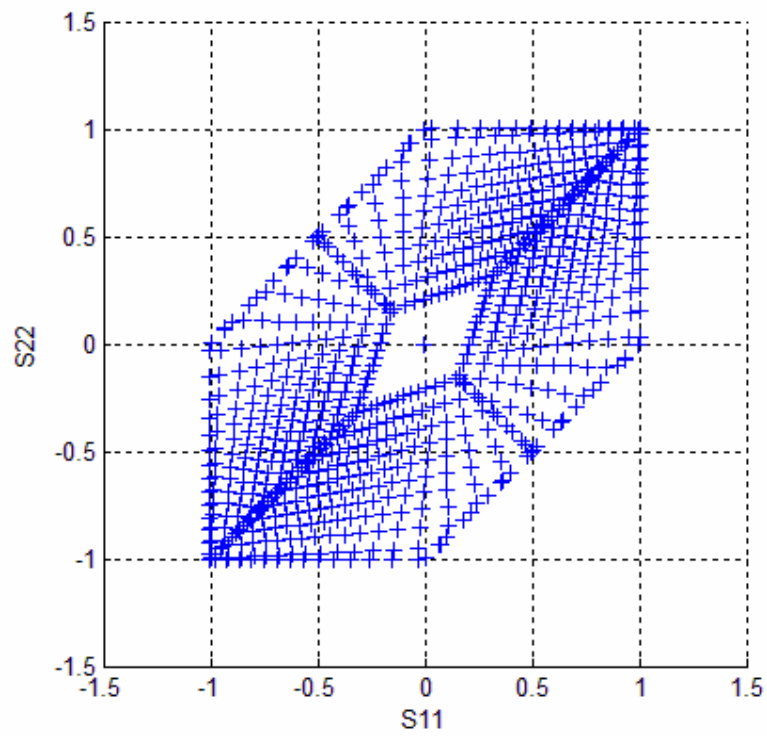

Figure 18. Single crystal (0,0,0). Distribution of stresses corresponding to an even distribution of strain rates at high elasticity.

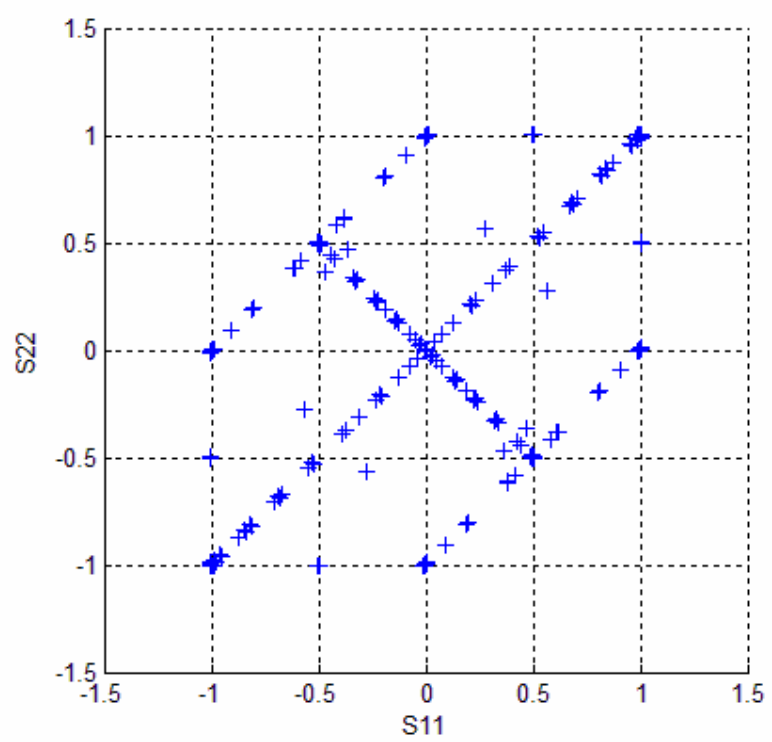

Figure 19. Single crystal (0,0,0). Distribution of stresses corresponding to an even distribution of strain rates at low elasticity.

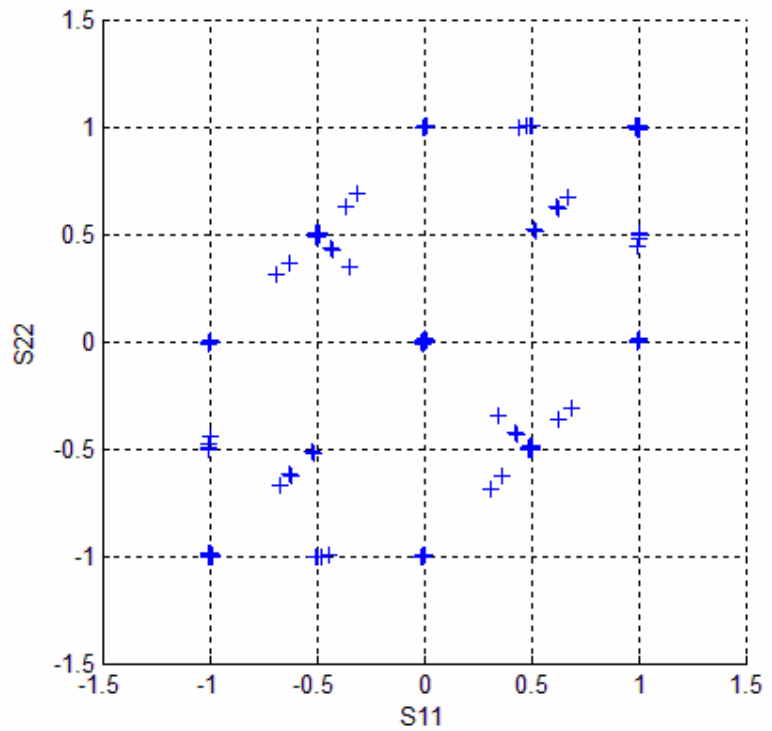

Figure 20. Single crystal (0,0,0). Distribution of stresses corresponding to high plasticity

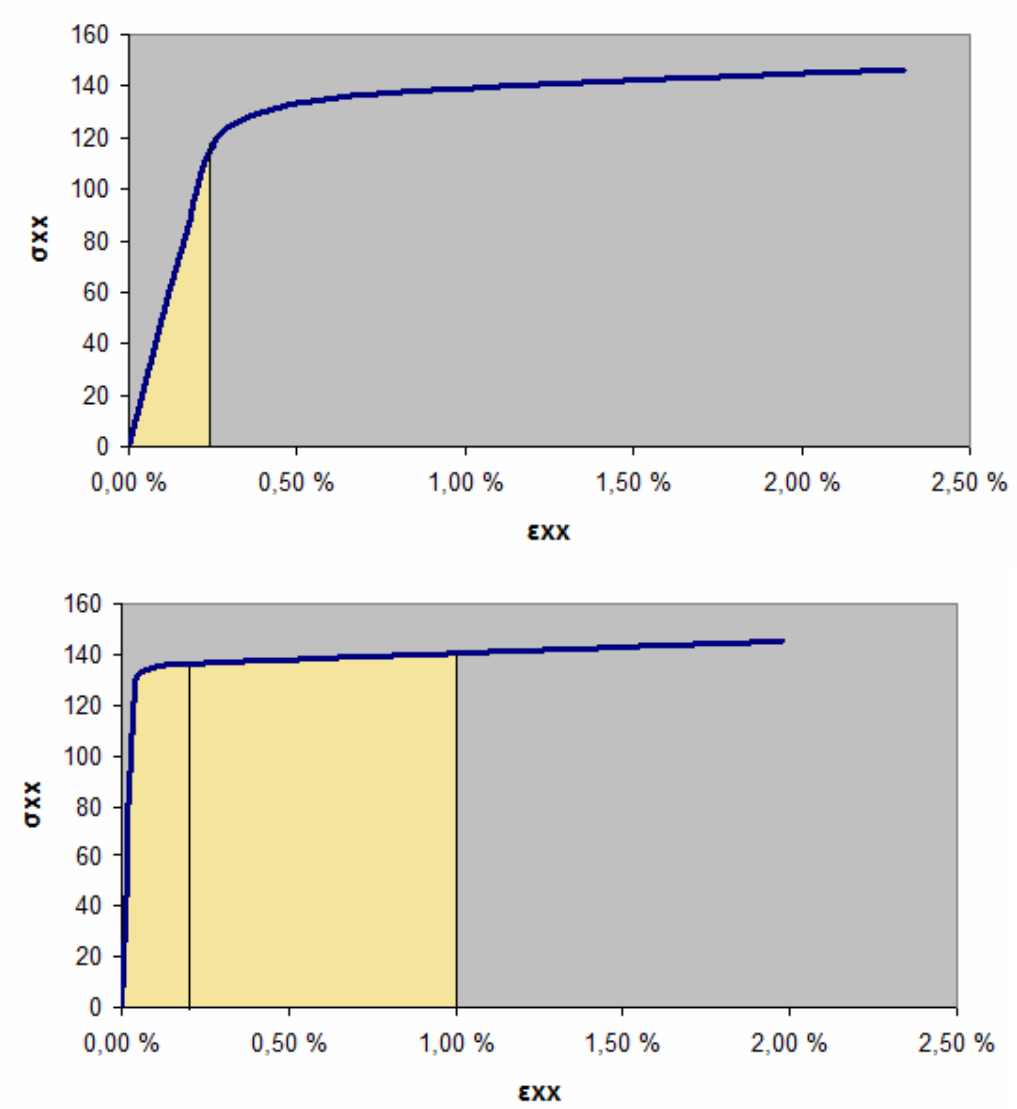

Figure 21. Stress-strain curves for elastic constants multiplied by factor 1 (upper) and 10 (lower). Work is equal to the area under curves. Saturation stress is the same, independent on elastic constants.

on the straight lines starting at the origin. Hookes proportionality law will transfer this pattern into the stress space without change. Several simulations were performed, with different proportion of elastic and plastic parts in the total work. Figure 18 corresponds to a high elasticity situation. The total strain equal to 0,2% was chosen as the stopping point. The points of the discrete yield surface are arranged in the same way as the strain rates in the strain rate space.

Figure 19 corresponds to the higher influence of plasticity. The points start to gather around the edges and vertices of the polyhedron and are almost absent on the faces. Figure 20 corresponds to the total strain of 1%. Plasticity is dominating and the points gathered at the vertices for the most part, so that a major part of all the different straining directions is provided by several discrete stress states.

The ratio between the elastic and plastic work for all three cases is shown on Figure 21. To reduce the simulation time in the latter two cases the elastic constants were multiplied by the

factor of 10, so that the total elastic work decreased correspondingly. Note that they are not corresponding to the uniaxial test, which is difficult to perform accurately by controlling the strain rate tensor, but to a stress and strain component along the x axis, corresponding to the strain rate tensor $\begin{pmatrix} 1 & 0 & 0 \\ 0 & -0.5 & 0 \\ 0 & 0 & -0.5 \end{pmatrix}$.

3.3 Generating textures.

The textures that are of particular interest are the typical textures in rolled and annealed aluminium, described in the previous chapter: Copper, Brass, S, Goss and Cube. To simulate the samples with more natural textures we use the same technique as in [6]. The texture is composed of a number of grains with orientations distributed around the ideal orientation and an equal number of randomly oriented grains. Both the directional part and the random part are generated by the software. The generated orientation part obeys Gaussian law. The distributions spread function is given as

$$G(\omega) = G(0)\exp(-\frac{1}{2}\frac{\omega^2}{\omega_0^2}) \tag{29}$$

where ω is the angle between a given orientation and the ideal orientation, ω_0 is represents the scatter width of the spread and must be chosen for generating the texture. To emphasize the effect of the texture on the yield surface we use the value of ω_0 equal to 5^0 which corresponds to a case of a very highly textured sample.

The pole figures for the generated textures may be compared with the pole figures obtained in [6]. On Figure 22 1 1 1 pole figure for the Copper texture with $\omega_0 = 5^0$ from [6] and the one for the generated texture are compared.

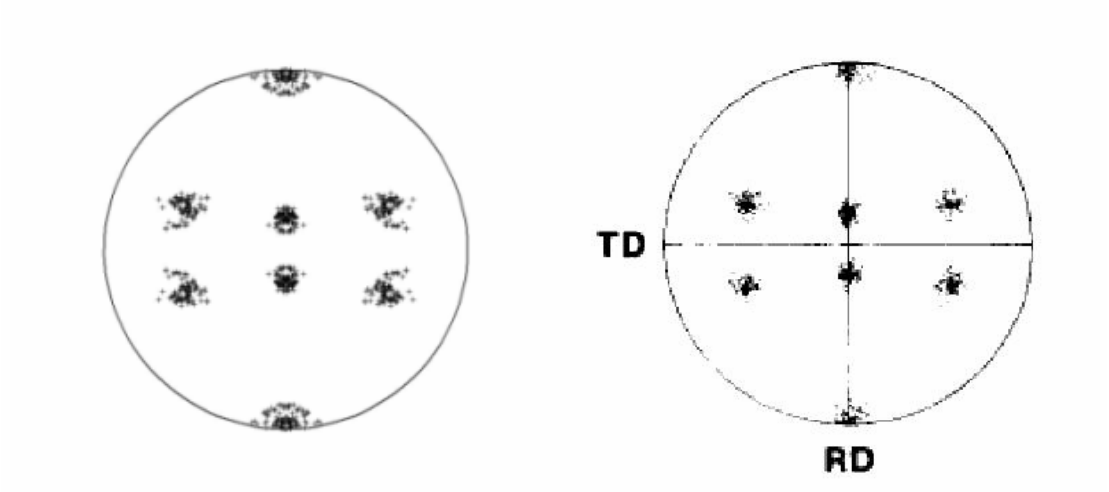

Figure 22. 1 1 1 pole figures for Copper texture with spread 5 degrees in [6] (right) and in this work (left).

3.4 Influence of plastic work on the yield surface.

We stated in the first chapter that the value of strain (and corresponding values of the elastic and plastic work) may be chosen arbitrarily, while usually it is chosen equal to 0.2%. The previous subchapter demonstrated that the ratio of the elastic-plastic in the total work at the end of the test is not so important for the form of a yield surface of a single grain, but has a certain influence on the distribution of the stresses. From this point of view it is worth investigating, which ratio of the elastic-plastic in the total work gives the most representative picture of plastic properties. The other 'reference point' is [6], who obtained these results before.

To make the evolutions in the yield surface more obvious the copper texture is shown. To estimate the relation between strain-stress and plastic-elastic work, firstly a simulation with one straining direction was performed. Results are shown on Figure 21. From the relations between elastic and plastic work found from this figure some predictions about the yield surface can be made by using the crystal plasticity theory. These predictions turned out to be correct.

Figure 23 shows the yield surface obtained for a very low ratio of plastic work, just in the beginning of the plastic deformations. The yield surface is rather linear and resembles the one for a (0 0 0) single crystal. The reason is that a large part of the slip systems with different orientations are not activated yet and the form is predominantly determined by a limited set of those that are activated. The form of the yield surface for different textures is almost the same at this level of plasticity, which confirms this assumption. The ρ=const lines are linear, showing that the proportionality determines the picture here.

Increasing the ratio of plastic work to about 50% leads to the yield surface, shown on Figure 24. Now more of the slip systems are activated and the form of yield surface is more curved, as in [6]. The ρ=const lines also start to curve. Also it is notable that it is more flat on top (so that a distinct line $S_{12} = 0.4$ could not be interpolated. The explanation may be that the slip systems that activate now give on average a contribution to yield surface that is lower than 0.4. Further activation of different slip systems cancels this effect.

Figure 25 shows how the yield surface looks when the plastic work is dominating. The form of it didn't change much, but the ρ=const lines now show a great deal of non-linearity. If we compare this picture with the yield surface of a grain that has Euler angles equal to (90.00 35.26 45.00) which corresponds to the orientation of the Copper component of the texture (Figure 29), we may see that the distortion of these lines has a tendency: they are denser around the vertices of the copper component yield surface and less dense on the facets. As we observed in the previous part the stresses tend to gather at the vertices at large plastic work, so averaging the stresses for the copper component with the randomly distributed stress points for the random part of the texture will likely result in such a picture. The yield surfaces found in [6] correspond to a high ratio of the plastic work, so it is chosen to use it here. We achieve it by reducing the elastic work by increasing the elastic constants by a factor of 10. Then we find the plastic work that corresponds to the 0.2% strain for the non-textured sample in a simulation of a single straining direction (we use the following values of the strain rate: the shear strain is 0, $\varepsilon_{xx} = 1$, $\varepsilon_{yy} = \varepsilon_{zz} = -0.5$), and then use this value of plastic work in the

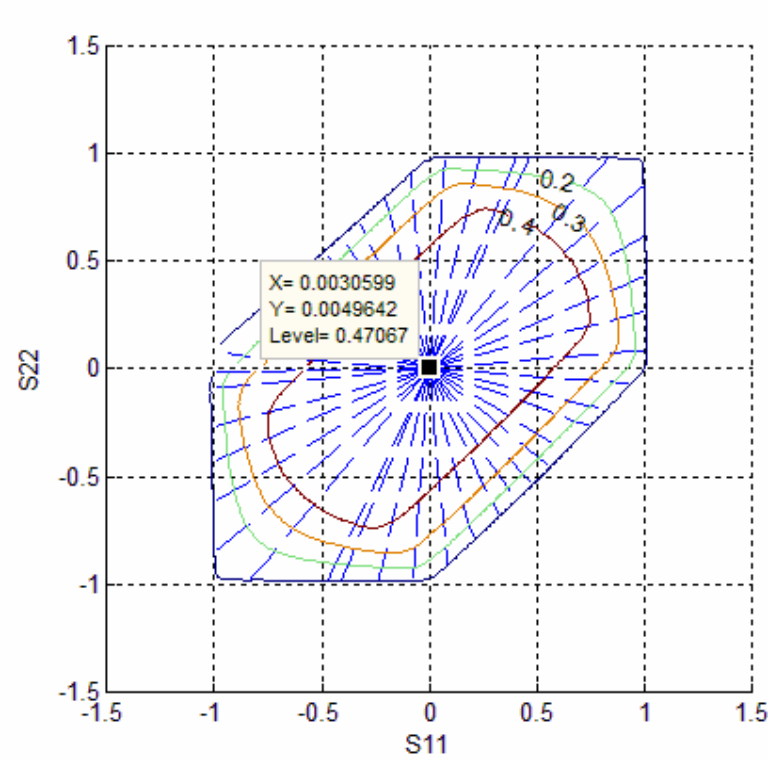

Figure 23. Yield surface for copper texture at high elasticity.

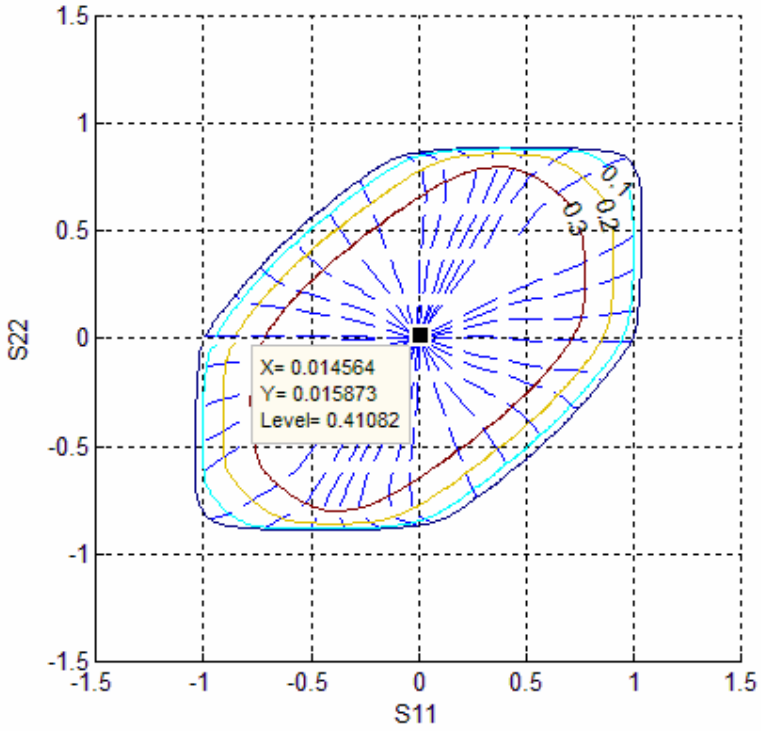

Figure 24. Yield surface for copper texture at low elasticity.

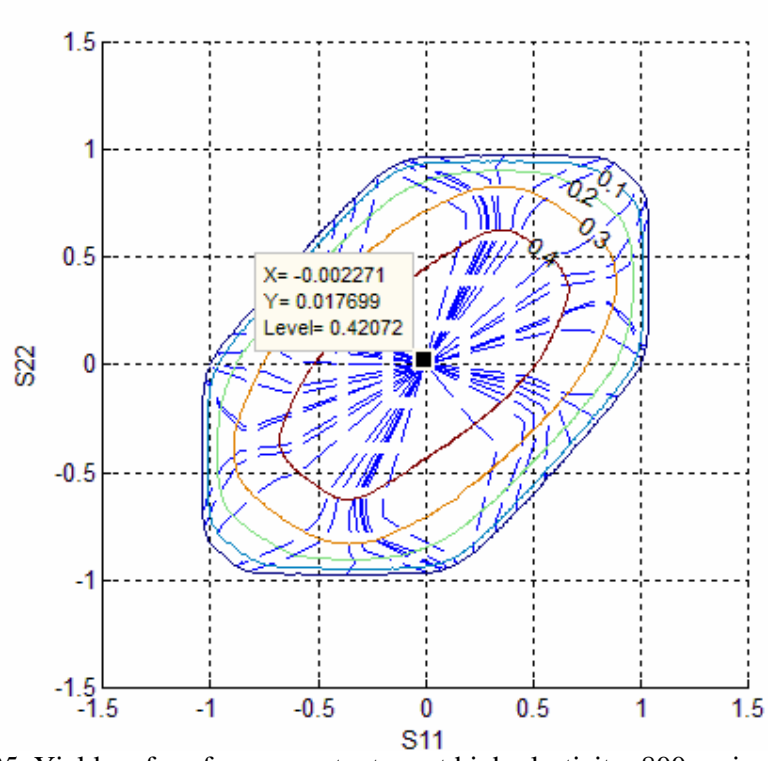

Figure 25. Yield surface for copper texture at high plasticity. 800 grains in total.

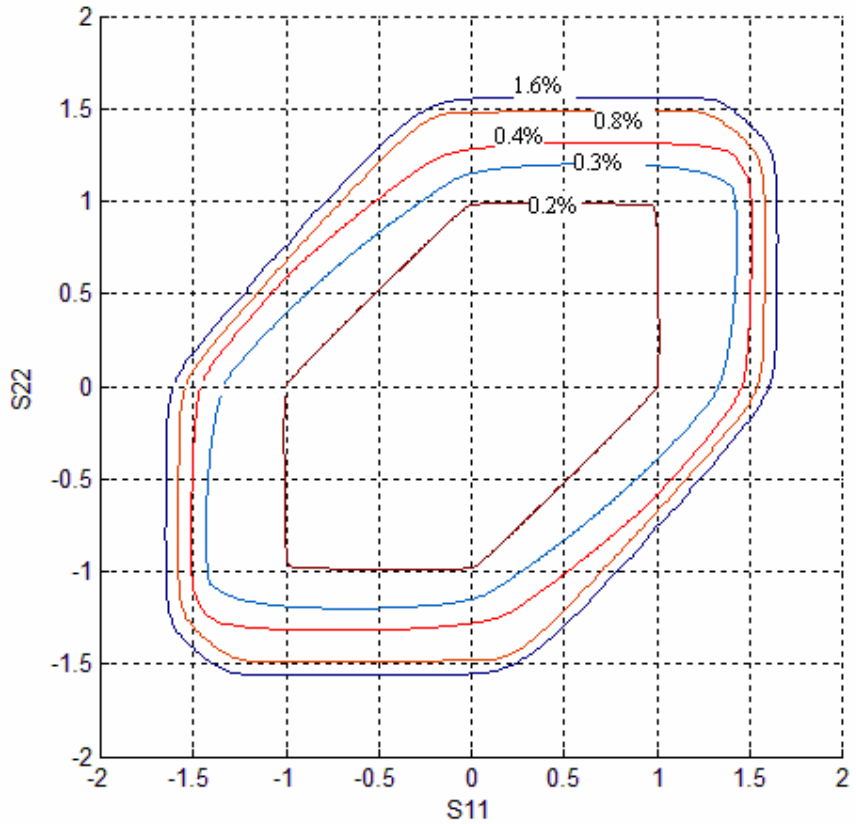

Figure 26. Hardening. Yield curves for different strains in $S_{12} = 0$ plane.

simulations for all textures. This value of plastic work is $w^p = 3.67053\text{E-}01$ The time step Δt was accordingly decreased to retain the stability of the solution.

To sum up what we know about the development of the plasticity with the increasing global strain, Figure 26 shows hardening by showing the intersects of the yield surfaces for the copper texture with the plane $S_{12} = 0$ at different values of strain.

3.5 Influence of number of grains.

F. Barlat and O. Richmond in [6] use 400 grains with distribution of the orientations around the ideal component. A fewer number of grains may lead to a worse representation of the component or the random part properties. To check if more grains will give some noticeable improvements, simulations with 600 and 800 'component' grains (1200 and 1600 total number) were performed. From Figure 27 it can be seen that the number of grains over 400 doesn't influence the yield surface. So, 400 grains with components' orientation and 400 random orientation grains were used for all the simulations.

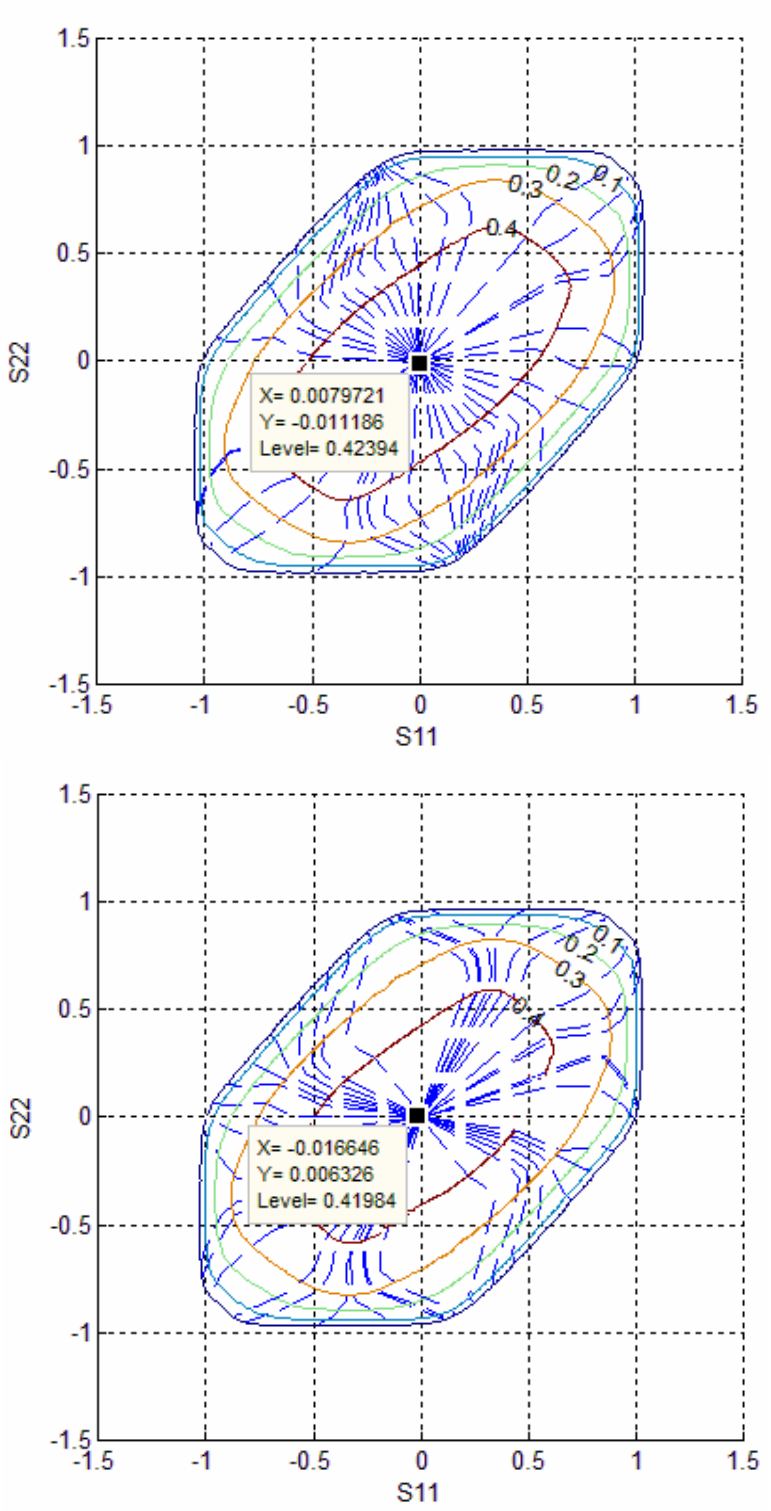

Figure 27. Yield surface for copper texture with 1200 (upper) and 1600 grains in total.

3.6 Generating yield surfaces for typical textures.

3.6.1. Non-textured case.

The yield surface for the non-textured case is presented on figure (28). 800 grains with random orientations were used. The surface is central-symmetric and symmetric relative to the lines $\rho = 1$ and $\rho = -1$. We can say that the isotropy expresses itself through the fact that the coordinates S_{11} and S_{22} are interchangeable. Normalization stress $\bar{\sigma} = 226$

3.6.2. Copper texture.

The central symmetry remains as may be expected for any yield surface, as well as the mirror symmetry relative to the $S_{12} = 0$ plane, but the other symmetries are gone and some anisotropy shows up. It may be explained if we look at this surface as the average of the previous one (Figure 28) and the component's surface (Figure 29). The randomly distributed grains smooth the edges and the corners, but the form of the single crystal polyhedron is still recognisable. The reduction of $\max S_{22}$ is f. ex. due to the horizontal edge at $S_{22} \approx 0.7$. The distortion of the $\rho = const$ lines was explained previously. The 'components' yield surface is also rather 'low' (has small value of $\max S_{12}$). It shows in the low max value of S_{12} of the whole texture, which is the lowest of the six. This sort of comparison helps to explain the properties of the other yield surfaces too. Should also be noted that the lines $S_{12} = const$ are more 'angular' than in [6], which is a result of the low density of the points in some areas and the linear interpolation. Either more points could be used or less plastic work, but by the time it was noticed there was little time left and both methods demand some lengthy simulations. Normalization stress $\bar{\sigma} = 249$

3.6.3. Brass texture.

A peculiarity of the brass texture component is that it has two modifications with equal total volume fraction. These two variants are basically the same, just rotated relative to each other. These two components are central symmetric, but they are not symmetric relative to the $\sigma_{xy} = 0$ plane. The yield surface of the whole texture meanwhile is still symmetric, because the two orientations 'cancel' each other to retain symmetry.

This yield surface is even more obviously anisotropic. The sharp edge of the components yield surface gives it a rounded highly curved 'edge' and higher values of S_{22}. The S_{12} of 'component' surface has max S_{12} at about 0.45, which reduces the S_{12}=0.542 of the random texture part but not as much as the copper texture. Normalization stress $\bar{\sigma} = 229$

3.6.4. S texture.

The S texture component has the same rotated variants as the Brass texture. The difference is that the S component has not so sharp and protruding edges as the Brass. As a result the yield surface is not that obviously anisotropic and resembles the non-textured one. Value of S_{12} at (0,0) is also expectedly lower than for the isotropic. Normalization stress $\bar{\sigma} = 233$

3.6.5. Cube texture.

This texture's peculiarity is that the basic single orientations surface is very symmetric (the same as in Figure 15). This symmetry remains in the texture surface. The difference with the non-textured one is the distortion of $\rho = const$ lines that now have several vertices to be attracted to. The main component also gives it a more round form, than oval isotropic surface. S_{12} of the single orientation surface is equal to 1, so it is the highest of the six for the total texture. Normalization stress $\bar{\sigma} = 204$

3.6.6. Goss texture.

The sharp edged and stretched up to almost 2 'component's' surface leads to a highly anisotropic and deformed surface of the total texture. S_{12} in pure shear is at about 0.7 which gives a higher value in the total texture. Normalization stress $\bar{\sigma} = 204$

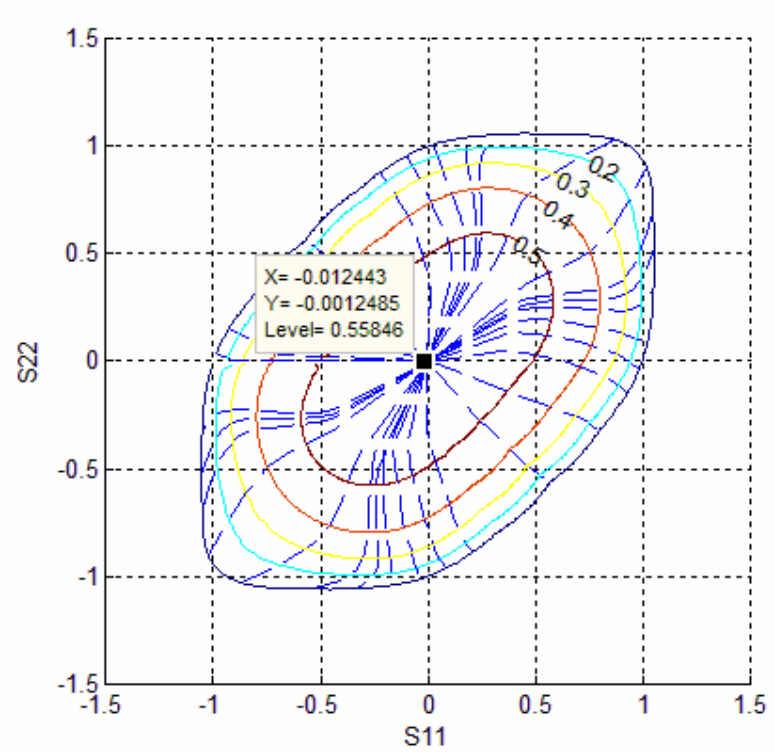

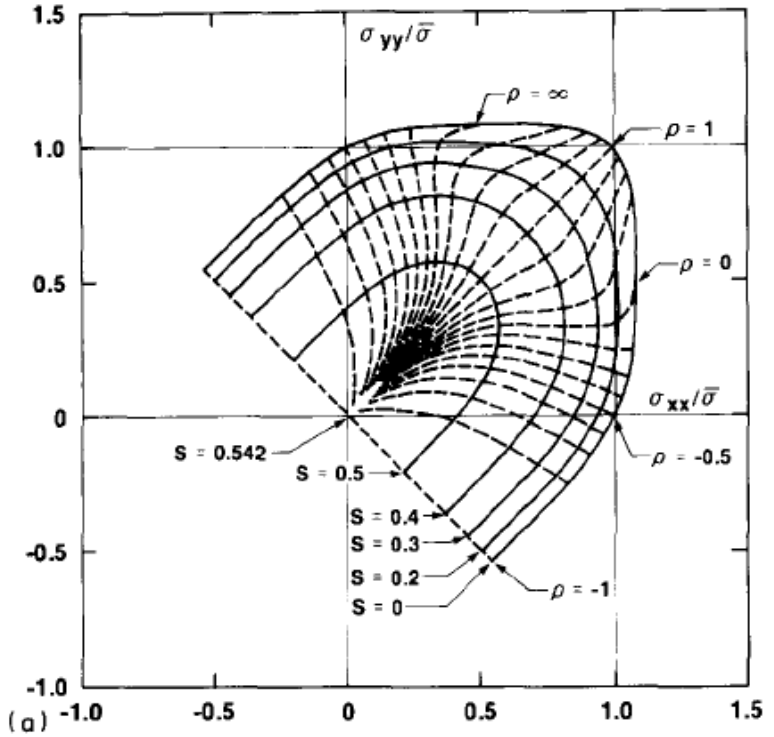

Figure 28. Yield surface for non-textured sample, 800 grains in total. Found in this work and in [6](lower).

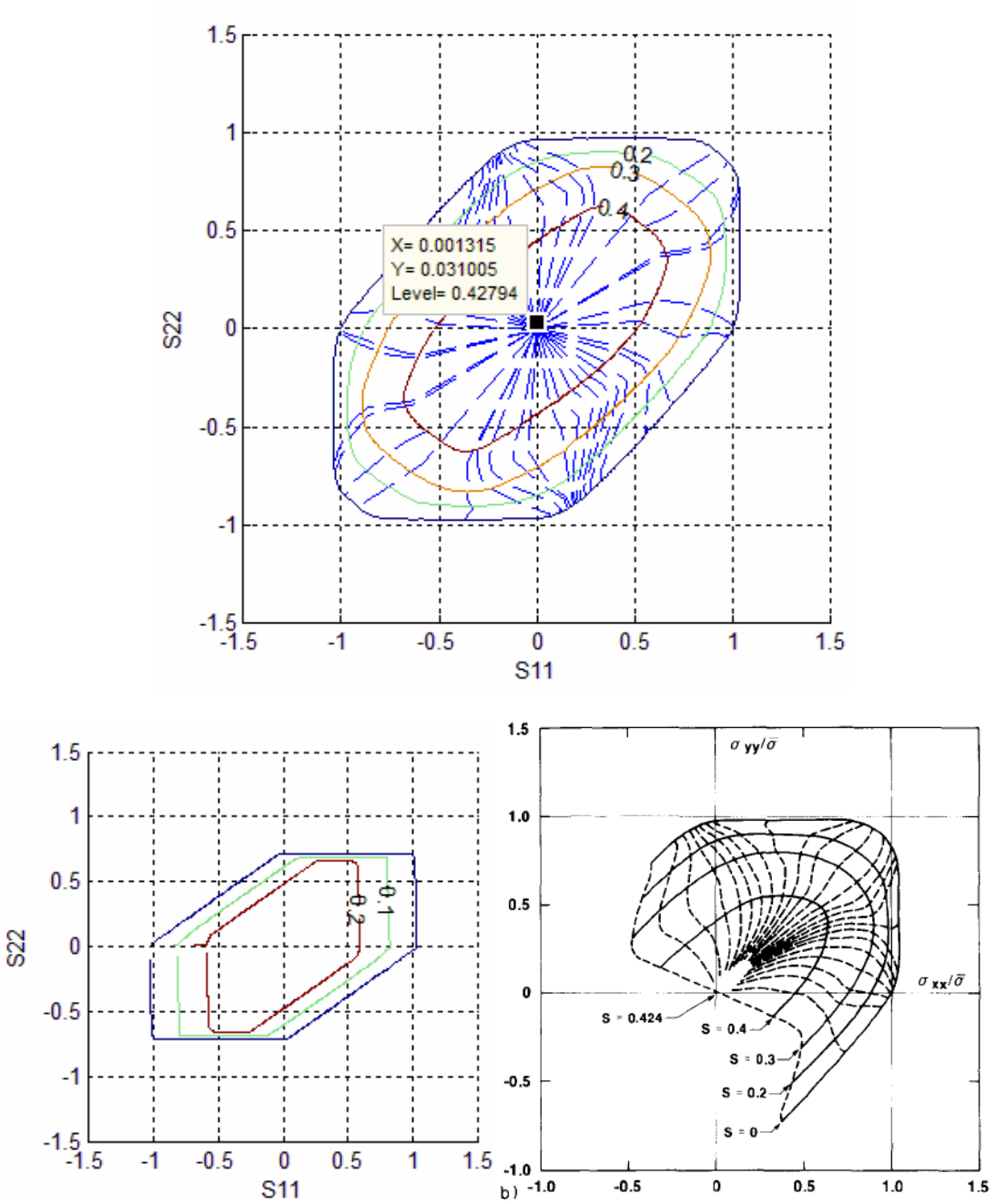

Figure 29. Yield surface for copper texture (upper), its main component (left) and as found in [6].

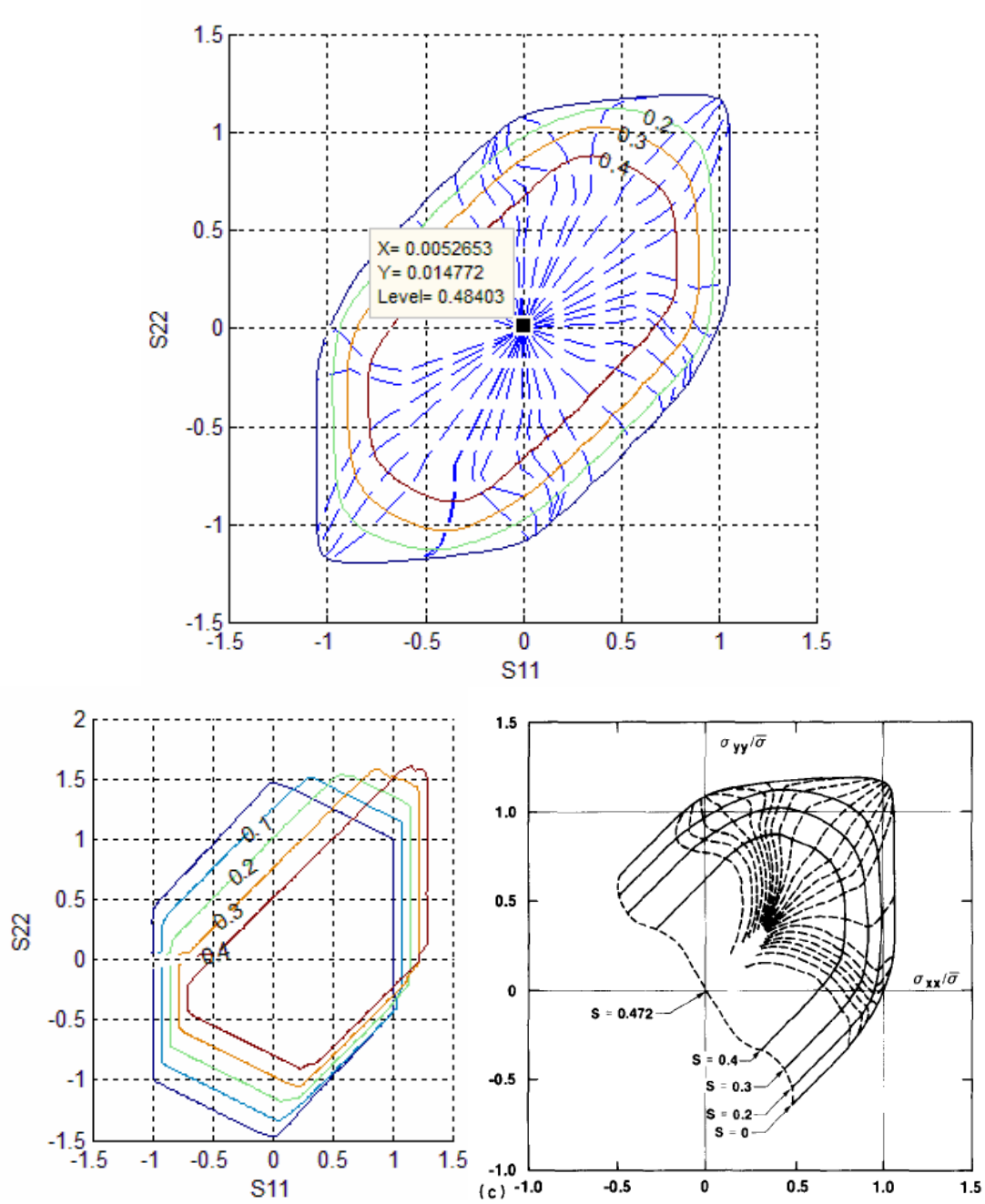

Figure 30. Yield surface for brass texture (upper), its main component (bottom left) and as found in [6] (bottom right).

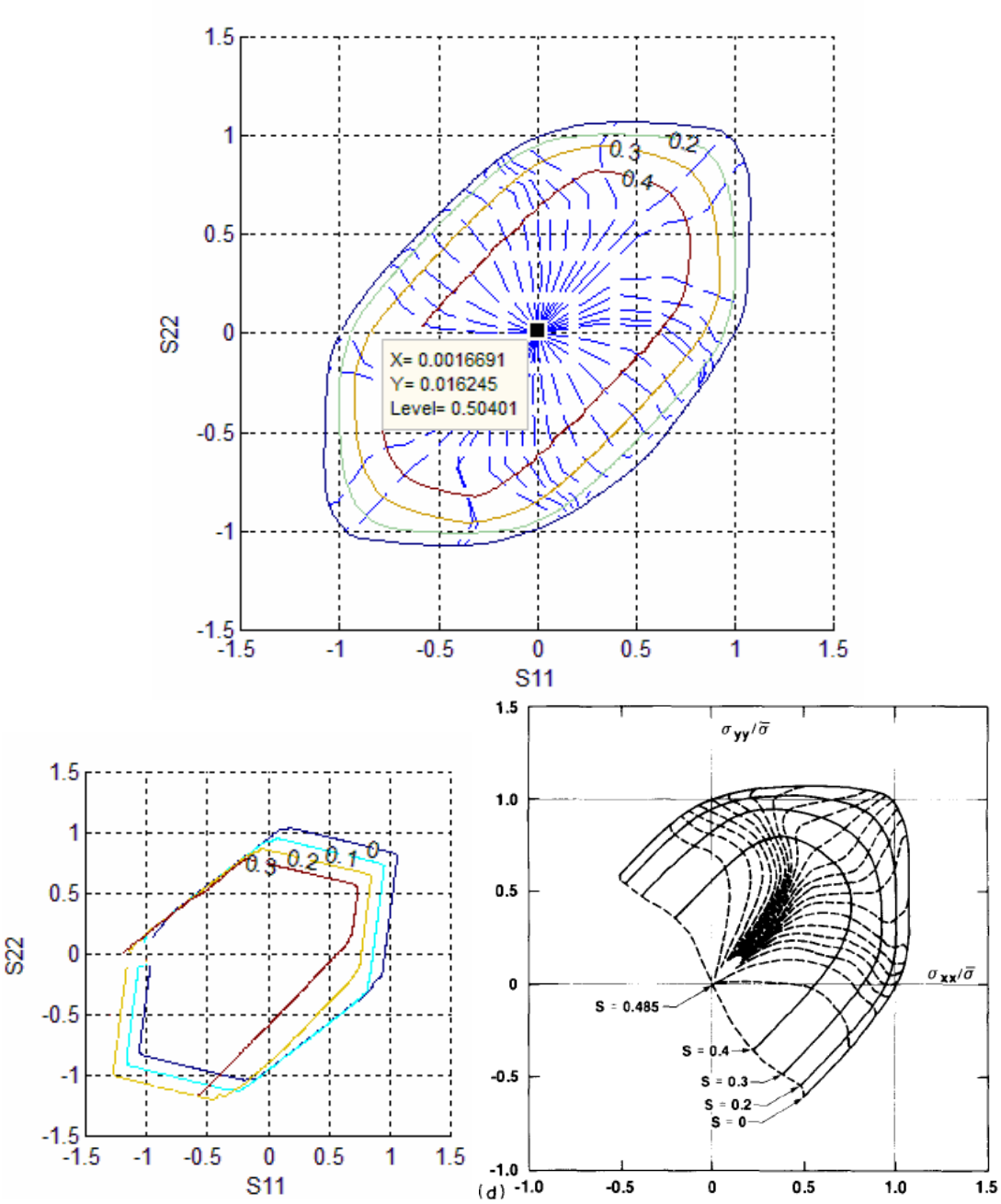

Figure 31. Yield surface for S texture (upper), its main component (bottom left) and as found in [6] (bottom right).

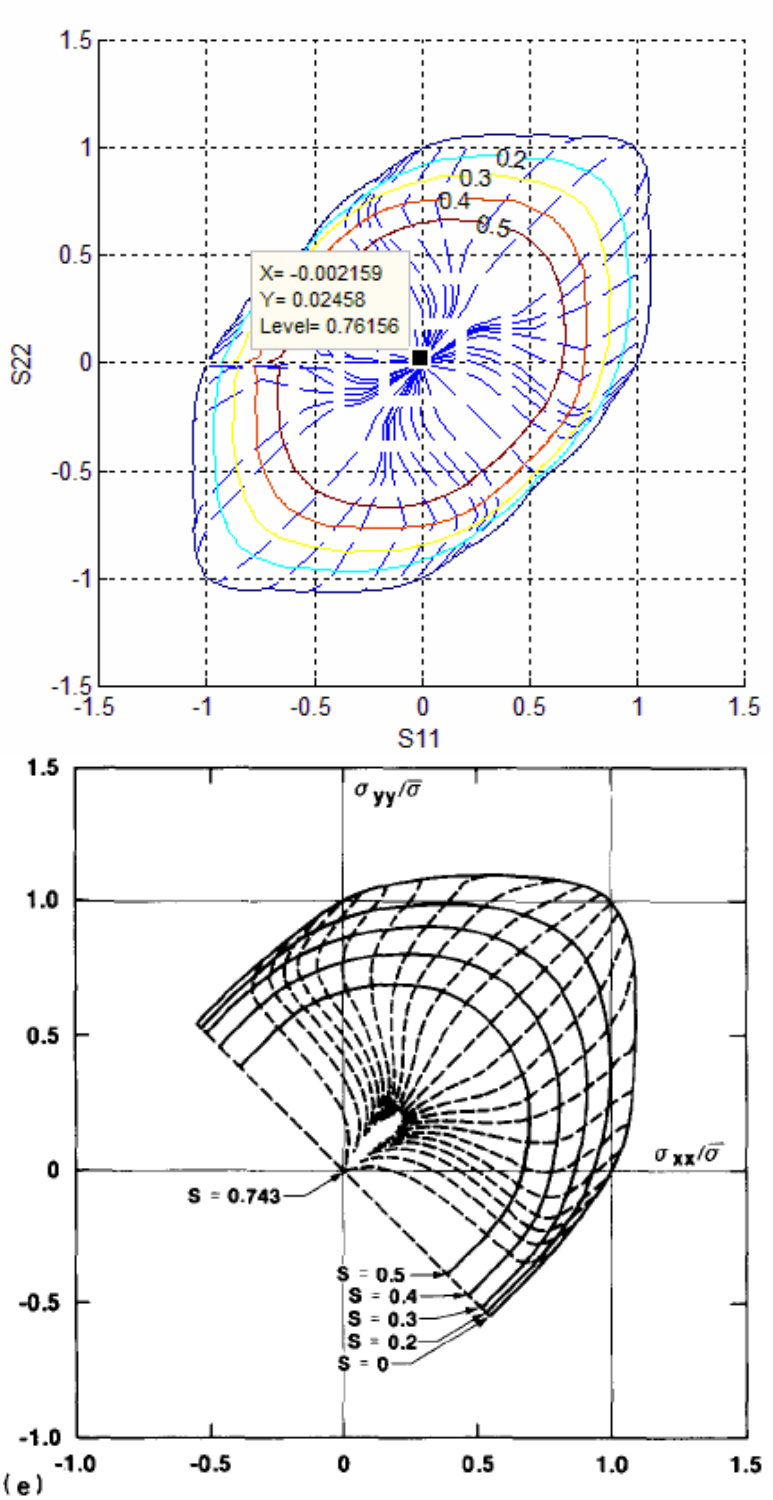

Figure 32. Yield surface for cube texture (upper), and as found in [6].

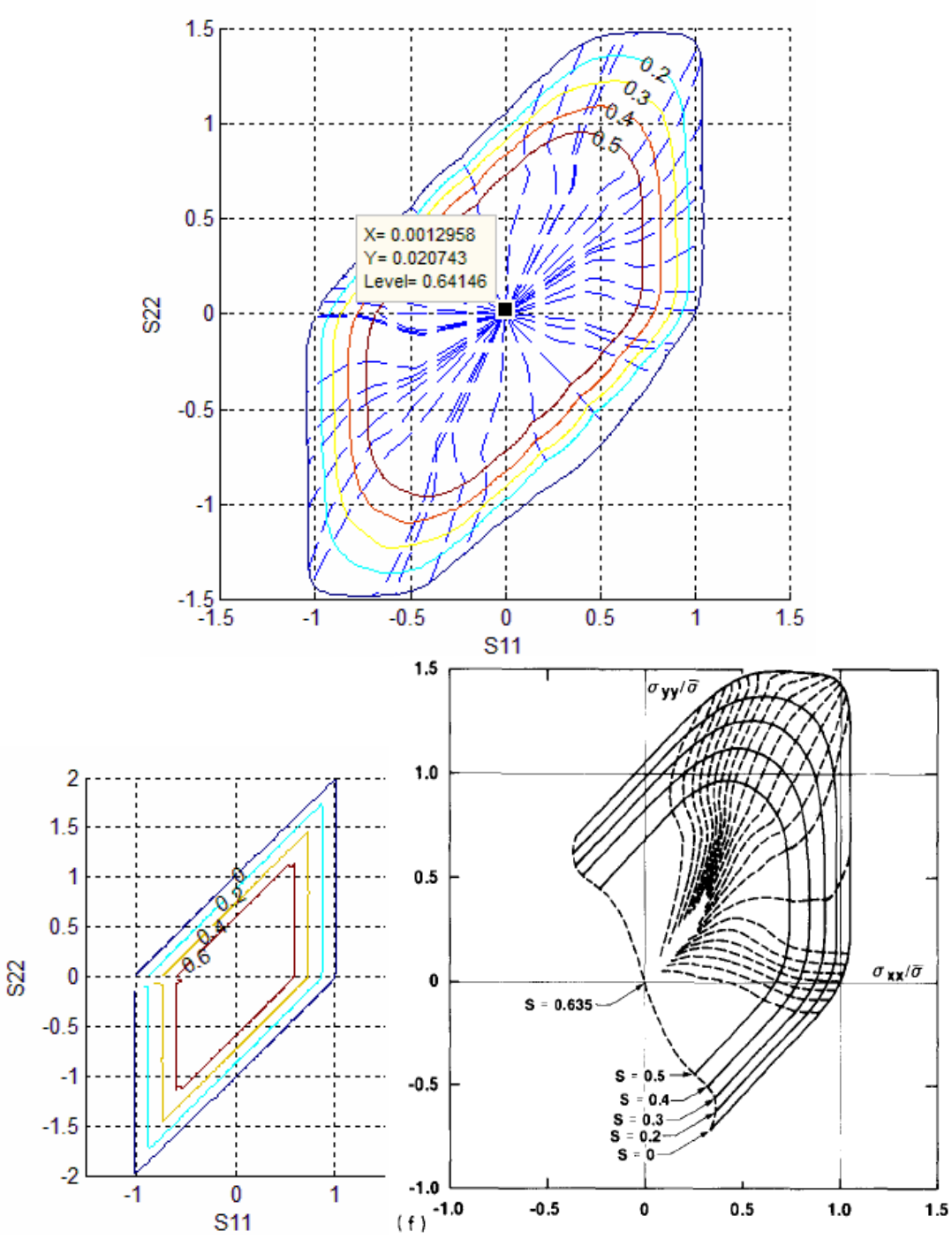

Figure 33. Yield surface for Goss texture (upper), its main component (left) and as found in [6].

All the obtained yield surfaces are very much like the ones that were found in [6]. The differences in S_{12} at (0,0) (pure shear) may be explained by the errors of interpolation. These errors are not more than several percent in all the cases. The interpolation method is also responsible for some minor irregularities in the yield surface projections (especially on Goss and Cube).

3.7 Concluding remarks

The program that we used showed good results that are in accordance with the crystal plasticity theory. The anisotropic samples were modelled by sets of grain orientations (textures) typical for aluminium, with strongly expressed texture components. The yield surfaces for these anisotropic samples were generated and they also showed anisotropy. That anisotropy may be explained in terms of the crystal plasticity theory, at least in qualitative sense. Hardening at different strain levels was also found and explained. The necessary number of grains, to represent these textures, was found to be not more than 400.

The next chapter will try using a different method of generating the yield surface. Comparison of the results will check the validity of some assumptions we made. Another useful step may be comparison of the obtained results with the experimental data and 'tuning' of the model parameters.

4. Generating yield surfaces with FEM.

4.1 Peculiarities of generating yield surfaces with FEM.

The next step is generating the yield surfaces using the FEM program LS-DYNA. It allows more control over the simulation in some respect, but has its own limitations. The main difference between the simulations performed for this chapter and the previous is that the boundary conditions become directly defined, not adjusted by superimposing a stress state. So this side of the previous simulation type may be checked for feasibility.

The sample is now represented by a rectangle element (in the previous simulation the sample geometry was not considered at all). It is an 8-node constant strain element with one integration point (reduced integration). The stress is calculated at the integration point (superconvergence point). So we can say that the Taylor model is still implemented here, because the strain is still constant throughout the sample, but the calculation method is different. Now, instead of applying the strain rate matrix to the whole set of grains, we may apply the velocities and constraints to the nodes. The boundary conditions used for the simulations are shown on Figure 34. Node 1 is prevented from lateral motion in all 3 axial directions. The rotations of the element around the x, y and z axes are prevented by preventing appropriate displacements in the nodes 2, 4 and 5. The velocities v_{xx}, v_{yy} and v_{xy} applied in nodes 2 and 4 give the strain rate components $\dot{\varepsilon}_{xx}$, $\dot{\varepsilon}_{yy}$ and $\dot{\varepsilon}_{xy}$. These strain components are connected by the parameters ρ and γ as stated in (27) and (28). The velocity field and the strain rate field are connected by expression

$$\dot{\boldsymbol{\varepsilon}} = \frac{d\mathbf{v}}{dx_i} \tag{30}$$

where x_i is one of the coordinates. So the velocities are connected by ρ and γ in the same way as the strain rates. By beholding v_{xx} and varying ρ and γ we obtain different points in the strain rate space and the corresponding points in the stress space in the same way it was done in the previous chapter.

To explain how uniform deformations of the element are provided by applying the velocities at just two nodes we must introduce the conception of the periodic representative volume element and the periodic boundary conditions. In chapter 2.4 it was stated that we find the properties of a whole sample by modelling a small part of it that still has the same properties as the whole (Representative Volume Element or RVE). In the present case RVE consists of one element, but generally it consists of a number of elements. In a sense, it is analogous to the unit cell, which is also representative for the whole lattice. This RVE that we consider must be a valid representation of a sample, remote from the influence of the boundaries (free surfaces, fixed displacements etc) i.e. without the effects of the constraints. To provide this it must fulfil some requirements. Let us say that we consider a sample of a material, divided into small parts, each of them is representative for the whole. If we deform the whole, each RVE must be deformed in the same way as all the others, so that they are fully interchangeable. In other words all possible RVEs are connected by the translational symmetry in the undeformed and all the deformed states. These parts must also naturally remain kinematically compatible. To provide both this translational symmetry and the kinematic compatibility, RVE must deform in a certain way, as e.g. is shown on Figure 35. Displacement at the edge 1-2 of element a is the same as at edge 3-4, same goes for edges 1-3 and 2-4 and for edges of element b. This type of boundary conditions that provide

translationally symmetric and kinematically compatible RVEs are called periodic boundary conditions [8]. Special subroutines in LS-DYNAprovide this kind of boundary condition

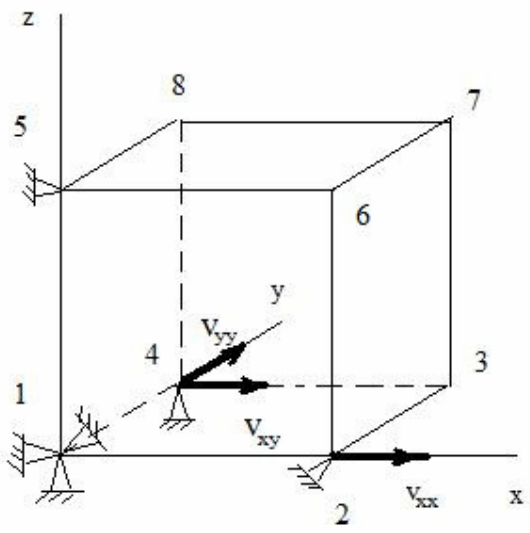

Figure 34. Boundary conditions of an element used in simulations.

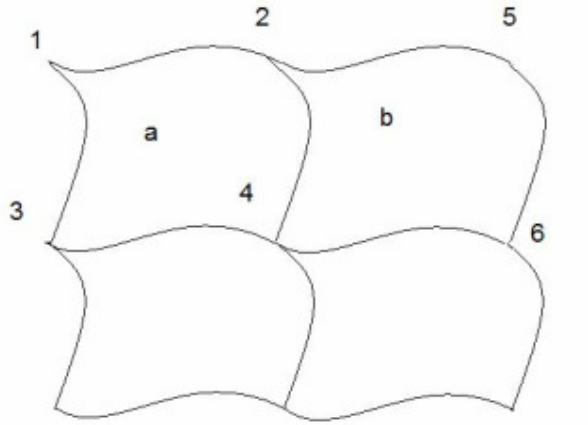

Figure 35. RVEs must provide both kinematic compatibility and translational symmetry.

in our element. It means that e. g. when node 2 starts moving in the positive x direction, nodes 3, 6 and 7 move accordingly, to behold the form of the element that will still fulfil the requirements.

The calculations of the stress are now performed in another way than in the previous chapter. Time is again divided into small steps. The crystal plasticity model is implemented in the material model. It is used to calculate the tangent stiffness matrix at every time step. This tangent stiffness matrix depends on the current state of strain-stress. Then the equilibrium equations are constructed and solved for the forces and displacement in the nodes iteratively

at each time step to account for the non-linearity. The stress is calculated from the strain, which in turn is calculated from the displacement.

4.2 Generated yield surfaces and comparison with previous results.

The first step was again to consider the stress-strain curve in the uniaxial test. This time we have full control of the boundary conditions and can produce an accurate uniaxial test. The obtained stress-strain curve is the same as shown in Figure 21, upper part. The use of larger elastic constants to reduce the influence of elasticity was unsuccessful – the solution could not be obtained. So another value of the plastic work was chosen, than in the previous chapter. The plastic work that corresponds to the plastic strain equal to 0.2% is approximately equal to 4. This value of the plastic work is used in simulation for a single crystal. A distribution of stresses, which was observed, is shown in Figure 36. The stresses again are attracted to the edges and especially vertices of the polyhedron, but in comparison to Figure 20, the points are much more scattered around the exact positions of the vertices. It may be explained by

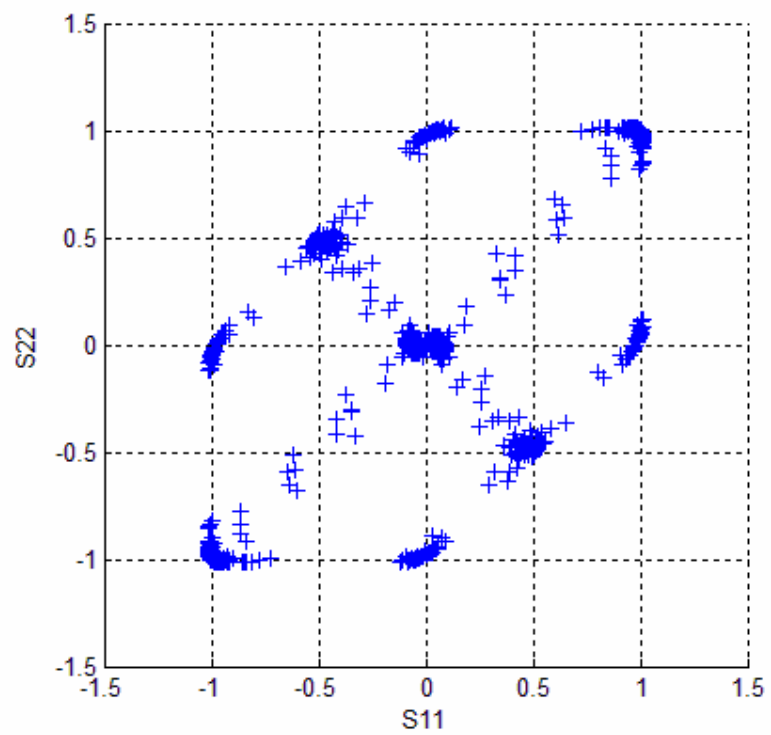

Figure 36. Distribution of stresses for a single crystal yield surface generated by LS-DYNA.

difference in the boundary conditions: in Taylor we apply a constant strain rate, while in LS-DYNA we apply a constant velocity, which gives a varying strain rate when the length of the sample is changing. And our model is rate dependent, so it gives some scatter in stresses.

But what is more important, at $w^p = 4$ the distribution of the stress points show little enough influence of elasticity, so this value may be used in the polycrystal simulations. This time we had to use a value that is about 10 times bigger than the one used for the previous type of simulations to reduce the contribution of elasticity in total picture, and the computation time also increased considerably.

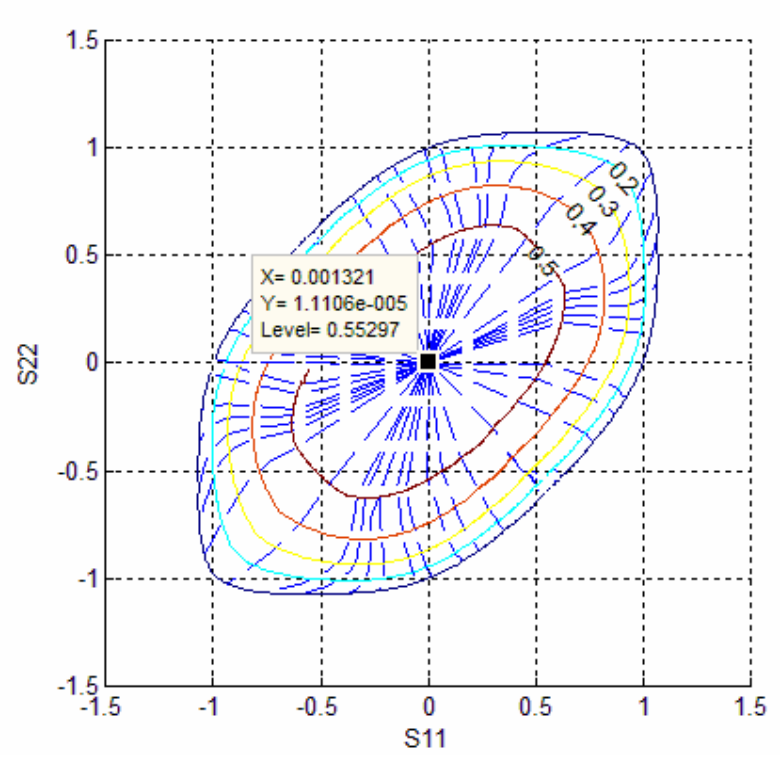

Figure 37. Yield surface by LS-DYNA for non-textured case, 800 grains.

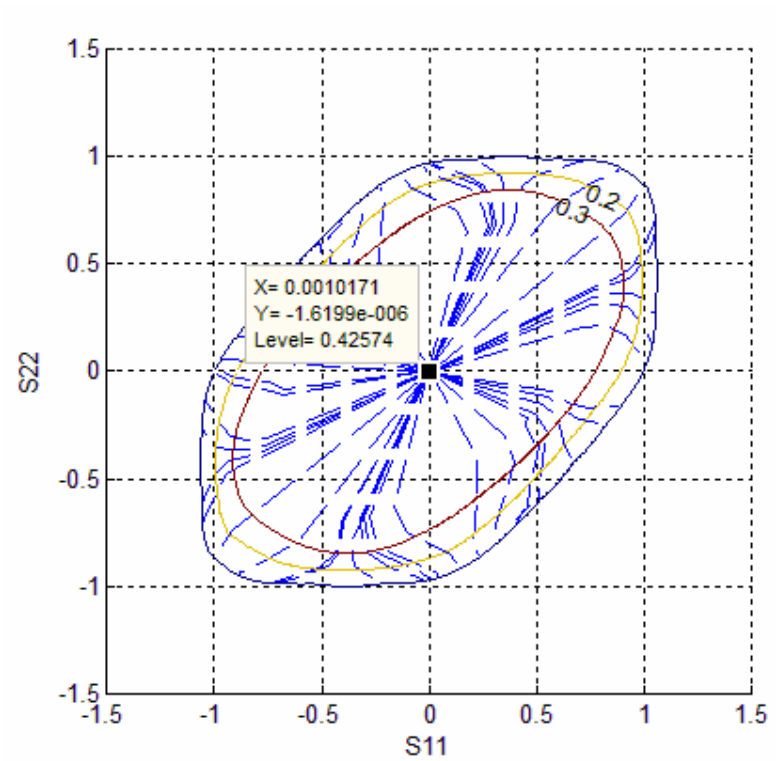

Figure 38. Yield surface by LS-DYNA for Copper texture component, 800 grains.

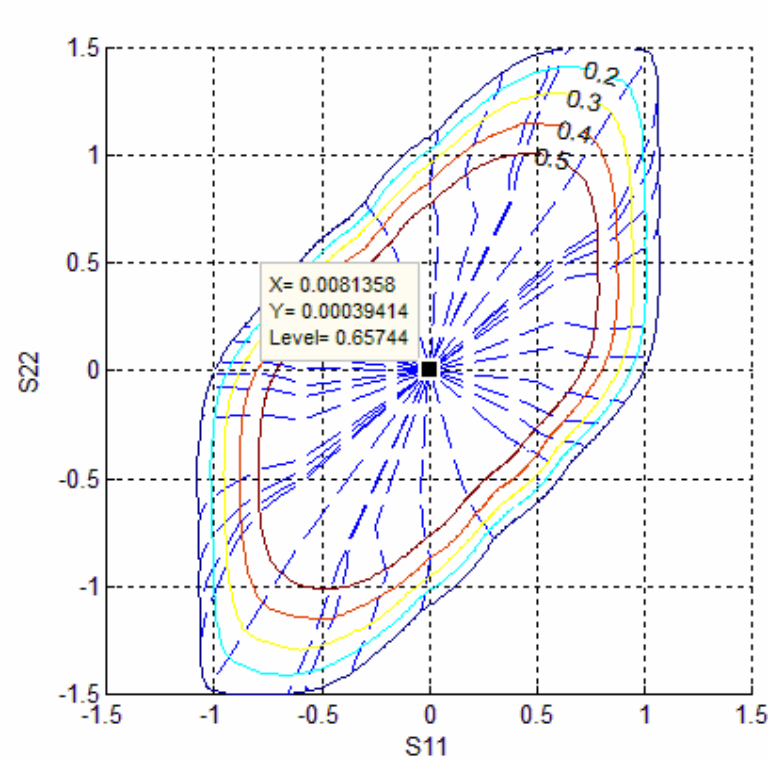

Figure 39. Yield surface by LS-DYNA for Goss texture component, 800 grains.

It may be expected from this that the yield surfaces of the polycrystals generated in LS-DYNA will not be very different from the ones generated by use of the Taylor model. The additional scatter may make them smoother and more rounded, though not much. This is what was observed. Figures 37, 38 and 39 show some of the results. The lines $S_{12} = const$ for the Copper component are more rounded than obtained by the Taylor model, and more like the ones found in [6]. Line $S_{12} = 0.4$ was again badly interpolated and is not shown in Figure 38.

The boundary conditions imposed on the element must lead to the plane stress state. The values of the stress components that must be equal to zero are negligibly low. We also get the same deviatoric stress states as in the previous chapter.

4.3 Concluding remarks

The FEM proved that the assumptions made in chapter 3 about the boundary conditions are reasonable. The results, obtained for the plane stress, provided by the boundary conditions and provided by superimposing the isotropic stress state are the same. The results also show that the crystal plasticity models may be successfully used as the material models in the FEM analysis, e.g. they may be used in the study of the morphology influence on the plastic properties.

5. Fitting of the generated surfaces to analytical expressions.

It may be useful for the practical purposes to represent the obtained yield surfaces by some analytical yield function. The exact function that fits all the data points that we generated may be difficult to find, but a good approximation may be reached. An example of such approximation is developed in [10, 31].

In 2.1.2 we stated that only the deviatoric component of the stress gives a contribution to plasticity. Then any isotropic yield function may be written as:

$$\varphi = \varphi(\mathbf{D}) \tag{31}$$

where $\mathbf{D}$ represents the principal values of the stress deviator $\mathbf{d}$. $\mathbf{d}$ may be found from the Cauchy stress tensor by a linear transformation. To use the isotropic yield function for an anisotropic material we can substitute $\mathbf{d}$ with $\tilde{\mathbf{d}}$, so that it takes account for the material anisotropy. $\tilde{\mathbf{d}}$ is also found by linear transformation of $\mathbf{d}$. The chain of transformations takes form:

$$\tilde{\mathbf{d}} = \mathbf{C}\mathbf{d} = \mathbf{C}\mathbf{T}\boldsymbol{\sigma} = \mathbf{L}\boldsymbol{\sigma} \tag{32}$$

where $\mathbf{C}$ contains the constant coefficients (not to be confused with stiffness matrix) and $\mathbf{T}$ transforms the Cauchy stress to its deviator component. Now the isotropic yield function becomes anisotropic, if we simply use $\tilde{\mathbf{d}}$ instead of $\mathbf{d}$. It will also behold the convexity.

We can use several linear transformations, to increase the number of the coefficients describing the anisotropy. The yield function will then take form:

$$\varphi = \varphi(\tilde{\mathbf{D}}^{(1)}, \tilde{\mathbf{D}}^{(2)}, ... \tilde{\mathbf{D}}^{(k)}) \tag{33}$$

for k transformations. In [10] $k = 2$ is described, which gives 18 parameters to describe the anisotropy. The transformed tensors are

$$\begin{aligned} \tilde{\mathbf{d}}' &= \mathbf{L}'\boldsymbol{\sigma} \\ \tilde{\mathbf{d}}'' &= \mathbf{L}''\boldsymbol{\sigma} \end{aligned} \tag{34}$$

and the yield function $\varphi = \varphi(\tilde{\mathbf{D}}', \tilde{\mathbf{D}}'')$. The yield function proposed by [10] and denoted Yld2004-18p is

$$\begin{aligned} \varphi = &\left|\tilde{D}_1' - \tilde{D}_1''\right|^\alpha + \left|\tilde{D}_1' - \tilde{D}_2''\right|^\alpha + \left|\tilde{D}_1' - \tilde{D}_3''\right|^\alpha + \left|\tilde{D}_2' - \tilde{D}_{\text{II}}''\right|^\alpha + \left|\tilde{D}_2' - \tilde{D}_2''\right|^\alpha + \\ &+ \left|\tilde{D}_2' - \tilde{D}_3''\right|^\alpha + \left|\tilde{D}_3' - \tilde{D}_1''\right|^\alpha + \left|\tilde{D}_3' - \tilde{D}_2''\right|^\alpha + \left|\tilde{D}_3' - \tilde{D}_3''\right|^\alpha \end{aligned} \tag{35}$$

The transformation matrix $\mathbf{C}$ takes form

$$\mathbf{C}' = \begin{vmatrix} 0 & -c_{21}' & -c_{31}' & 0 & 0 & 0 \\ -c_{21}' & 0 & -c_{23}' & 0 & 0 & 0 \\ -c_{31}' & -c_{32}' & 0 & 0 & 0 & 0 \\ 0 & 0 & 0 & -c_{44}' & 0 & 0 \\ 0 & 0 & 0 & 0 & -c_{55}' & 0 \\ 0 & 0 & 0 & 0 & 0 & -c_{66}' \end{vmatrix} \tag{36}$$

$\mathbf{C}''$ has the same form with the corresponding coefficients c_{ij}''. The exponent α is also a parameter that may be varied to find the best fit. It is interesting to note that if $\alpha = 2$ or 4 and the coefficients in $\mathbf{C}$ are equal to 1, then this yield function transforms into the von Mises yield function.

We have the stress tensor for different points of the yield surface from the simulations, so the problem is to find the coefficients in $\mathbf{C}$ for the anisotropic material. For this the error function is used:

$$E(c'_{ij}, c''_{ij}) = \sum_p w_p \left(\frac{\sigma_p^{pr}}{\sigma_p^{sim}} - 1 \right)^2 \tag{37}$$

where p is the number of the flow stresses σ_p^{sim} obtained in the simulations, σ_p^{pr} is the stress from the approximated function (35) and w_p is a weight coefficient. The coefficients in $\mathbf{C}$ are varied to obtain the minimal value of E.

The analytical surfaces were obtained for the same textures as in the previous chapters. To find the minimum of the error function (37) the solver module of MS Excel was used. A statistical analysis of the obtained analytical functions showed that most of them fit well into the analytical expression. The biggest maximum deviation is several percent and the biggest average deviation is less than one percent.

The yield function (35) proved to be a good approximate for even the most strong-textured materials. As expected the least error is for the most isotropic material (non-textured). The anomalously high difference between the analytical function and the data are found for the Copper (9.7%, the next highest is 4.0%) and Brass textures (4.8%, next highest is 2.4%). It corresponds to the pure shear points at (0,0). The Goss texture also has its maximum difference there although it is not as big as for the other two. The density of the data points around the pure shear point is low – the values of γ at this part of the surface are quickly going to infinity and values of ρ to the indeterminacy $\frac{0}{0}$, so this point is calculated separately as already mentioned, and the points in its neighbourhood are usually not calculated at all. So, if we prescribe a usual weight coefficient 1 to this point it will be 'ignored' by the solver and a surface that smoothly continues from the 'denser' parts of the simulated surface will be preferred. If the top of the simulated surface is not smoothly curved but instead flat, this will lead to a big difference between the analytical value and the simulated data. This may be solved by prescribing a higher weight coefficient to these points, but trying this showed that while the maximum difference reduced, the total accuracy of the solution suffered. Should be noted that the solver finds a local minimum of the error function, so different starting points of the c coefficients can give different results, but this process is complicated and unclear, so it was preferred to present the current results as is. But in the perspective, it may be investigated further, and may be better analytical surfaces could be found. The statistical diagrams for the 'anomalous' textures (Copper, Brass, Goss) are given without the pure shear points so as to be more representative.

The results are presented on Figures 40-45 by yield surface projections generated by the same Excel sheet. The lines $S_{12} = const$ start at $S_{12} = 0$ and have a step of 0.1 (same as in the Matlab representation from previous chapters). The lower diagram shows the fractions of stress points, which have the absolute difference between the simulated surface and fitted yield surface in a certain interval.

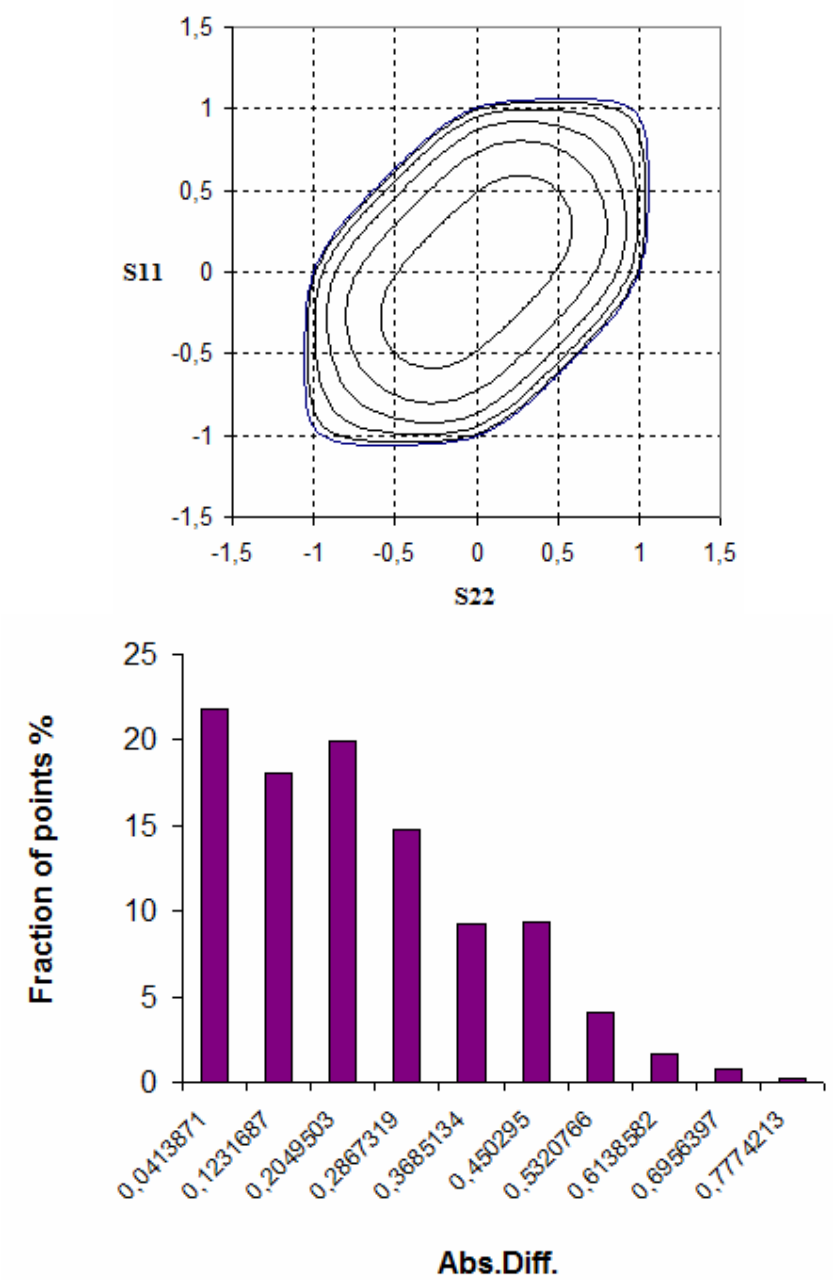

Figure 40. Fitted yield surface for the non-textured sample and the absolute error distribution. Max error is 0.80%, average 0.22%

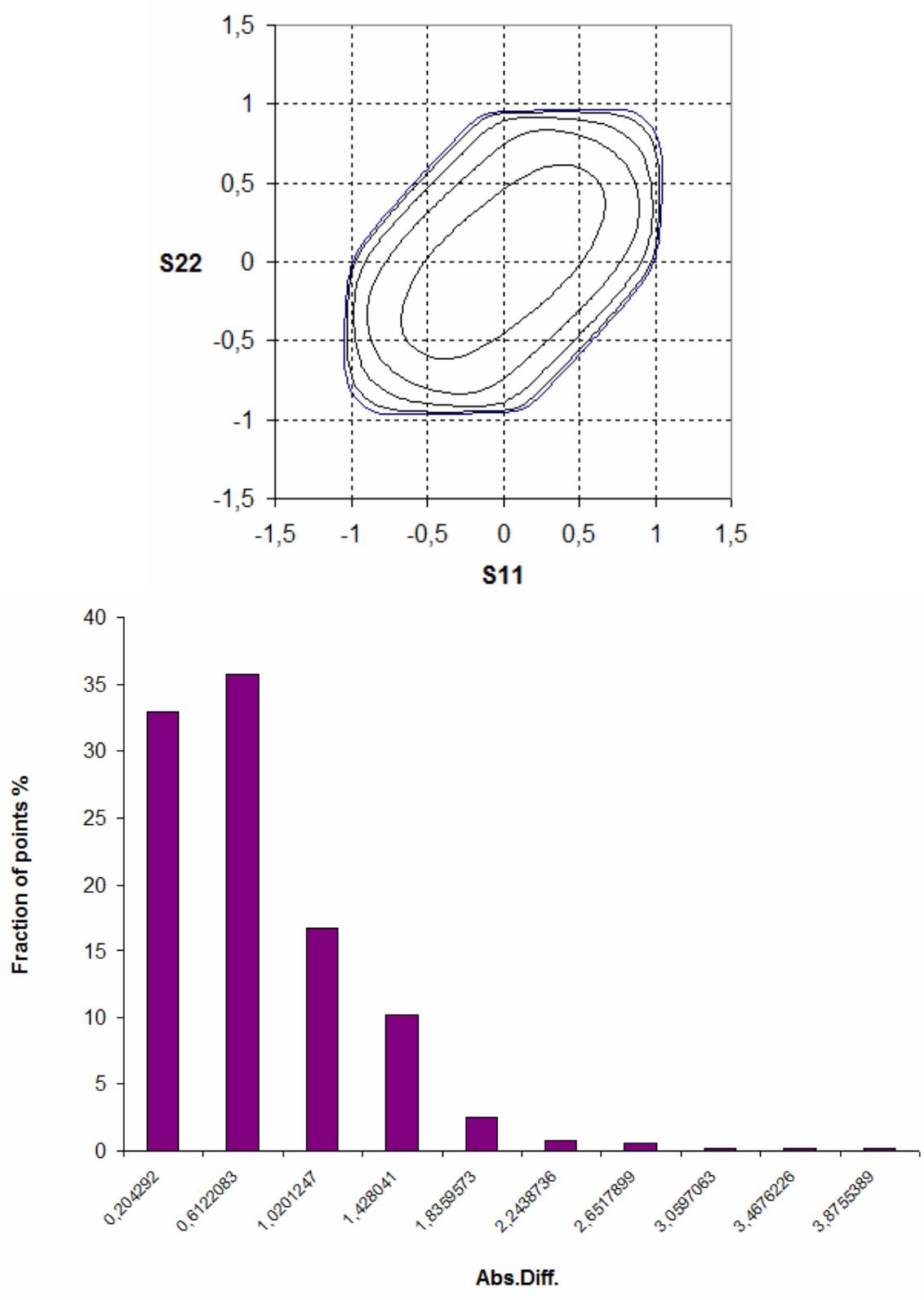

Figure 41. Fitted yield surface for Copper texture and the absolute error distribution. Max error 9.7%, average 0.70%.

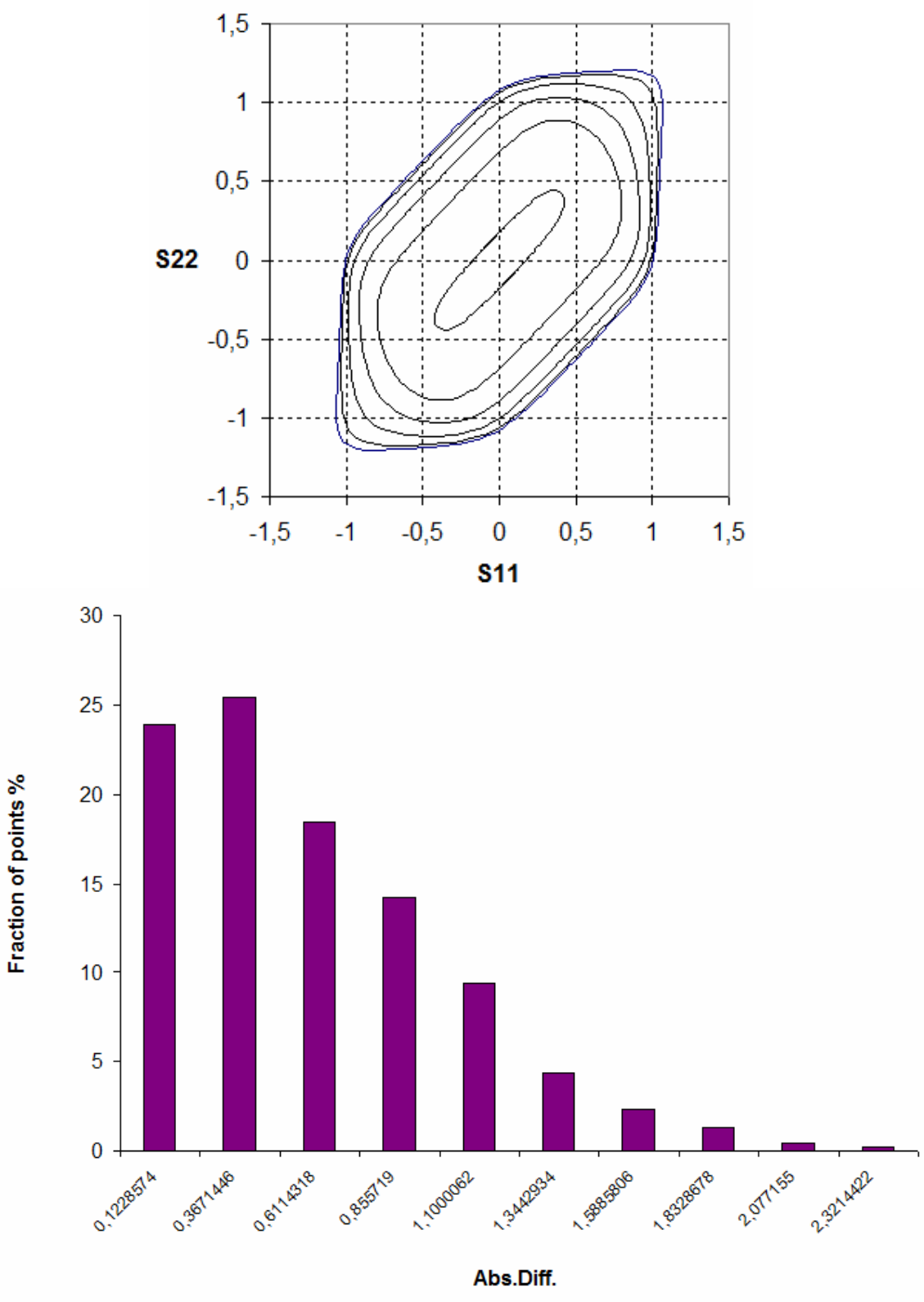

Figure 42. Fitted yield surface for Brass texture and the absolute error distribution. Max error 4.9%, average 0.59%.

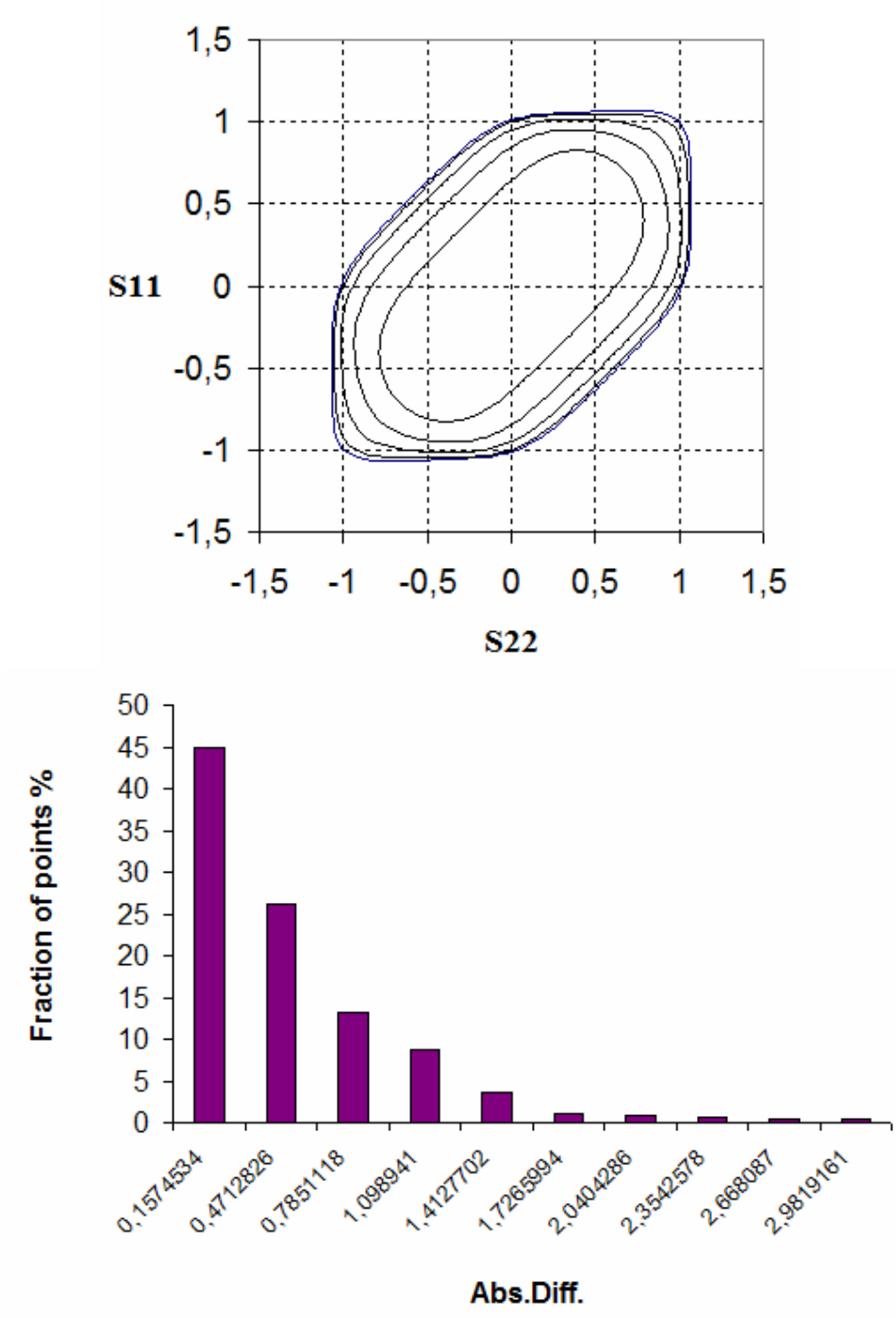

Figure 43. Fitted yield surface for S texture and the absolute error distribution. Max error 3.1%, average 0.50%.

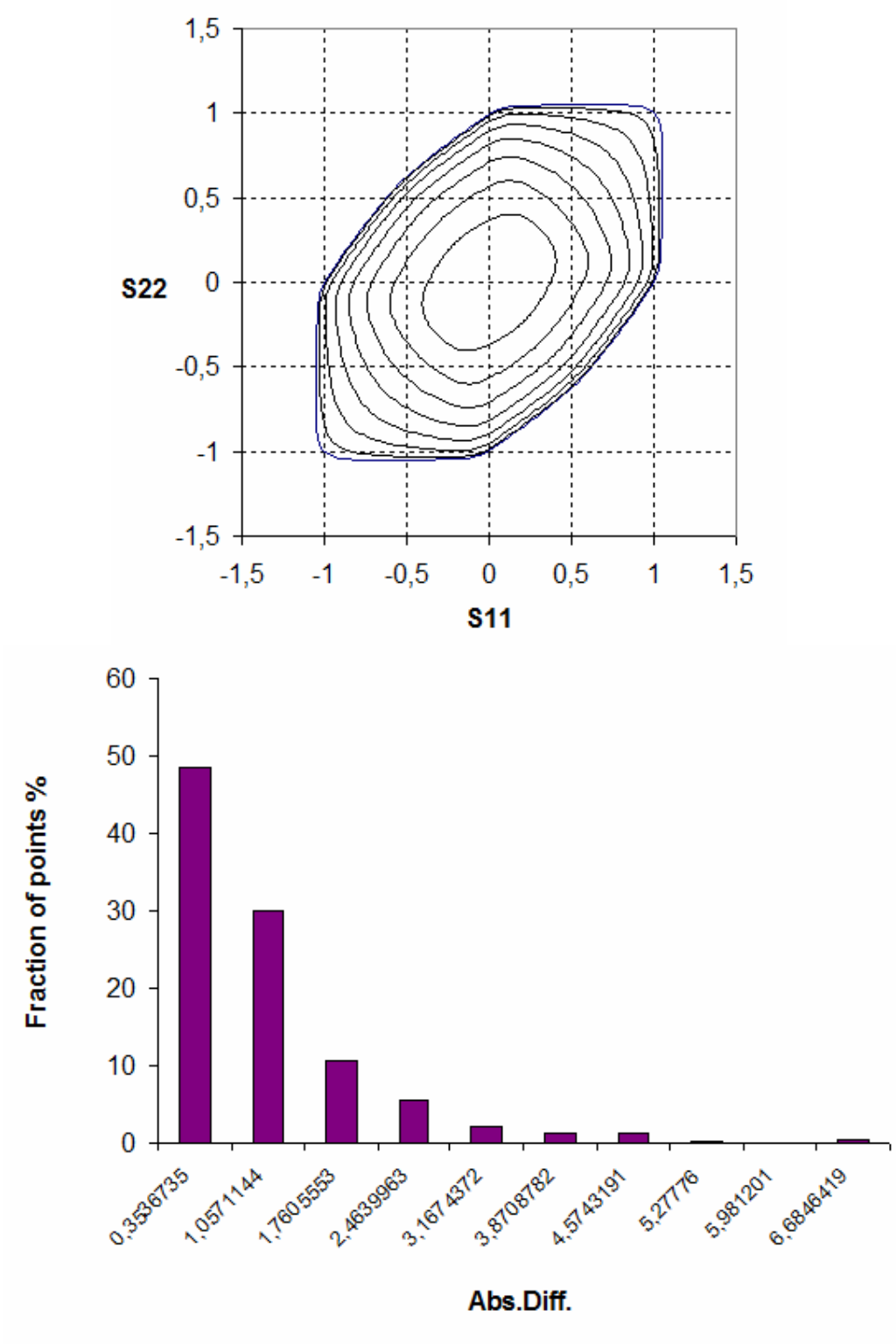

Figure 44. Fitted yield surface for Cube texture and the absolute error distribution. Max error 7.0%, average 0.99%.

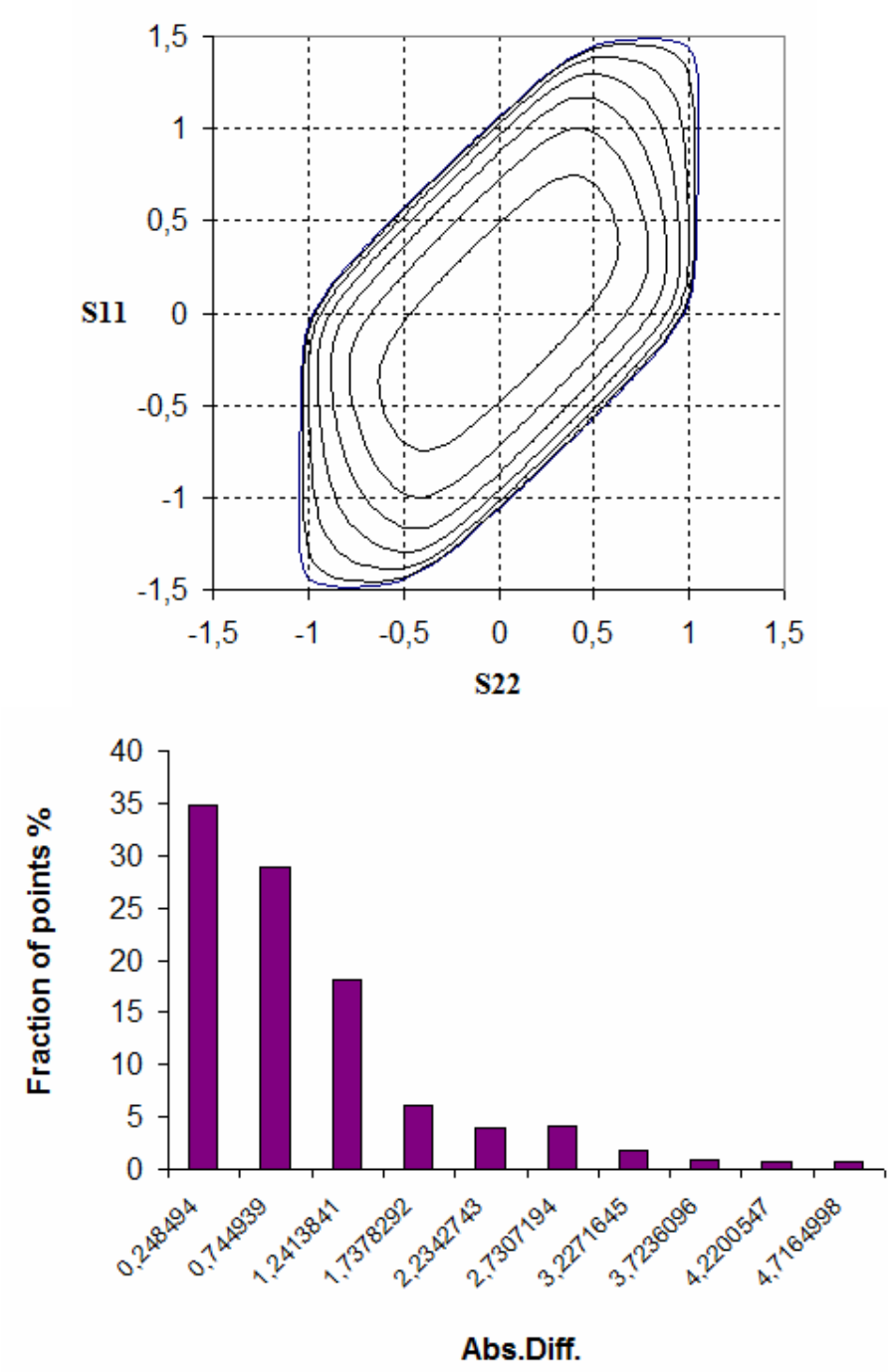

Figure 45. Fitted yield surface for Goss texture and the absolute error distribution. Max error 5.2%, average 0.97%.

6. Influence of grain morphology of the polycrystal on its plastic behaviour.

6.1 Introducing morphology into FEM analysis.

The goal of this work is to research the influence of the microstructure of aluminium on its plastic behaviour. One side of the microstructure – crystallographic texture – was shown to have a distinct influence. The other important side of the microstructure is the morphology of the grains or their shape, size and distribution in the polycrystal. The morphology was not considered at all in the analysis in chapters 3 and 4. The grains of different shapes and size interact through their grain boundaries and it leads to a complex distribution of the stresses in them. Nevertheless we modelled the material as a continuum, albeit with a texture.

Some studies (e.g. [9]) shows that the grain morphology has some influence on the properties of the polycrystals, though only a small number of grains was considered. The stresses and the strains inside the grains are heterogeneous. The stress redistribution on the grain level may lead to a "softer" response of the sample, in comparison to the Taylor approach (the models which account for the stress heterogeneity on the grain level are sometimes called "relaxed").

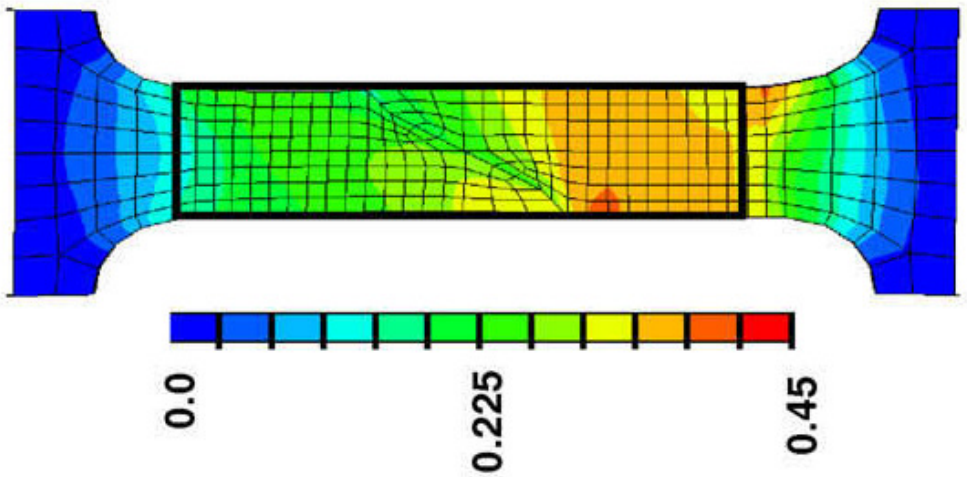

Figure 46. Strain field in a sample consisting of two grains with different orientations [9].

The study of this area has a limitation. These interactions together with the non-linear plastic behaviour usually result in a very big amount of the necessary calculations, which means the computational time. So a balance must be found, so that the morphology is described in enough detail and with enough precision, but the number of the elements must remain reasonably low.

A way to find this balance is to use the periodic RVE, described in the previous chapter. In case of the morphology study we apply the same requirements of the translational symmetry and compatibility to the grain morphology, as illustrated in Figure 47.

In this case it is impossible to use one element per RVE as we did in chapter 4. Each grain must consist of an appropriate number of the elements, enough to obtain a reasonable approximation of the intragranular stresses along with the evolving microstructure and texture.

To find the influence of morphology we may consider several samples with the similar geometry and texture and number of grains, but different grain form. Examples of such samples with different morphology are shown in Figure 48. Top left part shows a simplified description of grains by using one element for each grain. This representation will be more relaxed than a one-element description from the previous chapter. It contains 800 grains-elements. Dimensions of RVE: $1\times1\times0.8mm^3$. An orientation is assigned to each grain, so that 400 orientations represent a component with a 5 degree scatter and the other half represents the randomly distributed orientations (the same scheme as the one used in the previous chapters). The top right part shows a more complex representation – the grains are equiaxial, each grain is represented by 8 elements. Total number of grains is 800 (so the number of elements increases to 6400). Dimensions of RVE: $1\times1\times0.8mm^3$. An orientation is assigned to each grain again with the same scheme. The bottom part shows other grain morphology – the grains are elongated along one axis and also consist of 8 elements. 800 grains are used again. Dimensions of RVE:

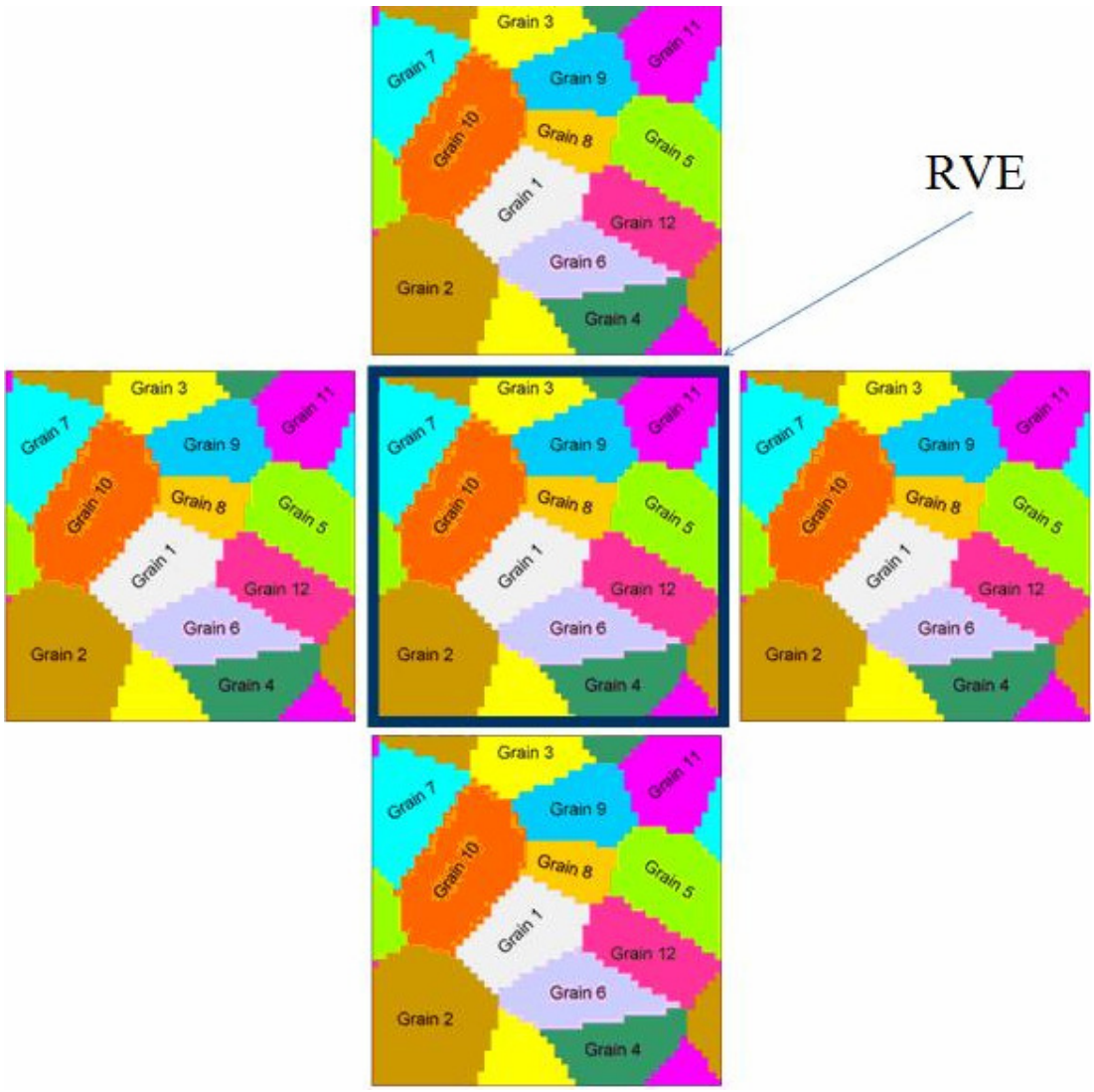

Figure 47. Representative volume element in morphology study [8].

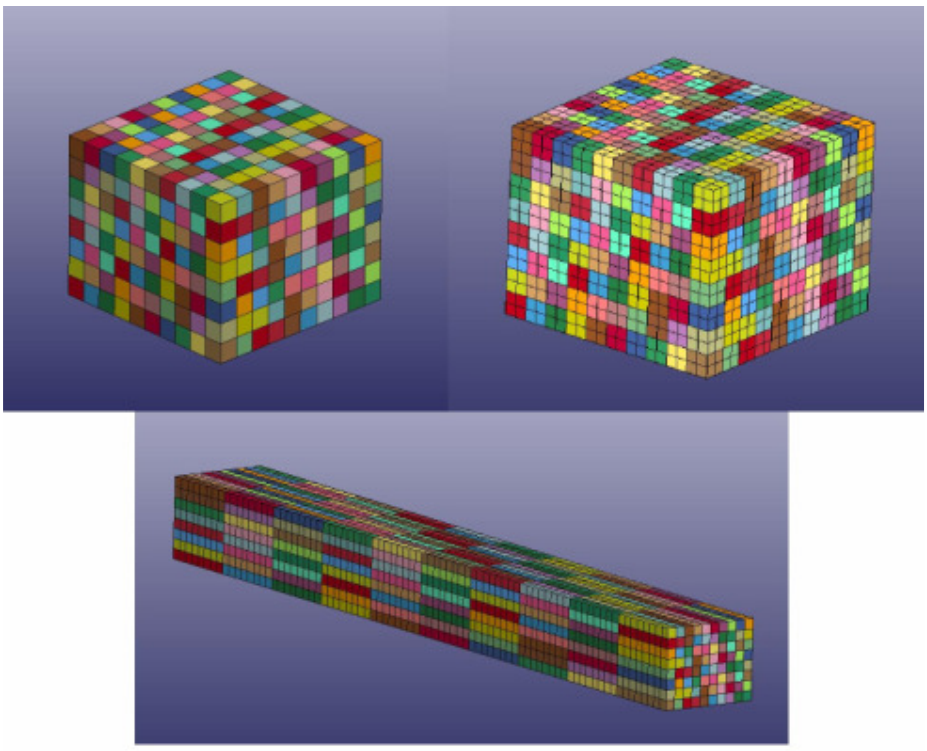

Figure 48. RVEs with different grain morphologies.

$8\times1\times0.8mm^3$. The same texturing scheme is used. This type of morphology is characteristic to e.g. drawn wires. Rectangular elements are used because of their better stability for FEM solution. Other possible geometry which could be considered is arbitrary irregular grain shape. But a solution for this type of morphology was not found before deadline, so no results can be presented.

6.2 Preliminary results and perspective for further study.

Some simulations of the samples with introduced morphologies were performed. These simulations, as already mentioned, take much longer time than the one-element simulations so it was impossible to perform all of them before deadline. One element per grain with equiaxial grains, 8 elements per grain with equiaxial grains and 1 element per grain with elongated grain all of them non-textured were tested. The obtained results show that yield surfaces for different morphologies also differ. If we use 1 element-1 grain morphology yield surface as a reference, we can see from Figure 49 that 8 elements per grain gives a yield surface that is 'compressed' along the $S_{11} = S_{22}$ line. But both of them behold symmetry relative to this line, because both morphologies are isotropic. The elongated grains morphology on the contrary is just orthotropic and its yield surface is distorted and symmetry relative to $S_{11} = S_{22}$ line is broken. The difference between the surfaces is not big, but quite visible. Another comparison between the yield surfaces for 1 element-1 grain and equiaxial grains and the isotropic von Mises yield function surface is shown on Figures 52 and 53. The equiaxial case is closer to isotropy. It may be that intragranular stress redistribution leads to weakening of anisotropic effects, but it is too early to make firm conclusions basing on just one simulation. One more simulations which we had time to perform is of cube texture and

elongated grain morphology as compared to 1 element-1 grain morphology. Results are shown on Figure 54. The elongated grains caused a 'rotation' of yield surface. The effect is more pronounced and somewhat different from the non-textured sample ('rotation' is more pronounced for Cube). A further study with different textures and morphologies is necessary to derive more regularities and tendencies. Figures 49-54 use the same representation the yield surface as in chapter 5.

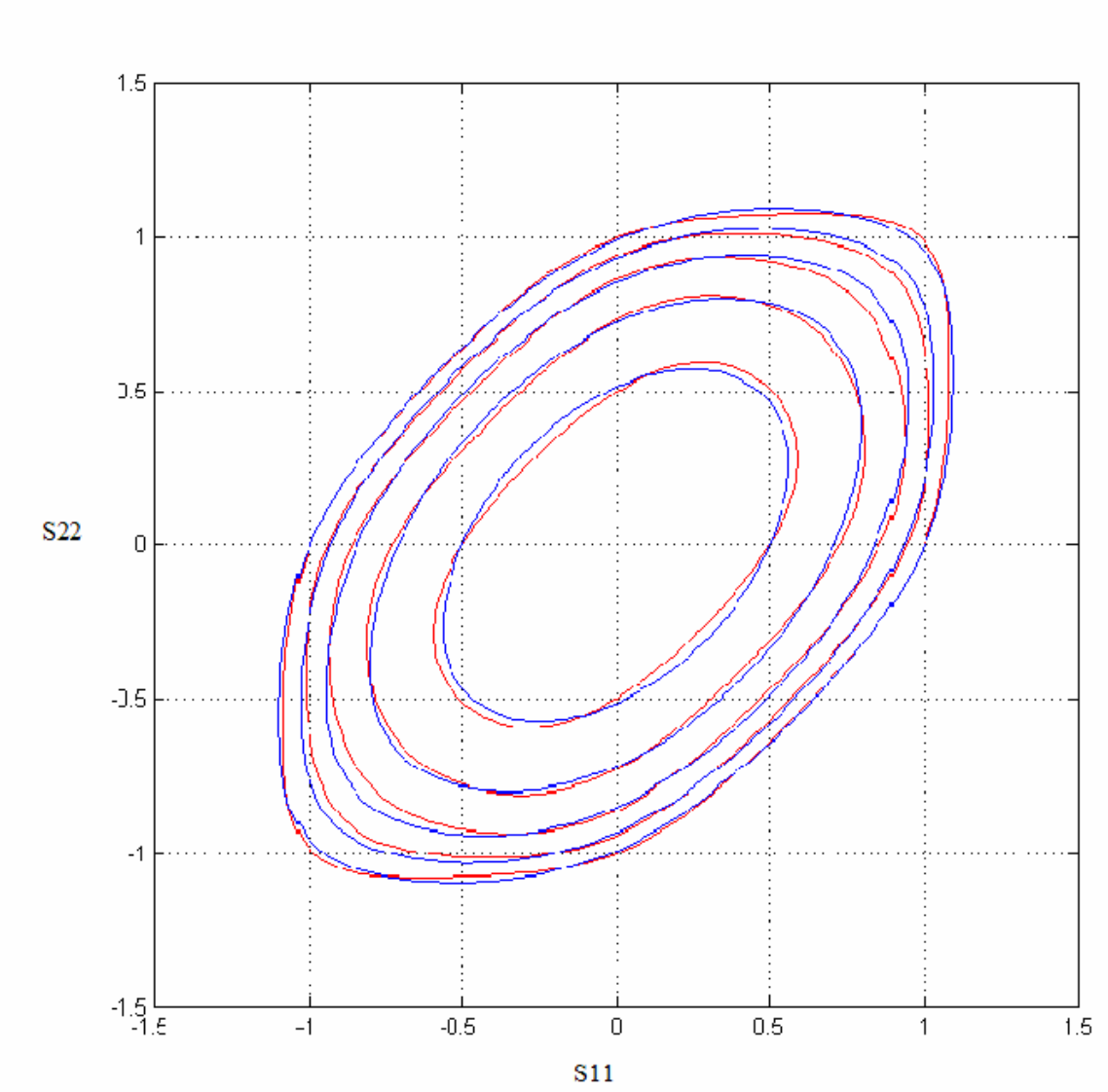

Figure 49. Yield surfaces for equiaxial 8 element grain morphology (blue) and equiaxial one element-one grain (red).

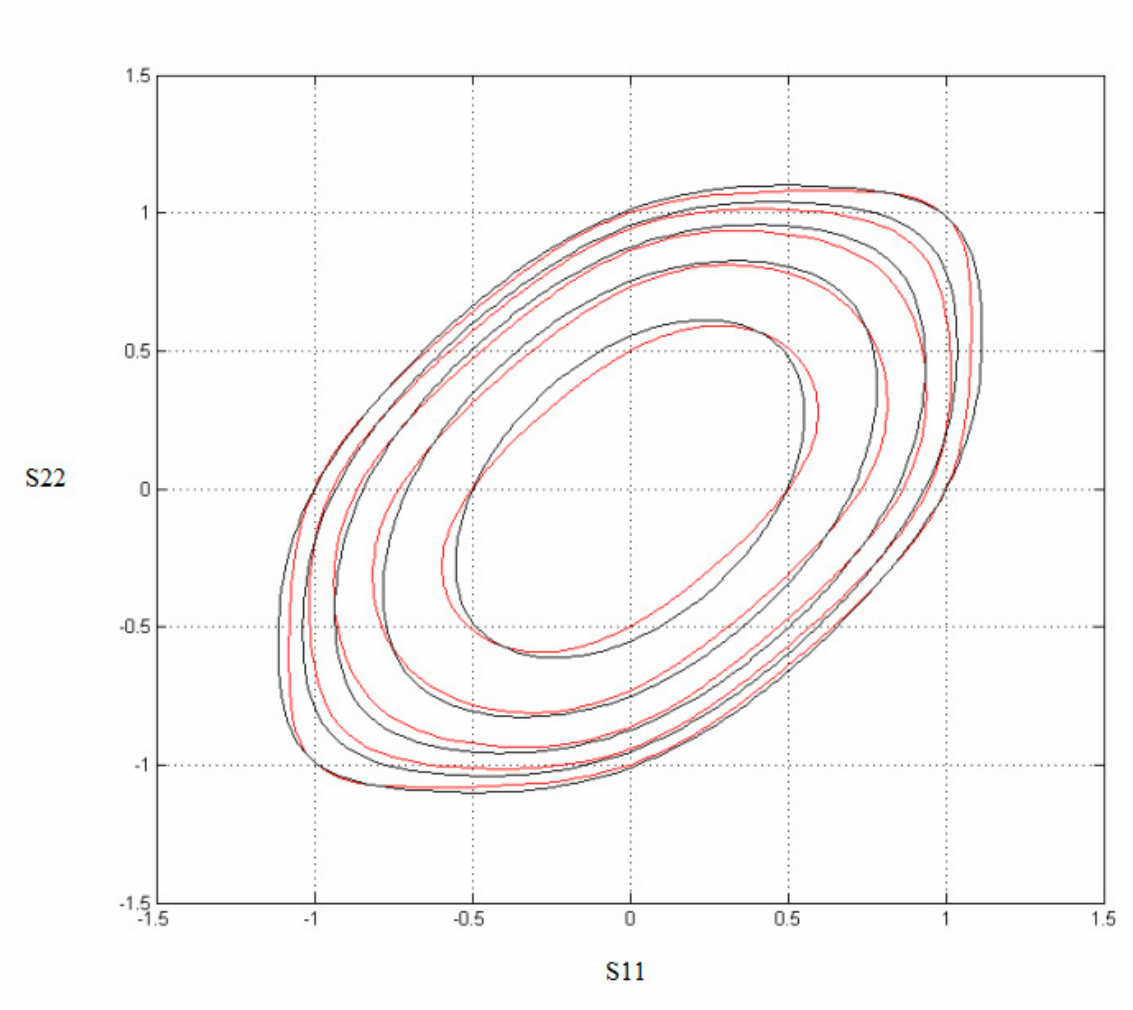

Figure 50. Yield surfaces for elongated grains (black) and 1 element per grain (red)..

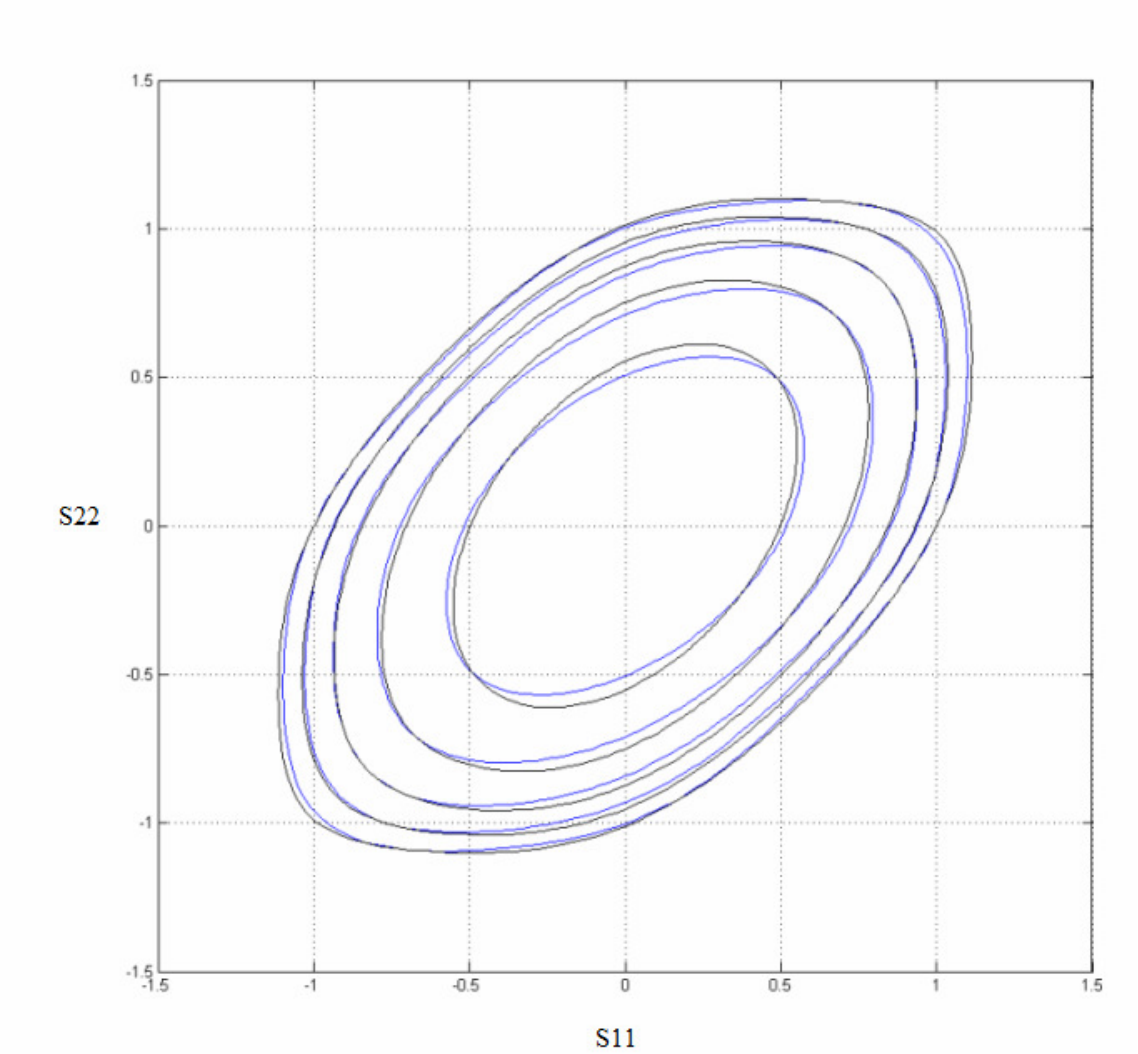

Figure 51. Yield surfaces for elongated grains (black) and equiaxial 8 element grains (blue).

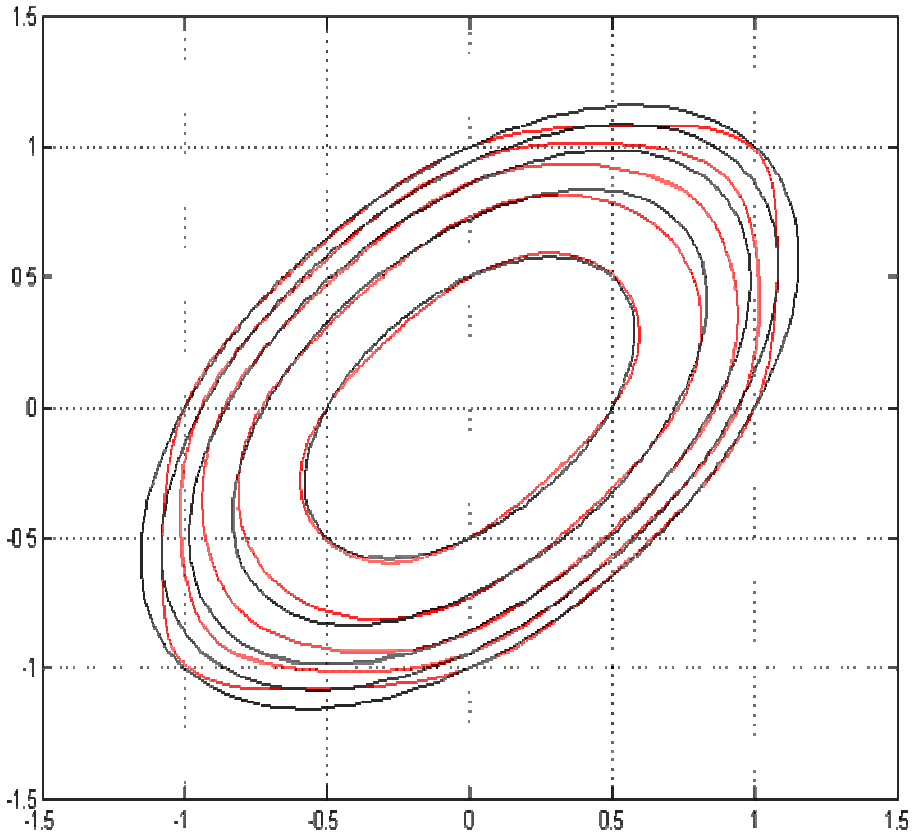

Figure 52. Yield surfaces for 1 element-1 grain (red) compared to von Mises yield surface (black).

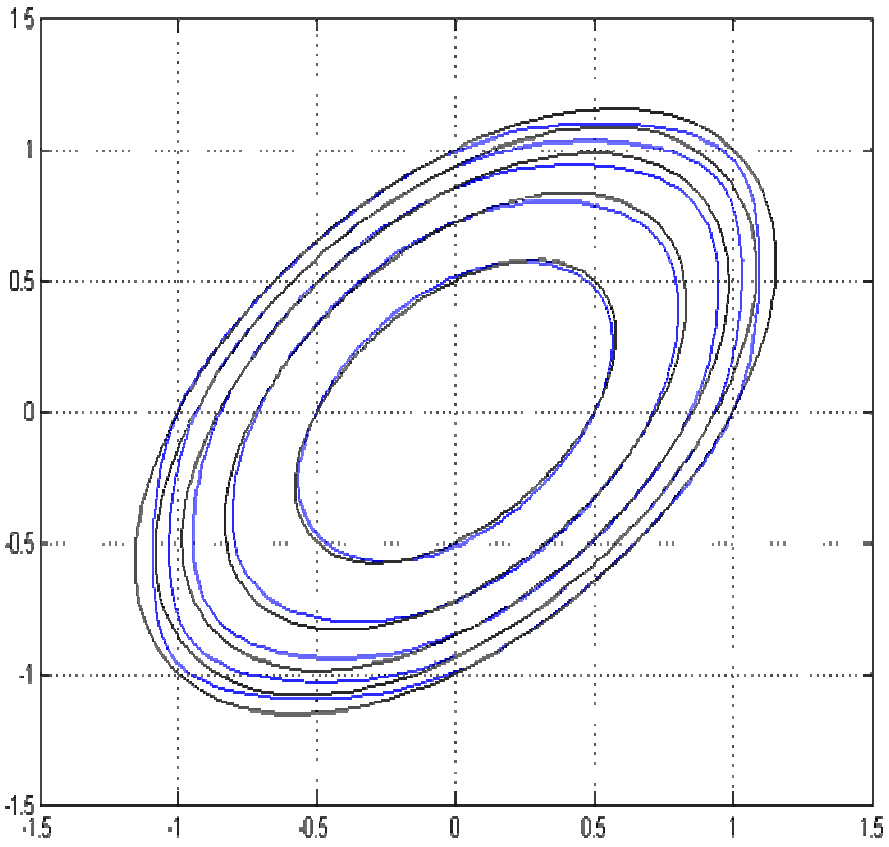

Figure 53. Yield surfaces for equiaxial grains(blue) compared to von Mises yield surface (black).

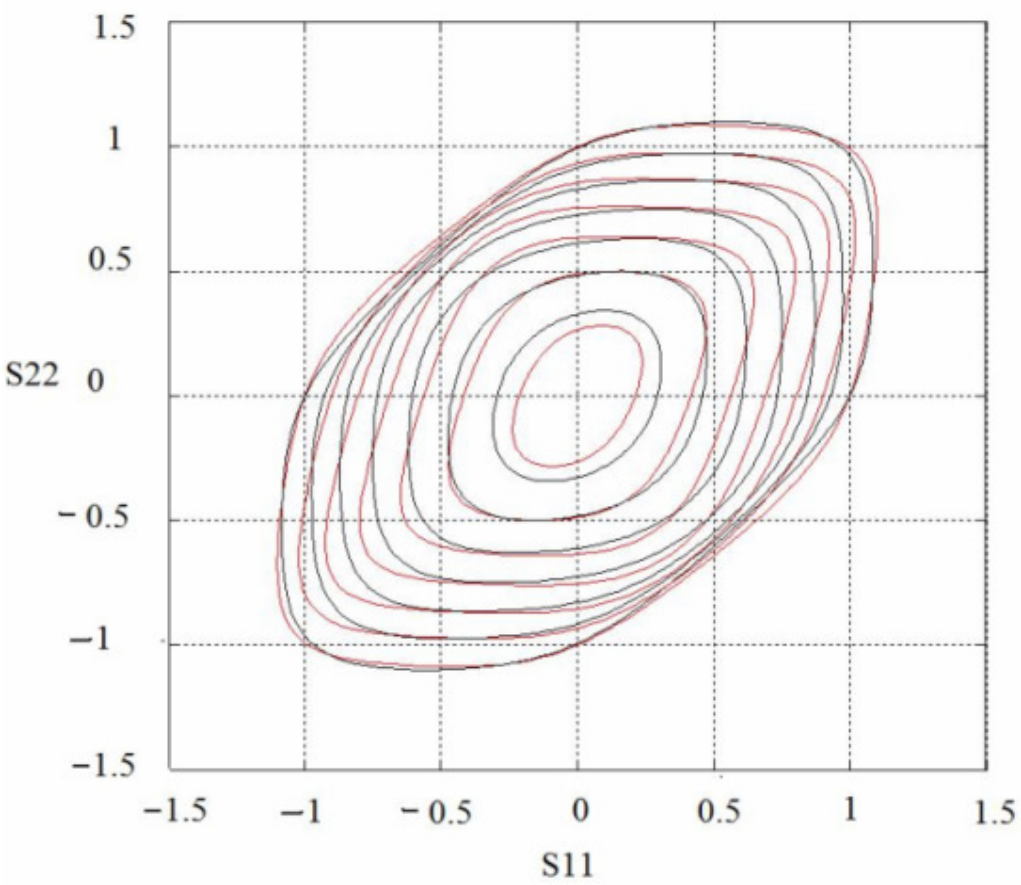

Figure 54. Yield surfaces for Cube textured elongated grain morphology (red) compared to 1 element-1 grain morphology (black).

7. Conclusion.

7.1 Obtained results and main observations.

After the literature study about the crystal plasticity theory and some of its models, a plane stress aluminium sample with distinct typical textures was numerically modelled in different ways and the following results were obtained:

1. The program based on the Taylor approach, rate-dependent constituent law and Voce hardening law with latent hardening was tested on several different textures and showed the results that both agree with the previous studies on this subject and can be clearly explained by the crystal plasticity theory. It gave us a material model that can be utilized in other applications for other purposes. It is not very useful by itself, because it ignores almost every other aspect of the sample like the geometry or morphology and boundary conditions are more a consequence of manipulations with the isotropic stress. Nevertheless, it allowed us to get used to the material model, investigate its properties at different plastic work and for different textures. The single crystals, as expected, have polyhedral yield surfaces that depend on the rotations of the crystal around its axes. Plastic strains are realized through stress states, lying in the vertices of the polyhedron. The total yield surfaces of polycrystals are an average of the yield surfaces of all the constituent crystals. As the main texture component is a big set of grains with similar orientations, the yield surface of a sample with strong texture is a polyhedral yield surface of a grain with this single orientation, smoothened and rounded by the randomly distributed rest part of the total texture (or alternatively, it is the smooth symmetrical isotropic yield surface, distorted by the component's polyhedral surface). Increasing plastic work leads to gradual activation of all slip systems. The starting yield surface for all textures is the same and coincides with the yield surface of a single crystal with (0,0,0) orientation. Then the other slip systems activate and after some value of plastic work (that corresponds to the strains $\varepsilon > 1\%$) all slip systems are activated, the yield surfaces reaches its form, characteristic for the given texture and hardening becomes isotropic.

2. This material model was introduced into the FEM program LS-DYNA. We started with one element mainly to check how the material model implements into LS-DYNA and if the assumptions made about the boundary conditions in the previous program are feasible. The boundary conditions could be implemented explicitly. The generated yield surfaces showed the same behaviour as for the previous program. The method of transforming a stress deviator into a plane stress state is found working. So a method of generating the yield surfaces for homogeneous polycrystals was tested.

3. We used the data from the previous simulations and tried to represent the yield surfaces as analytical yield functions. For the most part we succeeded – yield functions were found, which have a low difference between them and the simulated data. So a method of representing anisotropic yield criteria for a polycrystal was tested.

4. Some simulations on the samples with grain discretisation (morphology) were performed. The yield surfaces for the polycrystals with different grain morphologies are different to some degree. The influence of grain morphology of the polycrystals on some level was confirmed.

7.2 Unresolved questions and problems.

Most part of the work went smoothly with everything logical and explainable, but some unresolved problems remained.

1. The stress points of the single crystal yield surface at high plastic work obtained with LS-DYNA are distributed around the vertices' positions, while in the program that uses the Taylor model they lie exactly in the vertices. It may be the effect of varying strain rate, as explained in chapter 4, but this explanation may be wrong. Some calculations that prove or disprove it or some additional simulations which will investigate this aspect could be done.

2. The analytical functions obtained in chapter 5 seem to represent poorly the region of yield surface around the pure shear points (0,0). The yield surfaces for some textures seem to be rather flat there. The analytical yield functions tend to be smoothly curved. As explained in chapter 5 the MS Excel solver finds local minimum, so a more appropriate solution could be found if a good starting point was chosen. But how to find this good starting point is unclear. Some attempts were made but without success. If more time was given, may be a good fitting surface was found – some results of these attempts indicate it.

7.3 Suggestions for further study.

1. The simulations of samples with different morphologies should be continued. Solution for irregular grain form was not found. Other non-random textures should also be tested. It may show some tendencies and regularities and allow estimating how big the morphology influence is quantitatively, not just qualitatively.

2. A comparison between the results from the numerical modelling and the real sample test data should be performed. Model parameters could be 'tuned' better and the divergence between the two will indicate where the numerical model has its weaknesses.

Bibliography

1. O. S. Hopperstad, S. Dumoulin and A. Saai. A brief introduction to crystal plasticity. Draft report, SIMLab, NTNU (2010).

2. D W A Rees. Basic engineering plasticity. Elsevier (2006).

3. F. Irgens. Continuum mechanics. Springer (2008).

4. U. F. Kocks, C. N. Tomé, H.R. Wenk. Texture and anisotropy. Cambridge University press (1998).

5. Thomas H. Courtney. Mechanical behaviour of materials. McGraw-Hill (1990)

6. F. Barlat, O. Richmond. Prediction of tricomponent plane stress yield surfaces and associated flow and failure behaviour of strongly textured F.C.C. polycrystalline sheets. Material Science and Engineering (1987).

7. A.S. Khan, S. Huang. Continuum Theory of Plasticity. Wiley-Interscience Publication (1995).

8. A. Prakash, S.M. Weygand, H. Riedel. Modeling the evolution of texture and grain shape in Mg alloy AZ31 using the crystal plasticity finite element method, Computational Materials Science 45 744–750 (2009).

9. A. Saai, H. Louche, L. Tabourot, H.J. Chang. Experimental and numerical study of the thermo-mechanical behaviour of Al bi-crystal in tension using full field measurements and micromechanical modelling. Mechanics of Materials 42 275–292 (2010).

10. F. Barlat, H. Aretz, J.W. Yoon, M.E. Karabin, J.C. Brem, R.E. Dick. Linear transfomation-based anisotropic yield functions. International Journal of Plasticity 21 1009–1039 (2005).

11. http://www.absoluteastronomy.com/topics/Von_Mises_stress (20.02.2010)

12. http://www.bss.phy.cam.ac.uk/~amd3/teaching/A_Donald/Crystalline_Solids_1.htm (05.03.2010)

13. http://www.ndt-ed.org/EducationResources/CommunityCollege/Materials/Structure/linear_defects.htm (05.03.2010)

14. http://www.physics.thetangentbundle.net/wiki/Classical_mechanics/angular_velocity (05.03.2010)

15. G.I. Taylor and C.F. Elam. The distortion of an aluminium crystal during a tensile test. *Proc. R. Soc. Lond.* A102:643-67 (1923).

16. E. Schmid & W. Boas. Plasticity of Crystals. London: Chapman (1968).

17. J.F.W. Bishop and R. Hill. A theory of the plastic distortion of a polycrystalline aggregate under combined stresses. *Phil. Mag. Ser.* 7, 42:414-427 (1951).

18. G.I. Taylor (1938). Plastic strain in metals. *J. Inst. Metals* 62:307-24.

19. S.R. Kalidindi. Polycrystal plasticity: Constitutive modelling and deformation processing. PhD Thesis. Massachusetts Institute of Technology (MIT) (1992).

20. L. Tabourot, M. Fivel and E. Rauch. Generalised constitutive laws for f.c.c. single crystals. *Mater. Sci. Eng.* A 234-236:639-642 (1997).

21. L. Tabourot, S. Dumoulin and P. Balland. An attempt for a unified description from dislocation dynamics to metallic plastic behaviour. *J. Phys. IV France* 11:111-118 (2001).

22. Hill, R., A theory of the yielding and plastic flow of anisotropic metals. Proc. Roy. Soc. London A193, 281–297. (1948).

23. Z. Zhao, S. Kuchnicki, R. Radovitzky and A. Cuitiño. Influence of in-grain mesh resolution on the prediction of deformation textures in fcc polycrystals by crystal plasticity FEM. *Acta Mater.* 55:2361-2373 (2007).

24. E. Héripré, M. Dexet, J. Crépin, L. Gélébart, A. Roos, M. Bornert and D. Caldemaison. Coupling between experimental measurements and polycrystal finite element calculations for micromechanical study of metallic materials. *Int. J. Plasticity* 23:1512-1539 (2007).

25. D. Peirce, R.J. Asaro and A. Needleman. Material rate dependence and localized deformation in crystalline solids. *Acta metall.* 31:1951-1976 (1982).

26. S. Dumoulin and L. Tabourot, Experimental data on aluminium single crystal behaviour, *Proc. Inst. Mech. Eng. C* 219 (9) pp. 1159–1167 (2005).

27. D. Peirce, R.J. Asaro and A. Needleman, An analysis of nonuniform and localized deformation in ductile single crystals, *Acta Metall* 30 pp. 1087–1119 (1982).

28. U.F. Kocks, C. Tomé and H.-R. Wenk, Texture and Anisotropy. Preferred Orientations in Polycrystals and Their Effect on Material Properties. , Cambridge University Press, Cambridge, UK (1997).

29. Dierk Raabe, Franz Roters Using texture components in crystal plasticity finite element simulations. International Journal of Plasticity, Volume 20, Issue 3, pp 339-361 (2004).

30. G.R. Canova, U.F. Kocks, C.N. Tomé, The yield surface of textured polycrystals. J.Mech. Phys. Solids, Vol. 33, No. 4, pp. 371-397, (1985).

31. D. Achani, O.S. Hopperstad, O-G. Lademo, Influence of advanced yield criteria on predictions of plastic anisotropy for aluminium alloy sheets. Int. J. Mater. Form., Vol. 2 Suppl 1:487-490, (2009).